DISS. ETH NO. 20426

Investigation of Acetate and Oxalate Metabolism
in *Methylobacterium extorquens* AM1

A dissertation submitted to

ETH Zurich

for the degree of

Doctor of Sciences

Presented by

Kathrin Schneider

Dipl. Biol., University of Freiburg

Born on July, 21st, 1978

Citizen of Germany

Accepted on the recommendation of

Prof. Dr. Julia A. Vorholt

Prof. Dr. Jean-Charles Portais

Prof. Dr. Hauke Hennecke

2012

Table of Content

Table of Content

The results of this thesis were published in

Genome-scale reconstruction and system level investigation of the metabolic network of *Methylobacterium extorquens* AM1

KS performed analysis of (macro-) molecular biomass composition

AND

The ethylmalonyl-CoA pathway is used in place of the glyoxylate cycle by *Methylobacterium extorquens* AM1 during growth on acetate.

AND

Oxalyl-CoA reduction to glyoxylate is the preferred route of oxalate assimilation in *Methylobacterium extorquens* AM1

Abstract

Methylobacterium extorquens AM1 is a pink-pigmented facultative methylotroph that has been extensively studied for its one-carbon metabolism, but so far little is known about its growth with multi-carbon compounds such as acetate and oxalate. Assimilation of two-carbon compounds requires a strategy that allows producing the precursor metabolites required for biosynthesis, which contain three and more carbon atoms. Growth of organisms harboring the glyoxylate cycle for assimilation of acetyl-CoA has been investigated. However, this thesis gives new insights in acetate metabolism of *M. extorquens* AM1, which lacks isocitrate lyase, the key enzyme in the glyoxylate cycle. MS/MS-based proteomic analysis revealed that the protein repertoire of *M. extorquens* AM1 grown on acetate is similar to that of cells grown on methanol and includes enzymes of the ethylmalonyl-CoA (EMC) pathway that were recently shown to operate during growth on methanol. Dynamic ^{13}C-labeling experiments indicate the presence of distinct metabolic entry points for acetate, the EMC pathway and the citric acid (TCA) cycle. ^{13}C-steady state metabolic flux analysis showed that oxidation of acetyl-CoA occurs predominantly via the TCA cycle and that assimilation occurs via the EMC pathway. Furthermore, acetyl-CoA condenses with the EMC pathway product glyoxylate, resulting in malate formation. The latter, also formed by the TCA cycle, is converted to phosphoglycerate by a reaction sequence that is reversed with respect to the serine cycle. The results indicate that the metabolic flux distribution is highly complex in this model methylotroph during growth on acetate and is fundamentally different from organisms using the glyoxylate cycle.

Oxalate is the most oxidized two carbon compound and thus requires a different catabolic and anabolic strategy than acetate. Additionally to proteomics and dynamic ^{13}C-labeling experiments, mutant characterization was carried out to investigate the central metabolism of *M. extorquens* AM1 during growth on oxalate. The results confirmed that energy conservation from oxalate proceeds as previously described for *M. extorquens* AM1 and other characterized oxalotrophic bacteria via oxalyl-CoA decarboxylase, formyl-CoA transferase and subsequent oxidation to carbon dioxide by formate dehydrogenase. However, in contrast to other oxalate-degrading organisms, the assimilation of this carbon compound in *M. extorquens* AM1 occurs via the operation of a variant of the serine cycle: oxalyl-CoA reduction to glyoxylate, conversion to glycine and its condensation with methylene-H$_4$F (derived from formate) resulting in the formation of C3-units. The EMC pathway operates

during growth on oxalate but is nevertheless dispensable, indicating that oxalyl-CoA reductase is sufficient to provide the glyoxylate required for biosynthesis. Analysis of an oxalyl-CoA synthetase and oxalyl-CoA reductase deficient double mutant revealed an alternative, although less efficient, strategy for oxalate assimilation via one-carbon intermediates. The alternative process consists of formate assimilation via the tetrahydrofolate pathway to fuel the serine cycle, and in this case the EMC pathway is used for glyoxylate regeneration.

The results obtained reveal the utilization of common pathways during the growth of *M. extorquens* AM1 on one-carbon and two-carbon compounds, but with a major redirection of flux within the central metabolism. The plastic central metabolism featuring multiple assimilation routes for C1 and C2 substrates, may contribute to the rapid adaptation of *M. extorquens* AM1 to new substrates and the eventual co-consumption of carbon sources under environmental conditions.

Kurzbeschreibung

Methylobacterium extorquens AM1 ist ein pink-pigmentiertes fakultativ-methylotrophes Bakterium, dessen C1- (organische Substanzen ohne Kohlenstoff-Kohlenstoff Verbindung) Stoffwechsel gut erforscht ist. Über dessen Wachstum auf Substraten mit Kohlenstoff-Kohlenstoff Bindungen, beispielsweise Acetat und Oxalat, ist bisher jedoch wenig bekannt. Für die Assimilation dieser C2-Substrate wird eine Strategie benötigt, welche es erlaubt Vorläufermetabolite herzustellen, welche drei oder mehr Kohlenstoffatome besitzen und für die Biosynthese benötigt werden. Das Wachstum von Organismen, welche für die Acetat-Assimilation den Glyoxylat Zyklus nutzen, wurde bereits untersucht. Diese Arbeit gibt Einblicke in den Acetat-Stoffwechsel von *M. extorquens* AM1, welcher keine Isocitrat-Lyase, das Schlüsselenzym des Glyoxylate Zyklus, besitzt. MS/MS basierende Proteom Analysen zeigten, dass das Protein-Repertoire von *M. extorquens* AM1 während des Wachstums auf Acetat und Methanol sehr ähnlich ist. Auch die Enzyme des Ethylmalonyl-CoA (EMC) Wegs, welche, wie erst kürzlich gezeigt wurde, während der Assimilierung von Methanol in *M. extorquens* AM1 aktiv sind, wurden detektiert. Dynamische ^{13}C-Markierungsstudien deuteten darauf hin, dass zwei verschiedene Eintrittspforten für Acetat in den zentralen Stoffwechsel existierten, der EMC Weg und der Citrat (TCA) Zyklus. ^{13}C-Steady-State metabolische Flussanalysen zeigten, dass die Oxidation von Acetyl-CoA überwiegend über den TCA Zyklus stattfindet, und dass die Assimilation über den EMC Weg bewerkstelligt wird. Zusätzlich wird Acetyl-CoA mit Glyoxylat, dem Produkt des EMC Weges, kondensiert um daraus Malat zu bilden. Malat, ist ein Intermediat des TCA Zyklus, und wird nach Oxidation und einem Decarboxylierungsschritt zu Phosphoglycerat umgewandelt. Dies geschieht über die bekannten Reaktionen des Serin Zyklus, welche jedoch in umgekehrter Richtung ablaufen. Die Ergebnisse zeigen, dass die Flussverteilung im Zentralstoffwechsel in diesem Model-Organismus während des Wachstums auf Acetat sehr komplex ist, und diese unterschiedlich ist im Vergleich zu Organismen, welche den Glyoxylat Zyklus zur Acetyl-CoA Assimilation nutzen.

Oxalat ist die am höchsten oxidierte organische Verbindung und enthält zwei Kohlenstoffatome. Zusätzlich zur Proteome Analyse und dynamischen ^{13}C-Markierungsstudien wurden Mutanten charakterisiert, um den Zentralstoffwechsel von *M. extorquens* AM1 zu untersuchen. Die Resultate bestätigten, dass wie bereits in vorherigen Studien beschrieben wurde, *M. extorquens* AM1 Oxalat mittels Oxalyl-CoA Decarboxylase

Kurzbeschreibung

und Formyl-CoA Transferase zu Formiat umwandelt und es anschliessend mittels Formiat Dehydrogenase zu Kohlenstoffdioxid oxidiert. Im Unterschied zu anderen oxalotrophen Organismen, wird diese Kohlenstoffquelle von *M. extorquens* AM1 über eine Variante des Serin Zyklus zu Biomasse umgewandelt: Oxalyl-CoA wird zu Glyoxylat reduziert und schliesslich eine C3 Verbindung daraus gebildet. Hierfür wird Glyoxylat zu Glycin trans-aminiert und dieses anschliessend mit einer C1-Einheit ausgehend von Formiat kondensiert. Der EMC Weg ist aktiv in Zellen, welche mit Oxalat als Kohlenstoffquelle kultiviert wurden, jedoch ist dieser Stoffwechselweg nicht notwendig für das Wachstum auf Oxalat. Dies deutet darauf hin, dass die Aktivität der Oxalyl-CoA Reduktase ausreichend ist, um für das Wachstum genügend Glyoxylat zu synthetisieren. Das Wachstum einer Oxalyl-CoA Reduktase-negativen Doppelmutante zeigte, dass es noch eine zweite, wenn auch weniger effiziente, Strategie existieren muss, welche es ermöglicht Oxalat in Biomasse umzuwandeln. Diese alternative Stoffwechselroute besteht aus Enzymen des Tetrahydrofolat Weges, über welche Formiat reduziert wird. Das entstandene Methylen-Tetrahydrofolat wird anschliessend über den Serin Zyklus assimiliert. Der EMC Weg ist dann notwendig, um Glyoxylat zu regenerieren.

Die Ergebnisse dieser Arbeit zeigen, dass C1 und C2 Kohlenstoffquellen zwar über die gleichen Wege metabolisiert werden, es jedoch zu einer Neuausrichtung der Flüsse innerhalb des Zentralstoffwechsels kommt. Ein "formbarer" Zentralmetabolismus in *M. extorquens* AM1, welcher verschiedene Assimilationsrouten für C1 und C2 Substrate beinhaltet, könnte zu einer schnellen Anpassung des Organismus an neue bzw. ständig wechselnde Kohlenstoffquellen beitragen, oder sogar Co-Konsumation mehrerer Substrate ermöglichen. Dies könnte besonders in natürlichen Lebensräumen des Bakteriums von Vorteil sein.

Chapter 1

INTRODUCTION

Chapter I   Introduction

I. 1   The challenge of life

"The three main polymers of biology required for composition of living systems are the nucleic acids, the proteins, and the polysaccharides built from 20 amino acids, five nucleotide bases, and a few sugars, respectively. Together with lipids, these are the main constituents of biomass" (Lehninger, 1975). Form the so called precursor metabolites methylene-tetrahydrofolate (H_4F), acetyl-CoA, 3-phosphoglycerate, phosphoenolpyruvate (PEP), pyruvate, glyceraldehyde-3-phosphate, erythrose-4-phosphate, oxaloacetate, 2-oxoglutarate, erythrose-4-phosphate, ribose-5-phophate, glucose-6-phosphate, and fructose-6-phosphate all these bio-polymeres can be synthesized.

Depending on the availability of inorganic and organic matter, different anabolic and catabolic pathways are mandatory to allow energy conservation and biosynthesis. Prokaryotes are highly diverse in their metabolic capabilities; they can use a broad range of energy and carbon sources. Organisms are classified by their metabolic characteristics in *phototrophs* able of using light as energy source, and *chemotrophs* depending on reduced organic (*chemoorganotroph*) or inorganic (*chemolithothroph*) compounds. The organism is called *autotroph*, if capable of synthesizing all necessary compounds from carbon dioxide and *heterotroph* if depending on the availability of reduced organic compounds. The simplest organic compounds, alcohols or organic acids, that function as energy and carbon sources consist of one or two carbon atoms. Methanol for example is an one-carbon (C1) compound with an alcohol group and formate with a carboxylic acid group. Acetate, a two carbon short chain organic acid, has one carboxylic acid group and is a weak acid (pK_a 4,79), oxalate (also a two carbon compound) is a strong acid, it has two carboxylic acid groups and a pK_a of 1.46 and 4.40.

I. 2   Short chain organic acids and their toxicity

On the one hand short chain organic acids serve organisms as carbon and energy sources, on the other hand, they are known as important antimicrobial compounds. The acidification of nutrients with organic acids is commonly used for food conservation, e.g. production of yoghurt, vinegar, salami, sauerkraut and silage. *Acetobacter* and *Gluconobacter* species use incomplete oxidation of alcohols or sugars to produce acetic acid and to acidify their

environment to prevent growth of competitive species. Acetate is also a product of mixed acid, butyric acid, butanol, and homoacetogenic fermentation processes (Fuchs, 2007).

The antimicrobial activity of weak organic acids is related to their ability to travel across the cytoplasmic membrane in their undissociated form (Casal *et al.*, 1996; Salmond *et al.*, 1984). The idea of short chain organic acids acting as uncouplers was discussed versus toxicity being related to anion accumulation (Russell, 1992). Organisms which tolerate a decline in their intracellular pH are more resistant to the toxic effects of fermentation acids than those which do not. Maintaining a constant pH gradient across the membrane prevents the accumulation of high and potentially toxic concentrations of short chain organic acids (Diez-Gonzalez & Russell, 1997a; Diez-Gonzalez & Russell, 1997b; Russell, 1992). The toxicity of weak organic acids might be multifactorial. Roe *et al.* demonstrated growth inhibition of *Escherichia coli* by acetate is caused by a block in methionine biosynthesis (Roe *et al.*, 1998; Roe *et al.*, 2002). The addition of methionine to the medium relieves the growth inhibition in the presence of acetate to 80% relative to untreated controls. The intracellular homocysteine concentration increases upon acetate treatment, and supplementation of the medium with homocysteine was found to be toxic. Thus, the inhibitory effect of acetate is not only based on the depletion of methionine but also on the accumulation of toxic homocysteine. Furthermore, Steiner and Sauer (2003) demonstrated a second toxicity effect of acetate in *E. coli*, which is DNA damage. Over-expression of ATP-dependent helicases (RegG and RuvAB) was shown to improve resistance to organic acids, which is in line with DNA repair mutants to be more sensitive to weak organic acids compared to wild-type cells.

Oxalic acid, the simplest dicarboxylic acid, is not only a strong acid, but also a strong chelator. It forms highly insoluble crystals with calcium (solubility product, K_{sp}, at 25 °C of 2.32×10^{-9} for the monohydrate), but soluble salts with sodium and potassium. Calcium is involved in signal transduction pathways and in the regulation of other biochemical cellular processes. Plants use synthesis of oxalate to maintain stable calcium levels by precipitation of excess calcium into a physiologically and osmotic inactive form (Franceschi & Nakata, 2005). They accumulate calcium oxalate crystals up to 80% of their dry weight, which additionally can be used in mechanical defense mechanisms. The acid is formed through the oxidation of glyoxylate by activity of glyoxylate oxidase. However, ascorbate might be the major source of oxalate production in plants, but the enzymes of this pathway have not yet been identified. Furthermore, hydrolysis of oxaloacetate to oxalate and acetate was found in few plant species (Franceschi & Nakata, 2005). Oxalate is not only produced in large quantities by plants, but also by different classes of fungi by hydrolytic cleavage of

oxaloacetate or oxidation of glyoxylate (Dutton & Evans, 1996). The function of oxalate in fungi includes (*i*) pathogenesis during plant infection by disrupting the integrity of the host plant cell wall, (*ii*) inhibition of competing fungi and other soil microorganisms, (*iii*) the control of the availability of environmental nutrients like phosphate and iron, and (*vi*) detoxification of heavy metals like copper. Oxalate is also a product of lignocellulose degradation and has various functions in the degradation process. It is required for acidification of the environment and acts as a chelator for manganese involved in lignin degradation (Dutton & Evans, 1996).

Although short chain fatty acids like acetic acid and oxalic acid have their toxicological effects they are produced by various organisms like bacteria, plants, and fungi and are in return available to these as carbon and energy sources.

I. 3 Growth with acetate as the carbon and energy source

The ability to convert acetate to carbon dioxide for energy generation and to assimilate the C2 compound into cell material is a property shared by plants, numerous microorganisms, and invertebrates. This particular characteristic is not solely of importance when considering growth with acetate but extends to the question how assimilation of numerous substrates is accomplished that have in common their initial conversion to acetyl-CoA as the entry point for central carbon metabolism. These include abundant substrates such as fatty acids, terpenes, alcohols, and esters, waxes, alkenes, and polyhydroxyalkanoates.

Krebs discovered in the 1940ies that acetyl-CoA is oxidized under aerobic conditions to carbon dioxide by the tricarboxylic or citric acid (TCA) cycle with the C4 and C5 precursor metabolites, oxaloacetate and 2-oxoglutarate, as its intermediates. However, the TCA cycle does not allow any net synthesis of these compounds. Thus, the depletion of TCA cycle intermediates needs an anaplerotic pathway to replenish the cycle. In 1957, the question how the anaplerotic sequence of reactions for acetyl-CoA occurs was initially answered with *E. coli* growing in the presence of acetate as a sole carbon source and with germinating seedlings during fat reservoir consumption by the seminal studies by Kornberg, Krebs, and Beevers (Kornberg & Beevers, 1957a; Kornberg & Beevers, 1957b; Kornberg & Krebs, 1957). These studies let to the identification of the glyoxylate cycle that in conjunction with reactions of the TCA cycle allowed for the net synthesis of C4 compounds from two molecules of acetyl-CoA. Thereby, isocitrate lyase, together with the enzymes of the TCA cycle, is responsible for the oxidation of acetyl-CoA to glyoxylate. Malate synthase, the

second enzyme of the glyoxylate cycle, condenses glyoxylate and another molecule of acetyl-CoA to malate. Soon after the discovery of the glyoxylate cycle, it became clear that other bacteria, fungi, and nematodes use the same sequence of reactions for acetyl-CoA assimilation (e.g. Patel & McFadden, 1978).

Acetate metabolism has been well described in isocitrate lyase positive organisms like *E. coli* and *Corynebacterium glutamicum* (Figure I.1) including determination of the metabolic network topology and absolute flux quantification (Gerstmeir *et al.*, 2003; Holms, 1996; Oh *et al.*, 2002; Peng & Shimizu, 2003; Walsh & Koshland, 1984; Wendisch *et al.*, 2000; Zhao & Shimizu, 2003). Acetate is activated to acetyl-CoA and either directly used for biosynthesis (5%) or converted into the TCA cycle upon condensation with oxaloacetate (76%). Isocitrate is oxidized by reactions of the TCA cycle to oxaloacetate (56%), or is cleaved by isocitrate lyase to succinate and glyoxylate (18%). Glyoxylate is condensed with acetyl-CoA to produce malate and then oxidized to oxaloacetate. The C4 compound is decarboxylated to PEP (13%) and used for biosynthesis or is further converted for gluconeogenesis (Wendisch *et al.*, 2000).
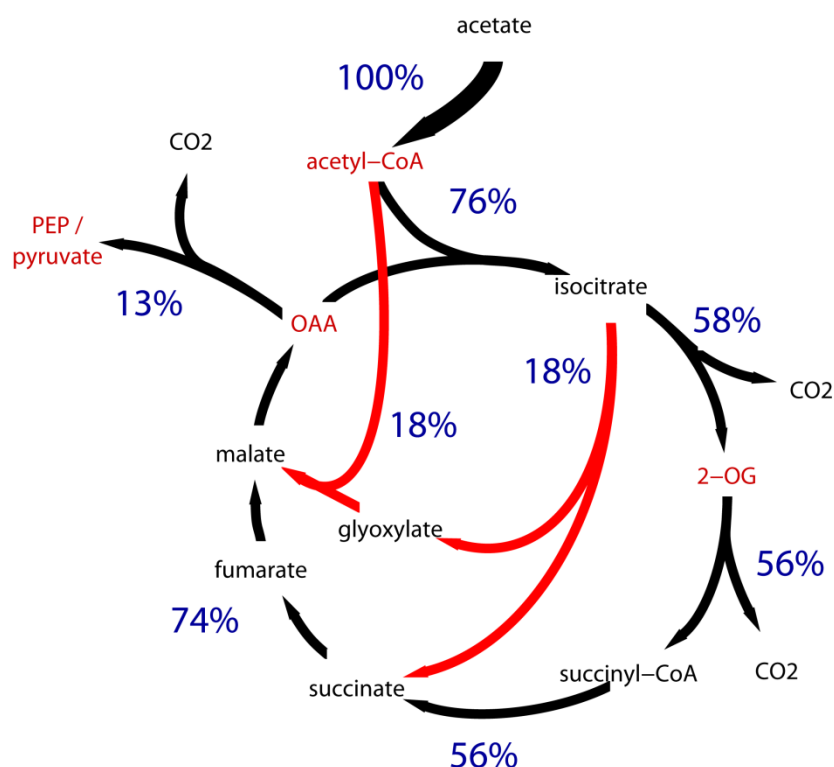
Figure I.1. Metabolic fluxes in the central metabolism of isocitrate lyase-positive *C. glutamicum* during growth on acetate according to data from Wendisch *et al.* (2000) . Fluxes are given in percent of acetate uptake rate. Precursor metabolites are labeled red and represent biomass exit fluxes.
OAA: oxaloacetate, 2-OG: 2-oxoglutarate.
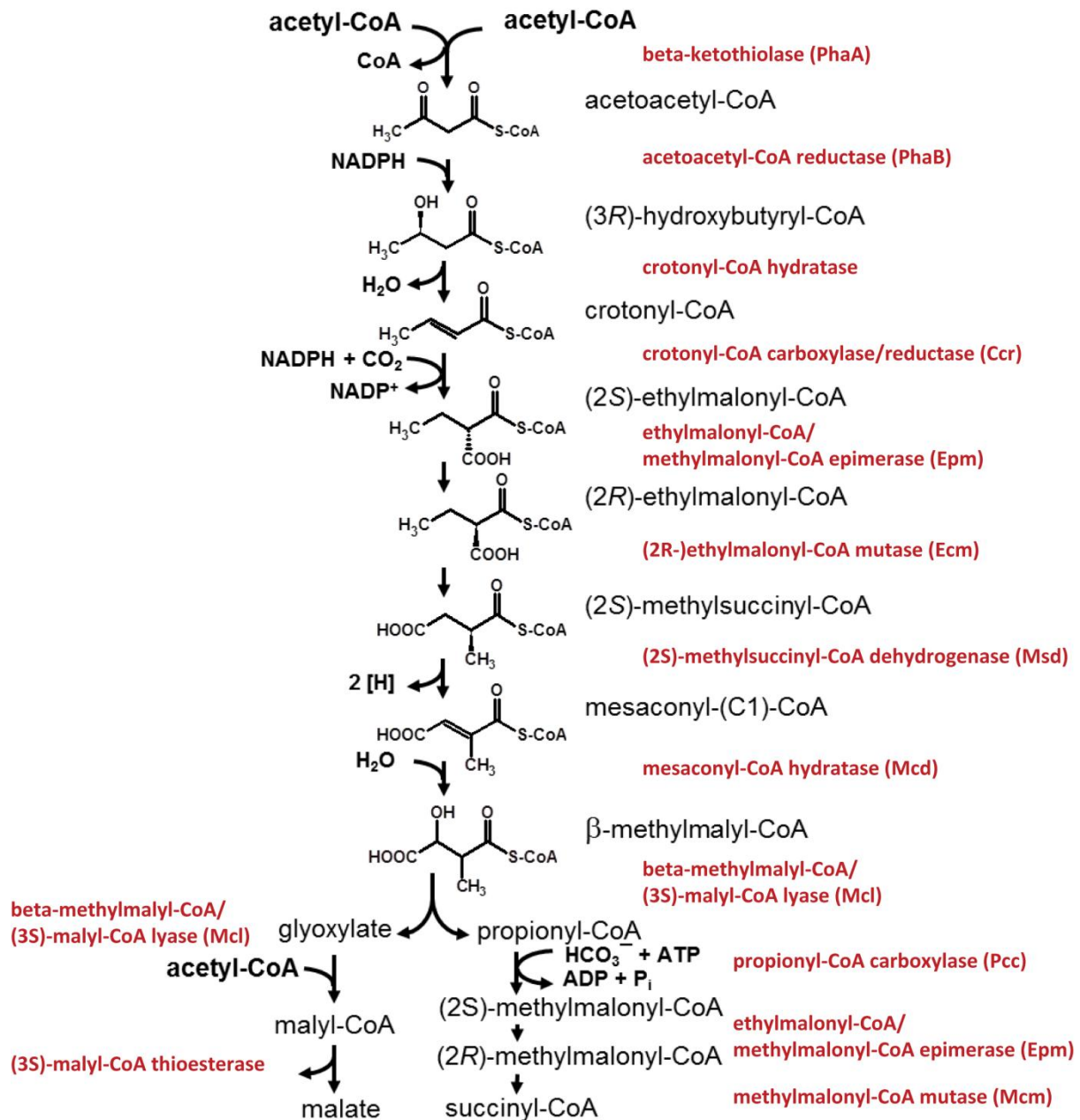
Figure I.2. The ethylmalonyl-CoA pathway is used for acetyl-CoA assimilation in *Rhodobacter sphaeroides*. The pathway and its enzymes are shown in detail (figure modified from Erb *et al.*, 2007).

But not all organisms possess the glyoxylate cycle. The pathway is conspicuously absent in vertebrates (Ensign, 2006). As a consequence, acetyl-CoA formed by catabolic reactions in vertebrates is committed to oxidation to CO_2 via the TCA cycle and no net conversion to a C4 precursor metabolite is possible. Also a number of bacteria lack the key enzymes of the glyoxylate cycle; however, they are able to grow on acetate and compounds that enter the central metabolism on the level of acetyl-CoA. Those isocitrate lyase-negative organisms, including *Methylobacterium extorquens* (Anthony, 1982), *Rhodopseudomonas* (Albers & Gottschalk, 1976), *Streptomycetes* (Han & Reynolds, 1997), and *Paracoccus* (Gottschal &

Introduction

Kuenen, 1980), must use another strategy for anaplerosis. The question how assimilation of acetyl-CoA occurs in organisms devoid of a functional glyoxylate cycle for a long time remained a mystery. Recently, Erb, Alber and coworkers have performed biochemical studies together with mutant analysis in *Rhodobacter sphaeroides* and provided evidence that anaplerosis occurs via a pathway that was named ethylmalonyl-CoA (EMC) pathway (Alber *et al.*, 2006; Erb *et al.*, 2007; Erb *et al.*, 2008; Erb *et al.*, 2009a; Erb *et al.*, 2009b; Erb *et al.*, 2010). This pathway (Figure I.2) includes the formation of ethylmalonyl-CoA, its characteristic intermediate formed from 2 acetyl-CoA and one carbon dioxide, which is further converted to methylmalyl-CoA, from which both glyoxylate and propionyl-CoA are released by cleavage. The propionyl-CoA is carboxylated to succinyl-CoA and glyoxylate is condensed with acetyl-CoA and converted to malate. The C4 compounds succinyl-CoA and malate refill the TCA cycle and are assimilated as cell material.

For evaluation of the relevance of the EMC pathway, the analysis of 1215 fully sequenced genomes for the presence of the minimum set of genes (crotonyl-CoA carboxylase/reductase, ethylmalonyl-CoA mutase, and methylsuccinyl-CoA dehydrogenase) was carried out (Erb, 2009). Around 5% of the bacterial genomes sequenced were predicted to harbor EMC pathway enzymes. This represents the alternative acetyl-CoA assimilation strategy in around 8% of the genera. In 28% of the genomes (34% on genus level) sequenced the isocitrate lyase gene was identified indicating the presence of the glyoxylate cycle. These numbers demonstrate the distribution of the two alternative pathways for anaplerosis amongst the bacterial genera, whose genomes have been sequenced. This demonstrates the EMC pathway is widespread and operating in a number of bacterial species. However, it has to be taken into account this may not necessarily reflect the actual distribution of the pathway with respect of the unknown bacterial species (Erb, 2009).

I. 4 Growth with oxalate as the carbon and energy source

Interestingly, not all C2 compounds are metabolized via acetyl-CoA. With two carboxylic acid groups oxalate has an oxidation number of plus three, and thus, is higher oxidized than acetate. The high oxidation state of the compound requires distinct catabolic and anabolic strategies that allow growth. Oxalate is often produced by plant and fungal species mostly as a metabolic end product. The carbon source is likely available as a nutrient for plant-associated microorganisms and particularly for those microorganisms found in the soil during the decay of plant material. Although calcium oxalate, which is likely to predominate in

nature, is less soluble than potassium or sodium oxalate, it supports growth of bacteria in soil (Bravo *et al.*, 2011).

A number of oxalotrophic bacteria have been isolated from various ecological niches, including terrestrial (Braissant *et al.*, 2004) and aquatic habitats (Smith *et al.*, 1985b), and the gastrointestinal tract, under both aerobic and anaerobic conditions. Phylogenetically, oxalotrophic bacteria belong to distinct groups (Khammar *et al.*, 2009; Sahin, 2003; Sahin & Aydin, 2006; Sahin *et al.*, 2008). The utilization of oxalate has been studied in *Oxalobacter formigenes* and *Cupriavidus oxalaticus* (formerly *Pseudomonas oxalaticus* (Vandamme & Coenye, 2004)), both members of the Burkholderiales. *O. formigenes* was found in the human gut and those of other warm-blooded animals and is an obligate anaerobe and oxalate-dependent organism (Allison *et al.*, 1985). Its presence in the gut is known to inhibit the formation of kidney stones (Allison *et al.*, 1986; Sidhu *et al.*, 1998). *C. oxalaticus* was isolated from the intestine of an Indian earthworm (Khambata & Bhat, 1953), and its oxalate metabolism was investigated under aerobic growth conditions by Quayle and co-workers in the 1960s (Quayle & Keech, 1959a; Quayle & Keech, 1959b; Quayle & Keech, 1960; Quayle *et al.*, 1961; Quayle & Taylor, 1961; Quayle, 1963a; Quayle, 1963b).

Oxidation of oxalate requires disruption of the carbon-carbon bond to release electrons used for generation of reductant. Three types of enzymes are known to catalyze the breakage of the carbon-carbon bond (Svedruzic *et al.*, 2005); (*i*) oxalate oxidase catalyzes oxygen-dependent oxidation of oxalate into two molecules carbon dioxide under the formation of hydrogen peroxide. This enzyme is predominantly found in higher plants but also in lignin degrading fungi. (*ii*) Oxalate decarboxylase catalyzes decarboxylation of oxalate to formate and carbon dioxide. The enzyme is present in different fungal species. (*iii*) Oxalyl-CoA decarboxylase exists in oxalate degrading bacteria such as *C. oxalaticus*, *Bacillus oxalophilus* and *O. formigenes*. The thiamin pyrophosphate-dependent enzyme converts oxalyl-CoA to formyl-CoA and carbon dioxide, the activity is stimulated by addition of Mg^{2+} and exhibits high substrate specificity to oxalyl-CoA. So far, oxalyl-CoA decarboxylase was not found outside Bacteria (Svedruzic *et al.*, 2005). The enzyme has been purified and characterized from *C. oxalaticus* (Quayle, 1963b) and *O. formigenes* (Baetz & Allison, 1989). The conversion of oxalate to its CoA thioesters is a prerequisite for its decarboxylation by oxalyl-CoA decarboxylase, and raises the question how organisms cope with the energetic cost of oxalate esterification. The solution was found by identification of a formyl-CoA transferase, which turns the CoA group from formyl-CoA over to oxalate (Baetz & Allison, 1990; Quayle, 1963b). This enzyme belongs to a group of CoA transferases, which differs in its

amino acid sequence from other well-known CoA transferase families (Heider, 2001). The overall reaction catalyzed by oxalyl-CoA decarboxylase and formyl-CoA transferase converts oxalate to formate and carbon dioxide by the consumption of one proton. By an antiporter two-fold negatively charged oxalate is imported by the export of the monoanion formate. The transport process creates a proton and electrochemical gradient across the membrane that can be used for ATP synthesis (Abe *et al.*, 1996; Fu *et al.*, 2001). The aerobe *C. oxalaticus* produces redox equivalents upon oxidation of formate to carbon dioxide by formate dehydrogenase (Quayle *et al.*, 1961), but generation of reductant by the anaerobe *O. formigenes* upon oxalate utilization is still unknown.

As mentioned, the oxidation number of oxalate is plus three and thus higher than of cellular carbon (the cellular composition $C_4H_7O_{1.5}N$ gives and average oxidation number of 0.5). Thus, a net reduction of oxalate is required for incorporation into biomass. Direct reduction of oxalyl-CoA to glyoxylate was detected in cell-free extracts of *C. oxalaticus* (Quayle *et al.*, 1961), and the corresponding enzyme oxalyl-CoA reductase was purified and characterized (Quayle & Taylor, 1961; Quayle, 1963a), but gene identification was missing. For synthesis of C3 and C4 precursor metabolites glyoxylate has to undergo condensation reactions. Via the glycollate pathway (Hansen & Hayashi, 1962; Kornberg & Gotto, 1959; Kornberg & Gotto, 1961; Kornberg & Sadler, 1961) (also referred as the glycerate pathway (Cornick & Allison, 1996b)), two molecules of glyoxylate are converted to tartronic acid semialdehyde by glyoxylate carboligase, which is subsequently reduced to glycerate by tartronic acid semialdehyde reductase. Glycerate, in turn, can be carboxylated to a C4 compound. The glycolate pathway is operating in *C. oxalaticus* (Blackmore & Quayle, 1970; Quayle *et al.*, 1961) and *O. formigenes* (Cornick & Allison, 1996b) during oxalate growth. The key enzyme glyoxylate carboligase was absent in oxalotrophs like *Methylobacterium* strains, and thus an alternative strategy for oxalate assimilation must exist (Blackmore & Quayle, 1970). Blackmore and Quayle detected oxalyl-CoA decarboxylase, oxalyl-CoA reductase and the presence of serine cycle enzymatic activities, i.e. serine glyoxylate aminotransferase and hydroxypyruvate reductase, in cell-free extracts of *Methylobacterium* species. Hence, they suggested oxalate assimilation via some variant of the serine cycle (Blackmore & Quayle, 1970). This variant of the serine cycle involves oxalyl-CoA reduction to glyoxylate and its condensation with the C1-unit precursor metabolite methylene-H_4F (produced from formate) via serine cycle enzymes to generate glycerate. However, due to the 20-30-fold lower specific activity of oxalyl-CoA reductase in *M. extorquens* AM1 than in oxalate-grown *C. oxalaticus*, it remained unclear whether oxalyl-CoA reduction is the major

pathway for glyoxylate generation (Blackmore & Quayle, 1970). The recently discovered EMC pathway (see Chapter I.3), which is operating in *Methylobacterium extorquens* during the assimilation of C1 compounds (Figure I.3) for glyoxylate regeneration (Peyraud *et al.*, 2009), was unknown when *Methylobacterium* was first studied during oxalotrophic growth (Blackmore & Quayle, 1970). The function of the EMC pathway during oxalate utilization has not yet been investigated.

I. 5   One-carbon metabolism and *Methylobacterium extorquens* AM1

Chemoheterotrophic growth on organic one-carbon compounds such as methanol and formate is called methylotrophy. Utilization of these carbon compounds requires specific enzymes for oxidation and *'de novo'* synthesis of carbon-carbon bonds to produce the precursor metabolites. Organisms are called obligate methylotrophs when growing exclusively on C1 compounds; facultative methylotrophs are able to also utilize a variety of other multi-carbon compounds. The first aerobic methanol-utilizing bacterium was already described in 1892, i.e. *Bacillus methylicus* (Loew, 1892). Ever since other methylotrophs have been isolated, they belong, amongst others, to the group of Alpha- Beta and Gammaproteobacteria, Verrucomicrobia, Cytophagales, Bacteriodetes, Firmicutes, and Actinobacteria (Kolb, 2009). The pink-pigmented facultative methylotrophs belong to the genus *Methylobacterium* and are known as major plant colonizers (Delmotte *et al.*, 2009; Knief *et al.*, 2011) but also have been isolated from soil, dust, and lake sediments (Green, 2006) and the human foot microflora and the mouth (Anesti *et al.*, 2004; Anesti *et al.*, 2005). These organisms have primarily a facultative methylotrophic lifestyle, only around 9% of the species are restricted to C1 compounds (Kolb, 2009).

Methanol utilization is well-studied and different pathways for oxidation and assimilation of this one carbon compound exist. Oxidation of methanol requires methanol dehydrogenase. Two types of methanol dehydrogenases are known, a periplasmatic PQQ-dependent and a cytoplasmic NAD^+-dependent enzyme. Formaldehyde, the product of methanol dehydrogenase, a highly toxic intermediate, is oxidized by cofactor-dependent pathways involving glutathione, H_4F, or tetrahydromethanopterin (H_4MPT) to formate (Vorholt, 2002). The product is oxidized by formate dehydrogenase to carbon dioxide (Chistoserdova *et al.*, 2004; Chistoserdova *et al.*, 2007). The H_4F-dependent pathway is not exclusively used in an oxidative manner but also for synthesis of methylene-H_4F (Vorholt, 2002). For carbon assimilation, three alternative strategies exist (Anthony, 1982), the serine cycle, the ribulose-

monophosphate cycle and the Calvin cycle. Serine cycle and ribulose-monophosphate cycle allow the *'de novo'* synthesis of carbon-carbon bonds from formaldehyde, and the Calvin cycle from carbon dioxide. By the overall reaction of the ribulose-monophosphate cycle one molecule of a C3 compound is synthesized from three molecules of formaldehyde, this compound being either pyruvate or dihydroxyacetone. The first step of the pathway is the condensation of formaldehyde with ribulose-5-phosphate followed by cleavage and rearrangement reactions of the Entner-Doudoroff and the pentose-phosphate pathway. The serine cycle differs from the formaldehyde assimilation pathway described above by its intermediates, which are carboxylic and amino acids instead of carbohydrates. The C1-unit assimilated via serine cycle is H_4F-bound at the level of a methylene group and not the free formaldehyde, as it is used within the ribulose-monophosphate cycle. Acetyl-CoA, the carbon fixation product of the serine cycle, is converted to glyoxylate to restore the serine cycle by either the glyoxylate cycle (Anthony, 1982) or, as recently demonstrated, by operation of the EMC pathway (Peyraud *et al.*, 2009).

In 1961, Peel and Quayle (Peel & Quayle, 1961) observed a pink pigmented probably airborne contaminant in a culture containing methylamine as sole carbon source. The organism was called *Pseudomonas* AM1 and later on reclassified as *Methylobacterium extorquens* AM1 (Bousfield & Green, 1985). The gram-negative organism belongs to the order of *Rhizobiales* and the class of Alphaproteobacteria; it is motile with a single flagellum and exhibits a size of 0.8 x 0.2 µm (Peel & Quayle, 1961). The interest in *M. extorquens* AM1 and its metabolism is in particular fueled by the potential of facultative methylotrophs for biotechnological applications (Schrader *et al.*, 2009) and by their general importance with respect to recycling of methanol, a plant product (Fall & Benson, 1996) estimated to be formed at a rate of 100 Tg per year by the global vegetation (Galbally & Kirstine, 2002). Utilization of methanol during plant colonization provides a selective advantage in competition experiments. However, methanol dehydrogenase-deficient and H_4MPT-deficient mutants of *M. extorquens* AM1 are still able to colonize the phyllosphere like wild-type under non-competitive conditions, indicating methanol is not the only carbon source accessible to *Methylobacterium* (Sy *et al.*, 2005).

In the past 50 years *M. extorquens* AM1 has been well studied for its C1 metabolism (Anthony, 1982; Anthony, 2011; Chistoserdova *et al.*, 2003). A draft genome is available since 2003 (Chistoserdova *et al.*, 2003) and the complete sequence was published in 2009 (Vuilleumier *et al.*, 2009). Together with transcriptomic (Okubo *et al.*, 2007) and proteomic

approaches (Bosch *et al.*, 2008; Laukel *et al.*, 2004), as well as genetic tools being applied (Marx & Lidstrom, 2001; Marx, 2008), the organism became an important model organism for facultative methylotrophs and systems-level approaches. Genome scale metabolic network reconstruction was carried out (Peyraud *et al.*, 2011) integrating information from (*i*) genome annotation, (*ii*) published physiological, genetic and biochemical studies of *M. extorquens* AM1 and closely related organisms, (*iii*) biochemical information contained in databases, and (*vi*) complementary investigations like biomass quantification (which is part of this thesis).

The metabolic network topology including flux values was determined during growth of *M. extorquens* AM1 on methanol using ^{13}C flux analysis (Figure I.3) (Peyraud *et al.*, 2011). The flux analysis confirmed that during methylotrophy 50% of carbon incorporated into biomass passed through carbon dioxide (Large *et al.*, 1961). Methanol is oxidized via the intermediates formaldehyde and formate to carbon dioxide (84%) by PQQ-dependent methanol dehydrogenase, the H$_4$MPT-dependent pathway, and formate dehydrogenase, respectively. Sixteen percent of the C1-units are converted to C3- and then C4-units: glyoxylate is converted by serine glyoxylate aminotransferase to glycine, which is condensed with methylene-H$_4$F to form serine. The latter is then converted to hydroxypyruvate by serine glyoxylate aminotransferase, reduced to glycerate, and converted to phosphoglycerate and then PEP, which is carboxylated to oxaloacetate. Oxaloacetate is converted to malate and subsequently to malyl-CoA, which is then cleaved to restore glyoxylate and to produce acetyl-CoA. Acetyl-CoA is converted by enzymes of the EMC pathway to succinyl-CoA and glyoxylate involving two carboxylation steps. Succinyl-CoA is converted by a reaction sequence of the TCA cycle to malate. The TCA cycle is operating during C1 assimilation in an incomplete manner, no flux through 2-oxoglutarate dehydrogenase was detected. The Entner-Doudoroff pathway was found to operate as one pathway for pyruvate synthesis amongst PEP conversion by pyruvate kinase and pyruvate synthesis via malic enzyme. During methanol utilization substrate cycles are active by simultaneous operation of (*i*) PEP carboxylase and PEP carboxykinase, (*ii*) malate thiokinase and malyl-CoA thioesterase, and (*iii*) pyruvate kinase and PEP synthase.

Although it is well understood how *M. extorquens* AM1 accomplishes growth with one carbon compounds such as methanol, there is rather poor knowledge about oxidation and assimilation of two carbon compounds like acetate and oxalate.
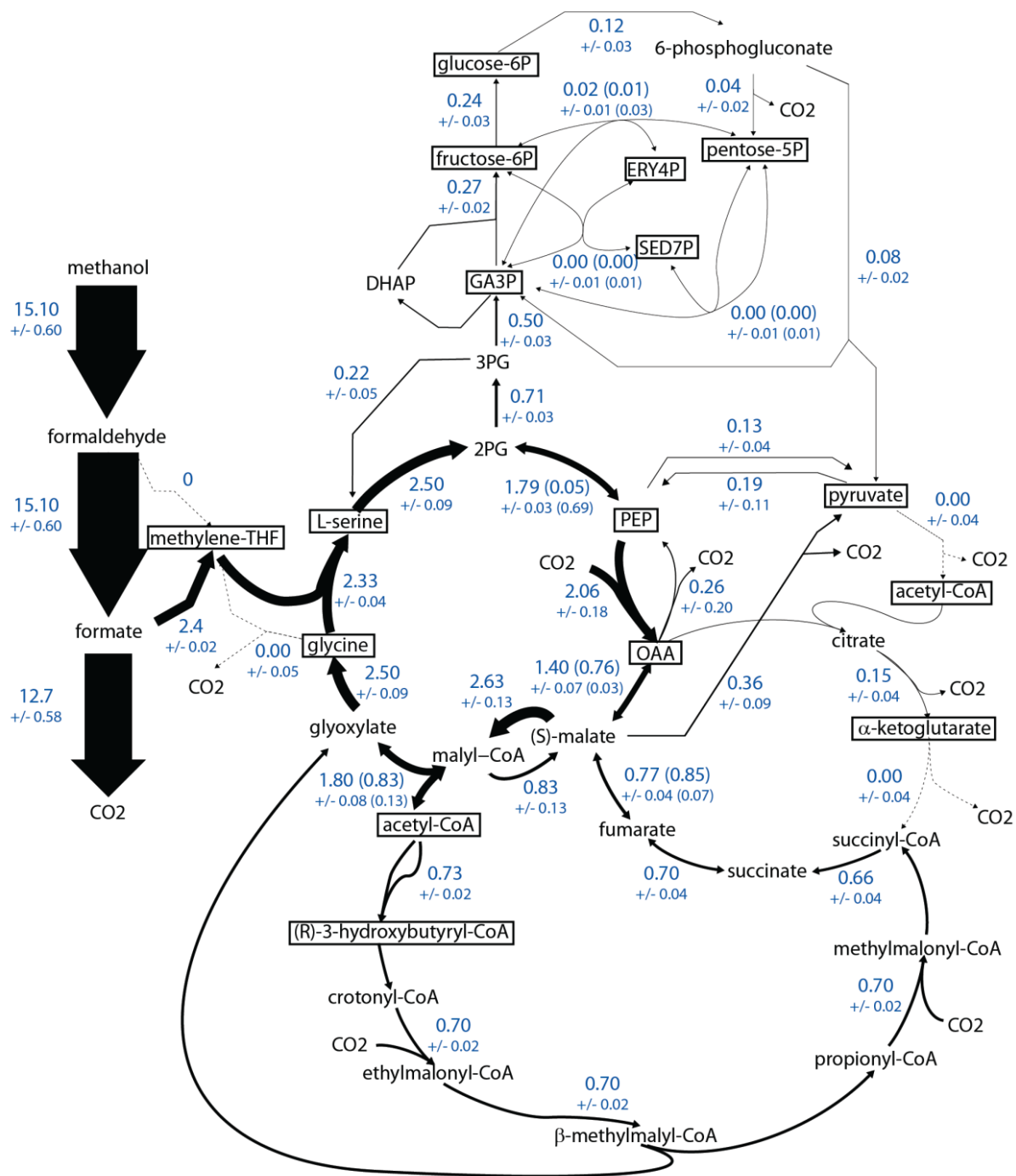
Figure I.3. Distribution of fluxes in the central metabolic network of *M. extorquens* AM1 during growth on methanol. Fluxes are given in mmol · g^{-1} (cell dry weight (CDW)) · h^{-1}, with standard deviations given below flux values. Exchange fluxes through reversible reactions are given within brackets. The width of the arrows is proportional to the flux value (figure was taken from Peyraud *et al.*, 2011).

I. 6 Omics and systems-level approaches

The suffix *-omics*, used to describe modern approaches in systems biology, refers to the totality of some sort. The term 'proteome' involves the set of proteins present in an organism under defined conditions. Different than the genome, the proteome of a cell is subjected to adaptions according to the changes in the environment of the biological system. The study of the cells proteome allows the identification of proteins present under specific growth conditions and gives valuable insight into the cellular condition.

Classical proteomic quantification methods require high-resolution separation by two dimensional gels in connection to dyes, fluorophores, or radioactivity labels. The classical approach has a very good sensitivity, linearity, and dynamic range, but does not reveal protein identity. High time and effort and the missing identification of proteins can be overcome by modern HPLC-MS/MS analysis of proteins and peptides, respectively. However, related to the physicochemical properties of peptides (size, hydrophobicity etc.) a large difference in mass spectrometric response has to be taken into account. Two different approaches are available for peptide quantification: (*i*) stable isotope labeling based on the addition of the labeled peptides as an internal standard, (*ii*) labeled-free quantification by mass spectrometric signal intensity or by the number of acquired spectra matching to a peptide/protein. Labeled-free quantification strategies can be used for comparison of two or more samples by comparing signal intensity or number of acquired spectra. The method comes with the cost of unclear linearity and relatively poor accuracy but is less time-consuming and of lower expenses than stable isotope labeling. Furthermore, mass spectral complexity is not increased with the labeled-free approach, which in turn provides for more analytical depth (i.e. number of detected peptides/proteins in an experiment) because the mass spectrometer is not occupied with fragmenting all forms of the labeled peptides (Bantscheff *et al.*, 2007).

Flux balance analysis is a mathematical approach for analyzing flux through a metabolic network obtained from a network reconstruction containing all known metabolic reactions in a biological system. Flux balance analysis gives one solution of flux distribution calculated based on maximizing or minimizing an objective function under monitored constraints. However, ^{13}C flux analysis gives the actual and quantitative flux distribution in the cell based on the proposed network topology plus the monitored constraints and in addition the experimentally determined ^{13}C-labeling patterns.

Introduction

Flux balance analysis. The metabolic reactions are represented by a stoichiometric matrix (**S**), every row represents one unique compound (**m**) and every column represents one reaction (**n**). **S = m x n.** Flux through all of the reactions is represented by the vector **v**, which has a length of n**.** Flux balance analysis uses linear programming to solve the equation **Sv = 0** considering the metabolism at steady state and stable intracellular metabolite concentrations. There are more unknown variables in genome-scale metabolic models than equations, thus there is no unique solution to this system. Constrains, such as the substrate uptake rate, define the range of solutions. The output of flux balance analysis is a particular flux distribution that maximizes or minimizes the objective function, e.g. growth rate (Orth *et al.*, 2010).

^{13}C flux analysis. Based on mathematical models, ^{13}C flux methods allow determining absolute fluxes through the central network of microbes grown on carbon substrates (Sauer, 2006). The fluxome, which describes the fluxes through the metabolic network topology, allows identifying the connectivity and the functions of pathways. Flux is the time-dependent motion of metabolites through a network. As flux cannot be measured directly it must be inferred from measureable quantities, which is for example substrate uptake and biomass production rate. To quantify pathway activity, additional intracellular information must be obtained from stable isotope tracer experiments. Typically, the cell population is grown with ^{13}C-labeled substrates for several generations until the isotope label is distributed throughout all cell constituents. As a function of the operating metabolic network a specific labeling pattern occurs in the metabolic intermediates and the cell constituents. Those patterns can be analyzed and used to reconstitute the metabolic flux distribution. Generally, ^{13}C-labeling patterns can be obtained by nuclear magnetic resonance (NMR) and mass spectrometry (MS) either from intracellular metabolites or from proteinogenic amino acids. Intracellular metabolites are of low concentration and subjected to high turnover rates, thus they are less suitable for this approach. However, protein is a stable and abundant source of labeling information, and the carbon backbones of the precursor metabolites are conserved in amino acids (Sauer, 2006). Prediction of labeling pattern of precursor metabolites from proteinogenic amino acids is called retro-biosynthetic approach, for example alanine, aspartate and glutamate are conventionally formed by transamination from pyruvate, oxaloacetate and 2-oxoglutarate (Eisenreich *et al.*, 1993). The mathematical evaluation effort is high; a more than 1000-dimensional non-linear equation system must be constructed and solved repeatedly to find the best fitting solution. A software called ^{13}C-FLUX was developed by Wiechert to model, simulate, design and evaluate the ^{13}C flux experiments

(Wiechert, 2001) and since 2012 a new software called influx_s is available (Sokol *et al.*, 2012) with an increased numerical stability and accuracy of flux estimation.

I. 7 Aims of the thesis

The aim of this thesis was to understand the central metabolism of *M. extorquens* AM1 during growth with acetate and oxalate, respectively, as the sole source of carbon and energy. Acetate was used as a model compound for all substrates that enter the central metabolism on the level of acetyl-CoA. Oxalate was of interest as it might be available for the bacterium in its plant-associated habitat.

- The operation of the EMC pathway, which was discovered in *R. sphaeroides* was demonstrated during growth of *M. extorquens* AM1 on methanol, but so far, it was not shown whether the pathway also operates during heterotrophic growth of *M. extorquens* AM1 on acetate, and how it is embedded in the metabolic network. It was one part of this thesis to investigate the role of the EMC pathway during acetate utilization in order to provide a better understanding of this rather long and complicated pathway compared to the glyoxylate cycle. The interest of studying this question in a context of a methylotroph extended to the operation of the TCA cycle upon generation of redox equivalents, and the role of the serine cycle during acetate assimilation, because a number of its intermediates are important branching points for biomass production.

- The second part of this thesis addressed the question, how oxalate is oxidized and assimilated by methylotrophs. Based on the enzymatic equipment of *M. extorquens* AM1 and the former studies of Blackmore and Quayle, two assimilation strategies are possible. Carbon assimilation by oxalate reduction to glyoxylate and conversion into a variant of the serine cycle, or alternatively, in a methylotrophic manner by oxalate conversion to formate and operation of the serine cycle in connection to the EMC pathway. The aim was to identify which of the two assimilation strategies is operating and to find the enzymes present in *M. extorquens* AM1 specific during oxalotrophy.

Chapter 2

EXPERIMENTAL

PROCEDURES

Chapter II   Experimental Procedures

II. 1 Chemicals

[^{13}C] sodium acetate and [^{13}C] sodium oxalate (99%) was purchased from Cambridge Isotope Laboratories. D$_2$O (99.8% and 99.97%) was purchased from Eurisotop; all other chemicals were purchased from Sigma.

II. 2 Medium composition and cultivation conditions

M. extorquens AM1 was grown on minimal medium (Kiefer *et al.*, 2009) supplemented with 5 mM sodium acetate. This substrate concentration was chosen because growth was inhibited by higher acetate concentrations. A preparatory culture was grown on minimal medium plates (1.5% agar); batch cultures were inoculated with cells washed from plates. All cultures were grown in a 500-ml bioreactor (Infors-HT) with a working volume of 400 ml at 28 °C, with an aeration rate of 0.2 l/min and stirring at 1000 rpm. The pH was kept constant at 7.0 by the addition of acetic acid (0.5 M), which allowed for substrate feeding and maintenance of the substrate concentration. Cells were harvested by centrifugation at 6000 x *g* at room temperature and frozen in liquid nitrogen until analysis.

M. extorquens AM1 was grown on minimal medium (Kiefer *et al.*, 2009) supplemented with 20 mM potassium oxalate in shake flasks, or cultures were grown in a 500-ml bioreactor as described above using 5 mM potassium oxalate. The pH of the bioreactor medium was maintained at 7.0 by the addition of oxalic acid (1 M). Cultures pre-grown with succinate in a shake flask were centrifuged ($3000 \times g$, 2 min), and the cell pellets were resuspended in fresh medium containing oxalate and used for inoculation. Alternatively, glycerol stocks from oxalate-grown wild-type cells were used for inoculation. Mutant growth characterization was performed in shake flasks inoculated with a low cell density corresponding to an initial optical density of 0.03 at 600 nm. After an overnight incubation, the optical density was measured every 2 hours.

II. 3 Quantification of acetate, oxalate, and formate

Quantification of acetate, oxalate, and formate was performed with a Waters Alliance 2690 HPLC system and a UV-VIS detector (DAD). Cell cultures were harvested with a 2 ml

plastic syringe and filtered through an RC syringe filter (0.2 µm); tartaric acid (acetate quantification) or succinic acid (oxalate and formate quantification) was added to the cell-free supernatant as an internal standard (500 µl sample and 500 µl internal standard were mixed). The concentration of tartrate and succinate was 10 and 50 mM, respectively, standard concentrations were between 0.5-100 mM acetate and 1-20 mM oxalate and formate. Organic acids were separated using a Phenomenex Rezex ROA-organic acid H+ (8%, 300 x 7.8 mm) column with a flow rate of 0.5 ml/min and detected at a wavelength of 210 nm. An isocratic method was employed as described by the supplier, using 2.5 mM H_2SO_4 as the solvent. Acetate and oxalate were quantified with a 0.3 mM standard deviation based on technical replicates.

In addition, formate identification was confirmed enzymatically using an NAD^+-dependent formate dehydrogenase (Chistoserdova *et al.*, 2007). The oxidation of formate was spectroscopically monitored at 365 nm and 37 °C using 0.5 ml of a reaction mixture containing 200 mM Tris-HCl buffer (pH 7.6), 0.75 mM $NADP^+$, and 2 Units formate dehydrogenase (*Candida boidinii*). The reaction was started by the addition of 100 µl of supernatant.

II. 4 (Macro-) Molecular composition of methanol- and acetate-grown cells

For cell dry weight (CDW) determination, 30 ml of culture were centrifuged in a 50 ml falcon tube and washed with deionized water and dried to constant weight at 80 °C. Falcon tubes were incubated for several days at 80 °C prior to use. For other measurements, cells were harvested by centrifugation at 6000 x *g* during 5 min. Cell pellets were frozen in liquid nitrogen and stored at -20 °C until analysis. Biomass yield (g of [C] per CDW / g of [C] from substrate) was calculated from the biomass production rate and the substrate uptake rate.

Polyhydroxybutyrate (PHB) content. Measurement of the PHB content was performed as described in (Braunegg *et al.*, 1978; Jan *et al.*, 1995) with some modifications. Cell pellets (3-4 mg CDW) were lyophilized and subjected to acid methanolysis with 2 ml 3% H_2SO_4 (v/v) in methanol (containing 0.05 mg/ml benzoic acid as internal standard) and 2 ml chloroform for 2.5 hours at 100 °C. PHB standard concentration was 0.1-2.0 mg/ml chloroform. Methyl-hyroxybutyryl monomers were extracted after addition of 1 ml water (20% v/v) and vigorous mixing. The organic phase was analyzed by gas chromatography - flame ionization detector (GC-FID) (Agilent Technologies 6850 with 7683B Series injector and FID detector) with a DB-WAX column, length 15 m, I.D. 0.32 mm, film 0.5 µm (Agilent

Technologies). Column flow was set to 1.8 ml/min, detector temperature to 270 °C and inlet temperature to 240 °C. A sample volume of 1 µl was injected with a split ratio of two. Temperature gradient was run from 90 °C to 230 °C at 40 °C/min.

Lipid Content. Whole cell hydrolysis with subsequent acid methylation of fatty acids was carried out as described in (Sasser, 1990) with slight modifications. Cells (10-20 mg CDW) were hydrolyzed with 4 ml of 15% NaOH (w/v) in methanol/water (1:1, v/v) for 30 min at 100 °C. Fatty acid methyl esters (FAMEs) were obtained by addition of 8 ml 6 M HCl/methanol (13:11, v/v) and incubation for 2.5 hours at 80 °C. An internal fatty acid standard (3 mg C15:0) was added before hydrolysis for quantification purpose. The methylation yield was measured from the addition of a FAME standard (3 mg C19:0 FAME) after the methylation step. FAMEs were extracted with 5 ml hexane/methyl-tertbutyl ether (1:1, v/v) and washed with 6 ml 1% NaOH in water (w/v). Extracted FAMEs were analyzed by GC-FID and a HP-5 column, length 30 m, I.D. 0.25 mm, film 0.25 µm (Agilent Technologies). Helium was the carrier gas with a column flow of 2.4 ml/min; detector temperature was set to 300 °C, and inlet to 250 °C. A temperature gradient was run from 190 °C to 260 °C at 5 °C per min. A sample volume of 1 µl was injected with a spilt ratio of thirty.

Carbohydrate Content. Carbohydrate content was measured after hydrolysis of the entire cell pellet. A two-step derivatization was used to convert carbohydrates into oxime trimethylsilyl derivates (Kiefer *et al.*, 2002), which were analyzed by GC-FID. For glucose and rhamnose quantification, cells (1-3 mg CDW) were directly subjected to 200 µl 2 M HCl at 80 °C for 4 hours or to 4 M HCl for 16 hours for glucosamine quantification, respectively; carbohydrates were stable under these conditions. After neutralization (pH 6.5-7.5), 50 µl of 25 mM lactose solution was added as an internal standard. Samples were vacuum-dried and derivatized for 40 min with 150 µl 0.5 M hydroxylamine·HCl in pyridine at 80 °C. After addition of 110 µl (trimethylsilyl)trifluoroacetamid (BSTFA), samples were incubated for another 20 min. Separation and quantification of the derivatives were performed by GC-FID as described under lipids except that column flow was set to 2.7 ml/min and temperature gradient was run from 160 °C to 310 °C with 7 °C per min. Peak identity in the GC-FID chromatograms was confirmed by performing GC-MS measurements of the same extracts.

Protein Content. Total proteins were quantified by the Biuret method (Herbert, 1971), using bovine serum albumine (2 mg/ml) as standard. This method is independent of protein composition (Sapan *et al.*, 1999). Cells were hydrolyzed in 0.75 ml 1 M NaOH (1-2 mg/ml

CDW) at 100 °C for 5 min. After addition of 0.25 ml of 2.5% $CuSO_4$ (w/v), samples were centrifuged and absorption was measured at 550 nm.

The composition in amino acids of proteins was analyzed by the Functional Genomics Center Zürich. Following hydrolysis in 6 M HCl at 110 °C for 22 hours under argon samples were dried and derivatized using the AccQ-Tag™ Ultra derivatization chemistry (Waters Corp., Milford, MA, USA) according to the manufacturer's instruction. Amino acid derivatives were separated by UPLC (Waters Corp., Milford, MA, USA) using the AccQ-Tag™ Ultra standard hydrolysate conditions. Amino acid derivatives were detected by UV absorbance.

DNA content. DNA content was calculated from that in *E. coli* (Neidhardt, 1996), using appropriate corrections to account for the size of *M. extorquens* AM1 genome and for its growth rate on methanol.

RNA content. RNA content was determined from the amount of ribose released after acidic hydrolysis (2 M HCl for 2 hours), assuming that all ribose was derived from RNA. The hydrolysis yield was determined from commercial RNA and data were corrected accordingly. Ribose was quantified as described under carbohydrate content.

Polyamine and carotenoid content. Polyamine content was calculated from that in *E. coli* (Neidhardt, 1996). The occurrence of putrescine in methanol-grown *M. extorquens* AM1 cells was also confirmed by GC-MS. Carotenoid data were taken from (Konovalova *et al.*, 2007).

II. 5 Proteome analysis

Cells were resuspended in deionized water supplemented with a protease inhibitor cocktail (Complete, Roche) and passed through a small French press cell 3 times, followed by centrifugation (5 min, 8000 x *g*) to remove cell debris. Proteins were separated by 1D-SDS/PAGE (Criterion Tris-HCl Gel, 10.5-14%, 13.3 x 8.7 cm, Bio-Rad Laboratories) and analyzed after tryptic digestion (trypsin, Promega) by reversed-phase high-performance liquid-chromatography coupled to high-accuracy mass spectrometers as described previously (Delmotte *et al.*, 2009). MS/MS spectra were searched against a database using Mascot (Matrix Science) and X!tandem. A database containing all annotated proteins in the *M. extorquens* AM1 genome was downloaded from the Genoscope website https://www.genoscope.cns.fr/agc/microscope/home/index.php (Vuilleumier *et al.*, 2009). Using a decoy database, the false positive rate was found to be less than 0.01%. To determine

significant changes in protein levels during growth on acetate and oxalate compared with methanol, spectral counts of each protein were normalized to the sum of all spectra detected for each sample. Average values for each substrate were obtained from three biological replicates and were used to calculate fold-changes of normalized spectral counts. To evaluate the statistical significance of observed changes, one-way analysis of variance with log2 transformation was used (Pham *et al.*, 2010). Prior to normalization, zero values were set to one. MS/MS data have been deposited in the PRIDE database (find methanol and acetate samples with accession numbers 17691-17696, and oxalate samples with 17697-17699).

II. 6 Dynamic ^{13}C-labeling experiment

^{13}C-labeling experiments with acetate grown cells were performed as described (Peyraud *et al.*, 2009) with adaptations. Cells were pre-grown on 5 mM acetate at natural ^{13}C abundance. Incubation of cells with labeled acetate was performed in 50 ml Falcon tubes containing 2 ml of minimal medium with 5 mM [U-^{13}C]-acetate. After the addition of 1 ml of culture (0.5 and 0.6 mg CDW) in exponential growth phase, the sample was continuously mixed and incubated for various times. Quenching and metabolite extraction were performed as detailed below. Calculations of ^{13}C-label incorporation were conducted as described (Peyraud *et al.*, 2009); the labeling fractions were normalized to the ratio of acetate with natural ^{13}C abundance from the culture and to ratio of ^{13}C that can be received from uniformly ^{13}C-labeled acetate.

The incubation of cells with labeled oxalate was performed in 50 ml Falcon tubes containing minimal medium with 3.4 mM [U-^{13}C]-oxalate. Cells were pre-grown on 5 mM oxalate at natural ^{13}C abundance. After the addition of exponentially growing culture to fresh medium containing [U-^{13}C]-oxalate (at a final concentration of 0.1 mg CDW/ml), the samples were continuously mixed and incubated for various times. During 10 min, the pH increased from 6.7 to 7.0, but the intracellular metabolite concentrations were stable. The calculation of ^{13}C-label incorporation was conducted as described (Peyraud *et al.*, 2009); the labeling fractions were normalized to the ratio of oxalate with natural ^{13}C abundance from the culture and to the ^{13}C-fraction of oxalate in the medium, which was between 70 and 80%.

II. 7 Sampling, quenching, and metabolite extraction

For the purpose of analyzing label incorporation by mass spectrometry, sampling, quenching and extraction of CoA thioesters were performed as described (Peyraud *et al.*, 2009) with adaptations. Sample volumes of 3 and 5 ml containing 0.5 mg CDW were added to 12 and 20 ml of -20 °C 95% acetonitrile containing 25 mM formic acid. After incubation for 10 min on ice with occasional mixing, samples were frozen in liquid nitrogen and lyophilized.

Sampling of keto acids was performed by fast filtration for salt reduction as described by Bolten *et al.* (Bolten *et al.*, 2007) with some modifications. Cell suspensions of 3 ml (0.6 mg CDW) were harvested by vacuum filtration and washed with 5 ml of phosphate buffer containing a 90% reduced salt concentration. Subsequently, the filter was transferred to a vessel containing boiling water as described (Kiefer *et al.*, 2008) for quenching and metabolite extraction.

The sampling of central metabolites was performed by fast filtration for salt reduction as described by Bolten et al. (Bolten *et al.*, 2007), with some modifications. Cell suspensions of 0.1 mg CDW (sample volume 1 ml) were harvested by vacuum filtration without washing. Subsequently, each filter was transferred to a vessel containing a mixture of acetonitrile (60% (v/v)), methanol (20% (v/v)) and 0.5 M formic acid (20% (v/v)) at -20 °C for quenching and metabolite extraction.

II. 8 HPLC-MS analysis

HPLC-MS analyses of CoA thioesters and keto acids were performed with a Rheos 2200 HPLC system (Flux Instruments, Basel, Switzerland) coupled to an LTQ Orbitrap mass spectrometer (Thermo Fisher Scientific, Waltham, MA, USA) equipped with an electrospray ionization probe. CoA thioester samples were resuspended in 100 µl of ammonium formate buffer (25 mM, pH 3.5). The supernatant collected after centrifugation was analyzed by HPLC-MS as described (Peyraud *et al.*, 2009) with slight modifications. For online desalting, two C_{18} analytical columns (Phenomenex, Torrance, CA, USA) were used. Samples were loaded onto a 50 x 2.0 mm C18 column (3 µm particle size, Gemini Phenomenex, Torrance, CA, USA), and the sample was washed for 5 min with 100% solvent A (50 mM formic acid adjusted to pH 8.1 with NH_4OH). During desalting, the short column was connected to waste via a 6-port-valve, and the 100 x 2.0 mm C18 column (3 µm particle size, Gemini, Phenomenex) was equilibrated with solvent A with an additional pump. After desalting, both

columns were connected in series, and the following methanol gradient was applied to separate CoA thioesters: 5 min, 5%; 15 min, 23%; 25 min, 80%; and 27 min, 80%. The HPLC-MS system was equilibrated for 6 min at initial elution conditions between two successive analyses.

Keto acids were analyzed after derivatization. To this end, samples were resuspended in 100 µl of 30 mM pentafluorobenzyl hydroxylamine (PFBHA) as the derivatization reagent, followed by incubation for 45 min at 45 °C. Subsequently, samples were centrifuged (4 °C, 5 min, 20,000 x g) and analyzed by HPLC-MS. The oximated acids were separated by reversed-phase HPLC after online desalting using the same setup described above for CoA thioesters. Solvent A was 2 mM acetic acid with 4 mM NH_4OH at pH 9.3, and solvent B was methanol. A gradient was applied as follows: after 5 min of online desalting, solvent B was set linearly from 3 to 90 % within 33 min.

Amino acids were analyzed as described (Kiefer *et al.*, 2008) using a pHILIC column.

The analysis of central metabolites was performed using nanoflow ion-pair reverse-phase HPLC coupled with nanospray high-resolution MS as described (Kiefer *et al.*, 2011) with a split-free nano-LC Ultra system connected to an LTQ-Orbitrap mass spectrometer.

II. 9 Sample preparation and NMR analysis

To extract proteinogenic amino acids, cell pellets were resuspended in 20 mM Tris-HCl (pH 7.6) and disrupted by three successive freeze-thaw cycles (submersion in liquid N_2 for 10 s), three passages through a small French press cell, and three rounds of sonication (30 s at 23 kHz). Cell debris was removed by ultracentrifugation, and proteins were precipitated in 70% ethanol (final concentration) and hydrolyzed in 6 M HCl for 12 hours. The amino acids were analyzed by HPCL-MS and after deuteriation, 2D-[^{1}H-^{13}C] HSQC and 2D-ZQF-TOCSY NMR spectra were recorded on a Bruker Avance II 500-MHz spectrometer as described (Massou *et al.*, 2007a; Massou *et al.*, 2007b; Peyraud *et al.*, 2009).

II. 10 Metabolic flux analysis

For the purpose of flux analysis, *M. extorquens* AM1 was grown in the presence of 5 mM ^{13}C-labeled acetate (80% [2-^{13}C] and 20% [U-^{13}C]-acetate), and the culture was aerated with synthetic air containing 5% ^{12}C-carbon dioxide. In total, three independent biological replicates were performed. Cells were inoculated at an optical density of 0.01 at 600 nm and

harvested at optical density one. Labeling of acetate was designed by simulation of label distribution using excel and ^{13}C-FLUX software (Wiechert *et al.*, 2001) to resolve fluxes in the TCA cycle, EMC pathway, serine cycle and C1 metabolism. Flux calculations were performed using the modified reaction network (Peyraud *et al.*, 2009; Peyraud *et al.*, 2011), in which the half-reaction model of the pentose-phosphate pathway (Kleijn *et al.*, 2005) and phosphoacetyl transferase were introduced (see Table SI_1.1). Biosynthetic requirements determined from the quantification of biomass composition were included. Flux distributions were calculated from the positional and mass isotopomers of amino acids obtained by NMR and HPLC-MS (as described above) using the ^{13}C-FLUX software developed by Wiechert (Wiechert *et al.*, 2001). Sensitivity analysis was conducted to establish the confidence interval of the calculated fluxes.

II. 11 Enzyme assays

The activity of oxalyl-CoA reductase [glyoxylate-NADP$^+$ oxidoreductase] was determined using the method of Quayle and Taylor (Quayle & Taylor, 1961). To measure oxalyl-CoA reductase activity in *M. extorquens* AM1, 400-600 mg frozen cells were resuspended in 0.5 ml of 200 mM Tris-HCl (pH 8.6) containing 4 mM dithiothreitol. After the addition of glass beads (0.1 mm in diameter), the cell solution was treated in a tissue lyser (Retsch, Haan, Germany) for 10 min at 30 Hz. Cell debris and glass beads were removed by centrifugation at 4 °C (Schneider *et al.*, 2012). Protein concentration was determined using the bicinchoninic acid (BCA) assay (Thermo Scientific, Illinois, (Smith *et al.*, 1985a)) according to the manufacturer's instructions, using BSA as a standard. The oxidation of glyoxylate was spectroscopically monitored at 365 nm (ε_{NADPH} = 3,400 M^{-1} cm^{-1}). The reaction mixture contained 100 mM Tris-HCl buffer (pH 8.6), 2 mM dithiothreitol, 3 mM CoA, 0.5 mM NADP$^+$, and 0.1-1.5 mg of protein. The reaction was started by the addition of 100 mM glyoxylate to the mixture. Enzyme activity is given in Units which correspond to μmol per minute.

II. 12 Mutant construction

Mutants not published previously were obtained from Elizabeth Skovran. Kanamycin insertion mutations in *panE2, oxs, frc1, frc2,* and *oxc* were constructed using the allelic exchange suicide vector pCM184 and mated into *M. extorquens* AM1 as described previously

(Marx & Lidstrom, 2002). Deletion mutants in the above strains were generated by introduction of the *cre* expression vector pCM157 in each mutant strain followed by plasmid curing and screening for Kanamycin sensitivity as described previously (Marx & Lidstrom, 2002). Mutations were confirmed by diagnostic PCR.

II. 13 Flux balance analysis

The previously described iRP911 genome-scale metabolic model of *M. extorquens* AM1 (Peyraud *et al.*, 2011) with the addition of oxalyl-CoA synthase was used to balance the energetic constraints on metabolism during growth with oxalate as the carbon source (Table SI_2.3). The computations were performed with the CellNetAnalyser (Klamt *et al.*, 2007) and MATLAB (Mathworks, Inc.) programs, as described (Peyraud *et al.*, 2011). The determination of biomass composition is a prerequisite to performing an accurate flux balance analysis. During growth on different carbon sources, the biomass composition of *M. extorquens* AM1 showed only minor changes, with the exception of PHB. PHB constituted <0.5 % of the CDW of oxalate-grown *M. extorquens,* which is a content similar to that of methanol-grown cells (~ 2%); thus, the biomass composition of cells grown on methanol was implemented in the metabolic model for flux calculation.

Chapter 3

RESULTS

Chapter III   Results

III. 1 Acetate metabolism

III. 1.1 (Macro-) Molecular composition of methanol- and acetate- grown cells

It is a prerequisite of metabolic flux analysis and flux balance analysis to implement the demand of precursor metabolites in the underlying metabolic model used for calculation of fluxes. To calculate the demand of those precursor metabolites a detailed analysis of the (macro-) molecular composition is required. Biomass composition of *M. extorquens* AM1 or closely related strains was not available before, thus it was determined using different analytical methods. Generally, cellular macromolecules are built from monomers: amino acids are building blocks of proteins, nucleotides (ribose or deoxyribose and a nucleobase) of RNA and DNA; lipids consist of two fatty acids and a lipid head, and lipopolysaccharides of lipids with an attached polysaccharide. Additionally, *M. extorquens* AM1 contains PHB, a polymer of 3-hydroxybytyrate, as an intracellular carbon-storage compound. To determine the biomass composition of *M. extorquens* AM1 analytical methods were established to quantify proteins, carbohydrates, fatty acids, and PHB in methanol and acetate grown cells. The macro-molecular composition was completed by estimation of the amount of DNA, polyamine, carotenoids, and intracellular metabolites based on literature data (Table III.1). In total 98% of the CDW of methanol-grown and 96% of acetate-grown *M. extorquens* AM1 cells was determined.

Table III.1. Macromolecular composition of *M. extorquens* AM1 cells grown on methanol or acetate.

	Methanol	Acetate	Method or Reference
Total % of CDW	97.7	95.8	
PHB	2.4 ± 0.1	13.2 ± 0.4	GC-FID
Normalized without PHB:			
Protein	62.0 ± 2.2	65.8 ± 1.0	colorimetric assay
Carbohydrate	17.3 ± 1.8	14.0 ± 0.2	GC-FID
Lipid	4.9 ± 2.2	6.4 ± 0.1	GC-FID
RNA	8.6 ± 0.5	6.7 ± 0.4	quantified via ribose
DNA	3.0	3.0	taken from Neidhardt (1996)
Intracell. metabolites	3.5	3.5	taken from Neidhardt (1996)
Polyamines	0.4	0.4	taken from Neidhardt (1996)
Carotenoids	0.01	0.01	taken from Konovalova *et al.* (2007)

Results

Table III.2. Composition of macromolecules in *M. extorquens* AM1 cells grown on methanol or acetate. Macromolecules were normalized to CDW, monomers were normalized to macromolecules.

	Methanol	Acetate		Methanol	Acetate
Protein	**0.591**	**0.544**	**DNA**	**0.030**	**0.030**
alanine	0.132	0.109	dATP	0.150	0.150
arginine	0.064	0.079	dGTP	0.350	0.350
aspartate	0.096	0.056	dTTP	0.150	0.150
cysteine	0.000	0.000	dCTP	0.350	0.350
glutamate	0.120	0.069	**Fatty Acid**	**0.047**	**0.053**
glycine	0.113	0.136	C14:0[?]	0.000	0.000
histidine	0.016	0.023	C16:0	0.025	0.014
isoleucine	0.040	0.046	C16:1	0.047	0.056
leucine	0.076	0.086	C:16:2[?]	0.016	0.015
lysine	0.056	0.034	C17:0	0.032	0.018
methionine	0.012	0.020	C18:0	0.050	0.045
phenylalanine	0.034	0.057	C18:1	0.815	0.830
proline	0.051	0.055	C20:0[?]	0.016	0.014
serine	0.046	0.047	**Lipid Head**		
threonine	0.053	0.054	phosphatidylserine	0.020	0.020
tryptophan	0.000	0.000	phosphatidylglycerol	0.680	0.680
tyrosine	0.021	0.036	phosphatidyl	0.300	0.300
valine	0.070	0.092	**Carbohydrate**	**0.165**	**0.116**
RNA	**0.061**	**0.055**	glucose (incl. trehalose)	0.420	0.407
ATP	0.150	0.150	rhamnose	0.539	0.550
GTP	0.350	0.350	glucosamine	0.041	0.043
UTP	0.150	0.150	**PHB**	**0.024**	**0.132**
CTP	0.350	0.350			

[?] Identity of fatty acids was estimated from retention time but identification by standard FAMEs is missing.

PHB was quantified by GC-FID after acid methanolysis of the entire cell pellet and extraction. PHB content of methanol- and acetate-grown cells was significantly different. While methanol-grown cells contained only 2% of PHB, it was about 13% in acetate-grown cells. As PHB is a carbon-storage compound, which is present in highly variable amounts depending on the growth conditions of the cell (Dawes, 1988; Reddy *et al.*, 2003) all other compounds were normalized without PHB on behalf of a better comparison between methanol and acetate grown cells (Table III.1). The biomass composition as it was used for ^{13}C metabolic flux analysis is presented in Table III.2.

The protein amount, quantified by a colorimetric assay, and amino acids composition, determined by UPLC, was very similar between methanol and acetate grown cells.

Fatty acids were quantified by GC-FID after acid methylation and extraction (Figure III.1). The major fatty acid detected was *cis*-vaccenic acid (C18:1ω7c). To calculate the lipid content the fatty acid amount was corrected for a lipid head (the estimated lipid

composition was 0.75 (w/w) fatty acid and 0.25 (w/w) lipid head). The lipid head composition was taken from Ames (1968) and adapted according to the genome scale metabolic netowork reconstruction (Peyraud *et al.*, 2011), see Table III.2. *M. extorquens* AM1 cells contained 5% of lipids of CDW after growth on methanol and 7% after growth on acetate; no significant changes in fatty acid composition were observed.

Carbohydrates were quantified using GC-FID after hydrolysis of the entire cell pellet and subsequent derivatization (Figure III.2). The following monosaccharaides were detected and quantified: glucose, rhamnose, ribose, and glucosamine. Furthermore, trehalose was detected (around 2% of CDW after 5 min incubation in HCl). Since trehalose is a disaccharide, it was not stable during hydrolysis and thus, glucose was detected. Carbohydrates account for 17% of the CDW after growth on methanol and for 14% of the CDW after acetate-growth; no significant changes in sugar composition were observed. RNA being hydrolyzed in HCl was used to determine RNA content by ribose quantification. Upon RNA hydrolysis three peaks were detected; a ribose peak and two others, one of which co-eluted with rhamnose (Figure III.1D). Thus, the peak area of rhamnose was corrected for the peak area deriving from the RNA compound (however, the substance co-eluting with rhamnose was less than 2 % of the total area of the rhamnose peaks). The amount of RNA quantified was around 9% of the CDW of methanol- and 7% of acetate-grown cells.
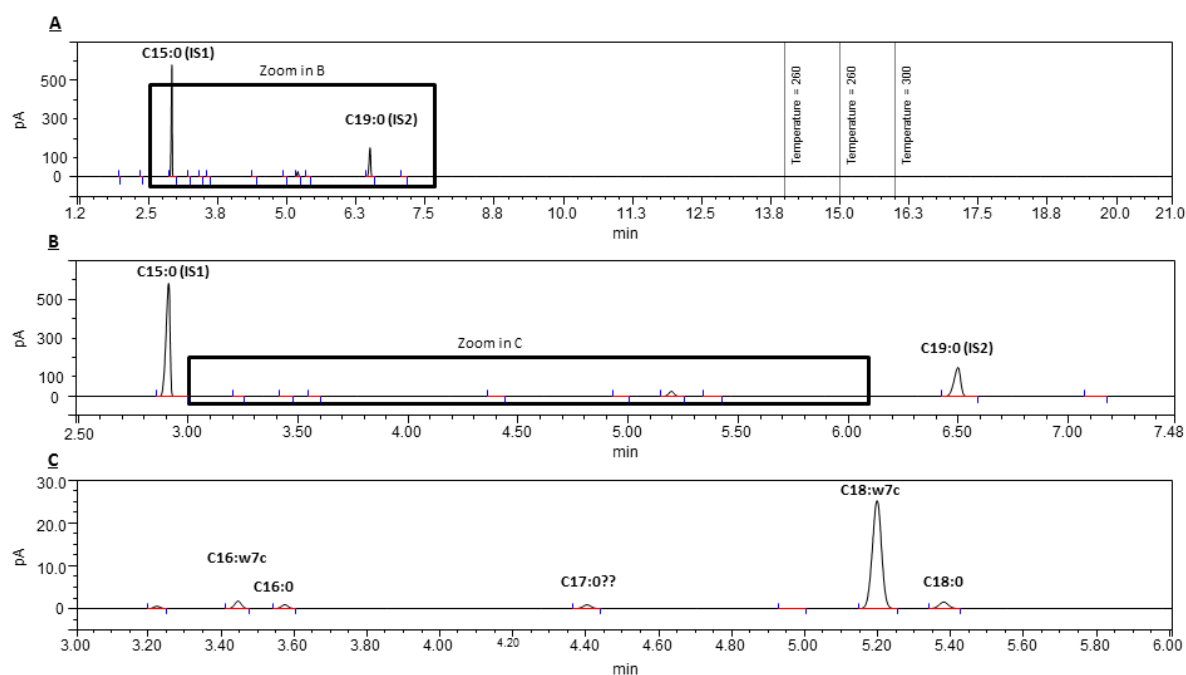
Figure III.1. Fatty acid quantification, GC-FID chromatogram. A-C: hydrolysis of methanol cells. IS: internal standard.
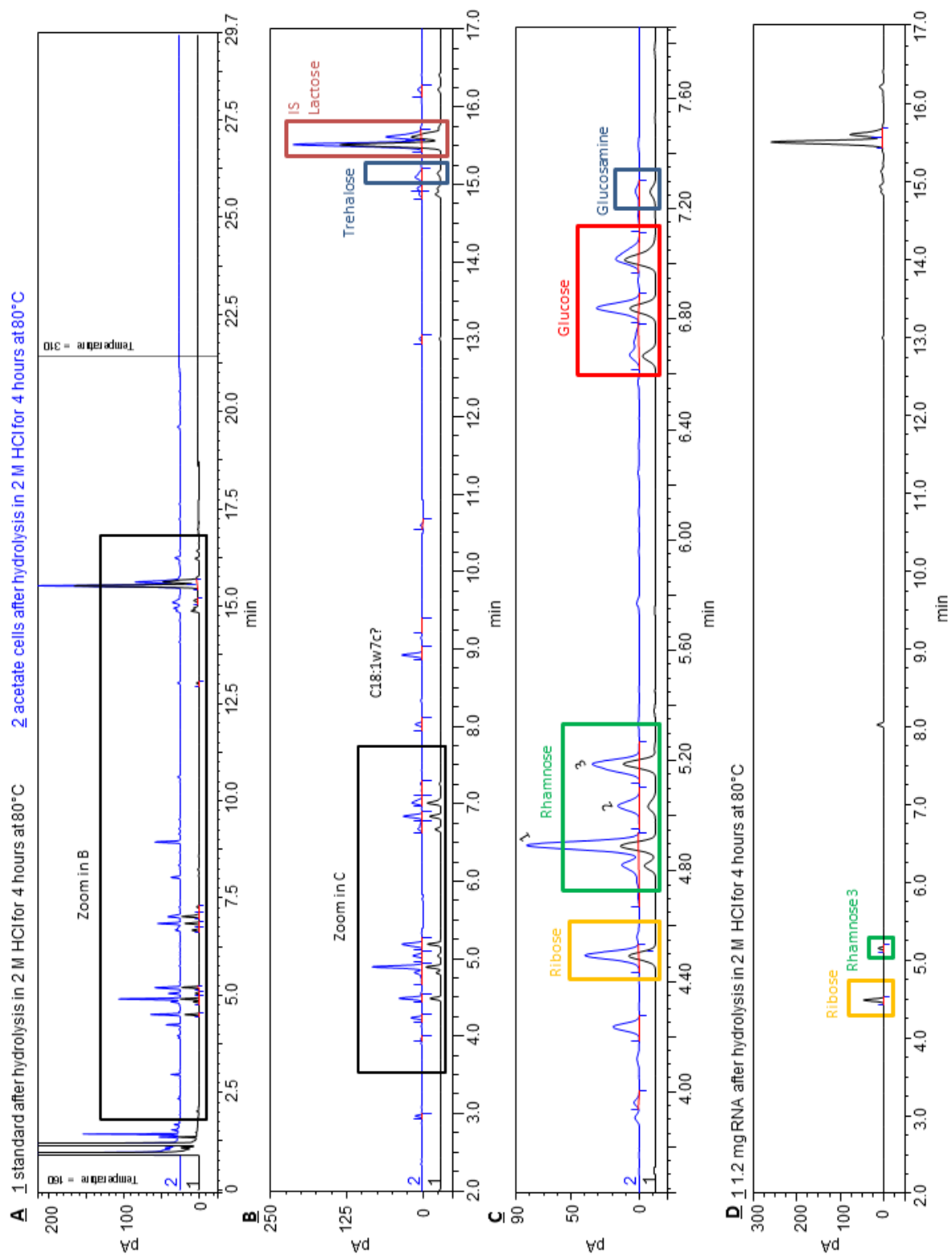
Figure III.2. Carbohydrate quantification, GC-FID chromatogram. A-C: hydrolysis of acetate cells (blue) and carbohydrate standard mix (black) in 2 M HCl for 4 hours at 80°C. D: hydrolysis of RNA as desribed.

III. 1.2 Macrokinetic growth characterization during growth on acetate

M. extorquens AM1 was grown in a bioreactor in the presence of acetate as its sole source of carbon and energy whereby the growth rate decreased with increasing substrate concentration (growth rate on 5 mM acetate was 0.068 h^{-1}, compared with 0.025 h^{-1} on 30 mM acetate, Figure III.3). The biomass yield for *M. extorquens* was 0.37 ± 0.01 (g of [C] per CDW / g of [C] from acetate (grown on 5 mM acetate)). The 1D-^{1}H-NMR analysis of the supernatant revealed no significant accumulation of cultivation products in the medium (limit of detection: 10 µM measured at OD 1). During growth on 5 mM acetate, the specific substrate uptake rate was determined to be 4.0 ± 0.4 mmol·g^{-1} (CDW)·h^{-1}, and the proton production rate was 0.53 ± 0.05 mmol·g^{-1} (CDW)·h^{-1}.
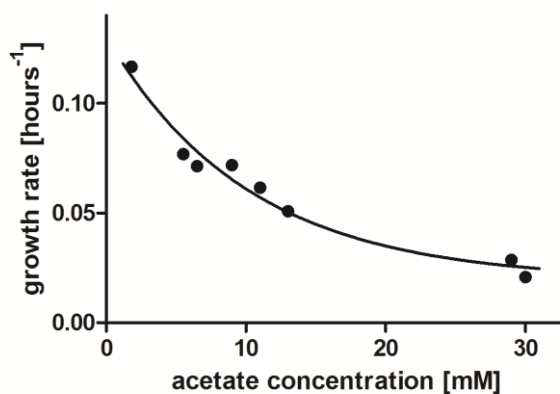
Figure III.3. Growth rate of *M. extorquens* AM1 versus different acetate concentrations determined during growth in a bioreactor.

III. 1.3 Identification of proteins present in cells grown on acetate

To determine the enzymatic framework underlying the metabolic network topology and to reveal proteins specific for growth on acetate, a proteome analysis of *M. extorquens* AM1 grown on acetate was performed. Cultures grown in the presence of methanol were used as the reference because metabolism under methylotrophic conditions is well characterized (Anthony, 1982; Chistoserdova *et al.*, 2003; Peyraud *et al.*, 2009; Peyraud *et al.*, 2011), as is the proteome (Bosch *et al.*, 2008; Laukel *et al.*, 2004). Cell extracts from cells grown on acetate and methanol were loaded onto a 1D-SDS-PAGE and were analyzed by HPLC-MS/MS after tryptic digestion. In total, approximately 2600 proteins were identified (Table SI_1.4). To this end, fold-changes in normalized spectral counts were determined, and statistical significance was tested by one-way analysis of variance. The majority of proteins detected under both growth conditions, i.e., acetate and methanol, did not change, thus indicating an overall consistency in the protein repertoire. Among all proteins with a *p*-value

Results

smaller than 0.05, 53 proteins from cells grown in the presence of acetate showed a fold-change higher than two relative to growth on methanol, and 9 of these exhibited fold-changes higher than five. Fifty-four proteins were less abundant on acetate (fold-change <0.5) compared to methanol, and 9 of these exhibited fold-changes smaller than 0.2. In total, 46 proteins were detected only in samples from cells grown on acetate, and 20 were detected only in samples from cells grown on methanol; however, most of these were of low abundance (detected with less than 0.3 ‰ of total spectral counts). All of these proteins are listed in Table SI_1.5, enzymes of central metabolism and their putative roles are highlighted in Table III.3.

Acetate must first be activated before it can enter central metabolism. Among the proteins specifically detected or enriched during growth in the presence of acetate, an acetate transporter and acetyl-CoA synthetase were found. Because higher expression of acetyl-CoA synthetase (fold-change 2.9) was detected in cells grown on acetate compared with methanol, and acetate kinase and phosphoacetyl-CoA transferase (both less than 0.01‰) were barely detected, acetyl-CoA synthesis by AMP-forming acetyl-CoA synthetase was predicted. Accordingly, a proton-translocating pyrophosphate synthase was found only in acetate-grown cells; this enzyme would allow for the effective conservation of energy by coupling proton pumping across the membrane to the cleavage of pyrophosphate, the product of acetyl-CoA formation via acetyl-CoA synthetase.

All TCA cycle enzymes were detected during growth on acetate; all of these (with the exception of aconitate hydratase and malate dehydrogenase) exhibited a fold-change greater than two relative to methanol-grown cells. The apparent increase in these proteins is consistent with the enhanced operation of the TCA cycle, which one would predict in the case of acetyl-CoA oxidation for energy generation. In principle, oxidation of C1-units to carbon dioxide could be an alternative to catabolic oxidation via the TCA cycle to generate reducing equivalents. In such a scenario, acetate could be converted to glyoxylate and subsequently to glycine, followed by decarboxylation by a glycine cleavage complex to methylene-H_4F, which is oxidized to formate via H_4F intermediates (though this would generate NADPH rather than NADH (Vorholt *et al.*, 1998)) or, indirectly, via H_4MPT intermediates (generating NAD(P)H (Hagemeier *et al.*, 2000)) and subsequent oxidation of formate to carbon dioxide (Chistoserdova *et al.*, 2004). The glycine cleavage complex was more abundant during growth on acetate, whereas it was weakly detected in methanol-grown cells. The operation of the enzyme complex can be expected to contribute to the synthesis of methylene-H_4F from glycine (Okubo *et al.*, 2010). Enzymes involved in one-carbon metabolism linked to H_4F and

H_4MPT were detected in acetate-grown cells. Whereas enzymes dependent on H_4MPT were present at the same order of magnitude in both acetate- and methanol-grown cells, enzymes involved in C1-unit conversion linked to H_4F were less abundant on acetate (fold-change $\approx$ 0.2). Tungsten-containing NAD^+-linked formate dehydrogenase 1 (Laukel *et al.*, 2003) was more abundant (fold change $\approx$ 3) during growth on acetate than on methanol. Otherwise, pyruvate dehydrogenase could contribute to the greater degree of NADH synthesis in cells grown on acetate than on methanol (fold-change $\approx$ 5-11). These alternative pathways may balance NADH/NADPH production, whereas the TCA cycle produces a fixed ratio of NADH to NADPH of 1:1. Membrane-bound $NAD(P)^+$ transhydrogenase was more abundant (fold-change $\approx$ 10) in acetate-grown cells than methanol, indicating that balancing redox equivalents is critical during growth on acetate.

All enzymes of the EMC pathway for acetyl-CoA assimilation and conversion to glyoxylate and succinyl-CoA were present in cells grown with acetate. Most enzymes of the EMC pathway were detected at a similar abundance during growth on acetate relative to methanol, with the exception of mesaconyl-CoA hydratase (fold-change 0.4) and malyl-CoA/β-methylmalyl-CoA lyase (fold-change 0.2). The latter is also part of the serine cycle, for which most proteins were less abundant during growth on acetate, suggesting a minor role for serine cycle enzymes during growth on acetate. All enzymes involved in the phosphoserine pathway (Harder & Quayle, 1971) were detected in both acetate- and methanol-grown cells; only phosphoserine aminotransferase was less abundant during growth on acetate (fold-change 0.4).

The storage compound PHB was increased more than 6-fold during growth on acetate compared to methanol. Accordingly, PHB polymerase and granule-associated 11 kDa protein, which are required for PHB granule formation (Korotkova *et al.*, 2002b), were more abundant in cells grown on acetate.

PEP carboxykinase, which catalyzes the decarboxylation of oxaloacetate into PEP, i.e., operating in reverse compared with the serine cycle PEP carboxylase, was detected in acetate-grown cells. Pyruvate kinase, which is required for the conversion of PEP to pyruvate (Anthony, 1982), was less abundant during growth on acetate than on methanol (fold-change 0.3), whereas pyruvate phosphate dikinase, which catalyzes the conversion of pyruvate to PEP (Anthony, 1982), was more abundant (fold-change 1.8). Pyruvate may be synthesized by malic enzyme, which was more abundant during growth on acetate than on methanol (fold-change 3.5).

Results

Table III.3. Results of proteome analysis from *M. extorquens* AM1 grown on acetate and methanol. Proteins of the central metabolism are listed.

Gene Number[a]	Description (Gene Name)	*p*-Value[b]	Fold-Change[c]
Substrate Uptake and Activation			
2531	acetyl-CoA synthetase (*acs*)	<0.01	2.9
2533	acetate transporter (*actP*)	0.12	1.7
3299	H$^{(+)}$ translocating pyrophosphatase (*hppa*)	<0.01	only on acetate
TCA Cycle			
5129	citrate synthase (*icdB*)	<0.01	3.1
2828	aconitate hydratase (*acnA*)	0.05	1.7
3354	NADP$^+$-dependent isocitrate dehydrogenase (*icd*)	0.01	2.4
1540, 1541, 1542	2-oxoglutarate dehydrogenase (*sucA, sucB, lpd*)	<0.01, 0.02, 0.01	2.7, 3.6, 3.8
1538, 1539	succinyl-CoA hydratase (*sucC, sucD*)	0.01, 0.07	2.0, 1.6
3860, 3861, 3863	succinate dehydrogenase (*sdhD, sdhA/B, sdhB*)	0.05, 0.01, 0.13	2.0, 3.6, 4.1
2857	fumarase (*fumC*)	<0.01	3.4
1537	malate dehydrogenase (*mdh*)	0.02	1.8
C1 Oxidation - H$_4$F/H$_4$MPT Pathway and Formate Dehydrogenase			
1729	H$_4$F pathway: methenyl- H$_4$F cyclohydrolase (*fch*)	0.01	0.2
1728	H$_4$F pathway: methylene- H$_4$F dehydrogenase (*mtdA*)	<0.01	0.2
0329	H$_4$F pathway: formate H$_4$F ligase (*ftfl*)	<0.01	0.3
1766	H$_4$MPT pathway: formaldehyde activating enzyme (fae)	0.01	0.6
1761	H$_4$MPT pathway: methylene-H$_4$MPT dehydrogenase (*mtdB*)	0.63	1.1
1763	H$_4$MPT pathway: methenyl-H$_4$MPT cyclohydrolase (*mch*)	0.20	0.7
1755, 1756, 1757, 1758	H$_4$MPT pathway: formyltransferase/hydrolase (*fhcC, fhcD, fhcA, fhcB*)	0.33, 0.04, 0.44, 0.07	0.8, 0.6, 0.8, 0.7
5031, 5032	NAD$^+$ dependent formate dehydrogenase (W-containing) (*fdh1A, fdh1B*)	0.01, 0.18	2.9, 1.7
4846, 4847, 4848, 4849	formate dehydrogenase (Mo-containing), (*fdh2C, fdh2B, fhd2A,fdh2D*)	0.37, <0.01, <0.01, 0.12	only on methanol
Redox Balance			
2956, 2958	NAD(P)$^+$ transhydrogenase (*pntA, pntB*)	<0.01, 0.85	12.5, 12.3
EMC Pathway			
3700	β-ketothiolase (*phaA*)	0.08	1.6
3701	acetoacetyl-CoA reductase (*phaB*)	0.79	1.0
3675	crotonase (*croR*)	0.85	1.0
0178	crotonyl-CoA carboxylase/reductase (ccr)	0.42	0.9
0839	ethylmalonyl-/methylmalonyl-CoA epimerase (*epi*)	0.82	1.1
0180	ethylmalonyl-CoA mutase (*ecm*)	0.07	0.7
2223	methylsuccinyl-CoA dehydrogenase (*msd*)	0.56	0.9
4153	mesaconyl-CoA hydratase (*mcd*)	0.01	0.4
1733	β-methylmalonyl-CoA/malyl-CoA lyase (*mclA1*)	<0.01	0.2
0172, 3203	propionyl-CoA carboxylase (*pccB, pccA*)	0.79, 0.06	1.1, 0.6
2390, 5251	methylmalonyl-CoA mutase (*mcmB, mcmA*)	0.33, <0.01	0.8, 0.5
2137	malyl-CoA thioesterase (*mcl2*)	0.07	1.3
PHB Metabolism			
3304	PHB polymerase (*phaC*)	0.72	8.2
2218	granule associated 11kDa protein	0.02	2.5
Serine Cycle			
3384	serine hydroxymethyltransferase (*glyA*)	0.03	0.7
1726	serine glyoxylate aminotransferase (*sga*)	<0.01	0.1
1727	hydroxypyruvate reductase (*hpr*)	<0.01	0.2
2944	glycerate kinase (*gck*)	<0.01	0.3
2984	enolase (*eno*)	<0.01	1.4
1732	PEP carboxylase (*ppc*)	<0.01	0.1
1730, 1731	malate thiokinase (*mtkA, mtkB*)	<0.01, <0.01	0.1, 0.1
Glycine Cleavage System and Phosphoserine Pathway			
0620, 0622	glycine cleavage system (*gcv*)	0.94, 0.21	34.7, 14.3
0485	phosphoserine aminotransferase (*serC*)	0.01	0.4
2848	phosphoserine phosphatase (*serB*)	0.35	1.3
0486	phosphoglycerate dehydrogenase (*serA*)	0.38	0.6
C3 Metabolism			
1533	PEP carboxykinase (*pckA*)	<0.01	only on acetate
0594	malic enzyme (*dme*)	<0.01	3.5
2941	pyruvate kinase (*pyk*)	0.01	0.3
3097	pyruvate phosphate dikinase (*ppdK*)	0.02	1.8
2987, 2986, 2989, 2990	pyruvate dehydrogenase (*pdhA, pdhB, pdhC, lpd*)	<0.01, 0.01, <0.01, <0.01	4.5, 5.5, 8.2, 11.2

[a] gene number (META1) reflects the order in the chromosome,
[b] obtained from statistical analysis by one-way ANOVA with log2 transformation,
[c] fold-change of averaged spectral counts acetate versus methanol

III. 1.4 Dynamic ^{13}C-acetate-label incorporation

A central question regarding growth on C2 substrates concerns the involvement of the EMC pathway, which converts acetyl-CoA to glyoxylate and succinyl-CoA. To demonstrate the presence of the enzymes involved (see above), as well as their operation, dynamic ^{13}C-labeling experiments were performed. To this end, fresh medium containing [U-^{13}C]-acetate was mixed with a culture of cells grown on naturally labeled acetate, and ^{13}C incorporation into EMC pathway CoA thioesters was measured by HPLC-MS. In addition, incorporation of the label into the central intermediate 2-oxoglutarate was followed to monitor operation of the TCA cycle. Results are presented in Figure III.4 as percentage of ^{13}C-atoms incorporated into the metabolite, normalized to the maximal number of ^{13}C-carbon atoms that can be incorporated from [U-^{13}C]-acetate according to the network topology.
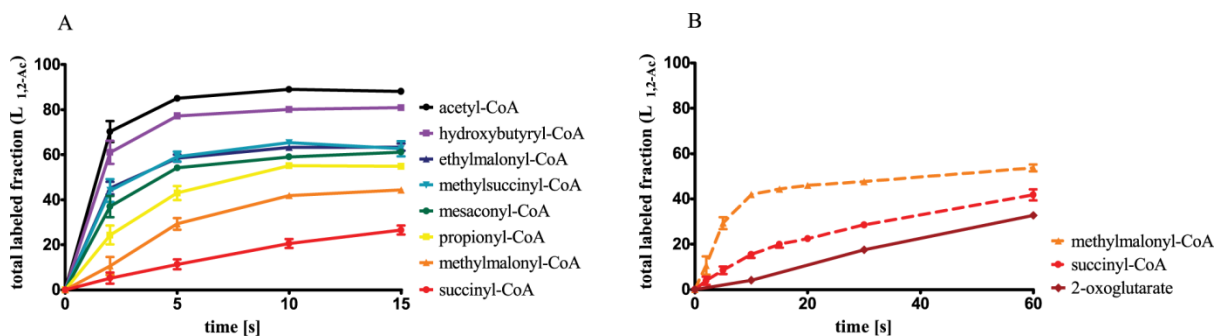
Figure III.4. Incorporation of the ^{13}C label in CoA thioesters (A) and 2-oxoglutarate (B) over time after incubation with [U-^{13}C] acetate. A culture of *M. extorquens* AM1 grown on naturally labeled acetate was mixed with fresh medium containing [U-^{13}C]-acetate, and label incorporation was measured in CoA thioesters and 2-oxoglutarate at different times; the average and standard deviation of three technical replicates are given in the graph. The total labeled fraction represents the percentage of ^{13}C carbon atoms that can be assimilated from [U-^{13}C]-acetate. The total labeled fraction was corrected for CO_2 incorporation for intermediates of the EMC pathway (A).

As expected, acetyl-CoA was the first metabolite in which the label was detected; subsequently, label incorporation into CoA thioesters of the EMC pathway was observed, in the following sequence: hydroxybutyryl-CoA, ethylmalonyl-CoA, methylsuccinyl-CoA, mesaconyl-CoA, propionyl-CoA, and methylmalonyl-CoA. After methylmalonyl-CoA, succinyl-CoA (Figure III.4A) was labeled, followed by 2-oxoglutarate (Figure III.4B). From these results, one can conclude that the EMC pathway represents an entry point for acetate. Labeling of 2-oxoglutarate was also observed, thus implicating TCA cycle activity for acetyl-CoA conversion. The slower increase in labeled succinyl-CoA relative to methylmalonyl-CoA might be indicative of a complete TCA cycle and the formation of succinyl-CoA from

the EMC pathway and TCA. However, exact pool sizes of intermediates or steady-state labeling experiments (see below) are required to confirm this statement.

Approximately 10 s after the addition of ^{13}C-acetate, EMC pathway intermediates reached an apparent isotopic steady state (with the exception of methylmalonyl-CoA and succinyl-CoA). Labeling did not increase further during the next 60 s without reaching enrichment similar to acetyl-CoA, which could be due to the recycling of PHB and/or the permanent hydrolysis and re-esterification of CoA intermediates.

III. 1.5 Steady-state labeling during growth on acetate

To quantify fluxes through the EMC pathway, the TCA cycle and more distant steps relative to the entry of acetyl-CoA, such as the operation of the serine cycle and the phosphoserine pathway and the potential oxidation of glyoxylate, a ^{13}C steady-state labeling experiment and ^{13}C metabolic flux analysis were performed. Isotopomer analysis was conducted by 2D-HSQC and 2D-TOCSY NMR measurement combined with HPLC-MS using the retro-biosynthetic approach and was based on three independent biological replicates. The absolute fluxes were calculated using ^{13}C-FLUX software with consideration of the acetate uptake flux and the biomass exit fluxes determined from substrate uptake, biomass composition, and growth rate. The metabolic network topology including *in vivo* flux values is presented in Figure III.5, and fluxes of the three biological replicates are provided in Table SI_1.2.

Flux calculations revealed that the majority of acetyl-CoA (68%) enters the TCA cycle. Notably, 98% of the acetyl-CoA entering the TCA cycle was found to be completely oxidized to CO_2; thus, the TCA cycle represents the main pathway for the generation of reducing equivalents and operates in an almost purely catabolic mode. Only 2% of acetyl-CoA entering the TCA cycle was oxidized to 2-oxoglutarate as a precursor for biomass synthesis. The second largest conversion of acetyl-CoA occurred via the EMC pathway, which converts acetyl-CoA to glyoxylate and succinyl-CoA (21%); thus, 0.8 mmol·g^{-1}·h^{-1} of CO_2 was assimilated, which corresponds to the recycling of 16% of the completely oxidized acetate. A smaller proportion of acetyl-CoA (5%) was condensed with glyoxylate to generate malate. Three percent of acetyl-CoA was used directly for biosynthesis, and 5% was used for PHB production. Oxidation of glyoxylate via glycine and methylene-H$_4$F to CO_2 could not be detected with a threshold of detection of 1%, similar to pyruvate dehydrogenase (maximum of two percent). Thus, the main pathway to generate redox equivalents upon acetate oxidation is the TCA cycle.
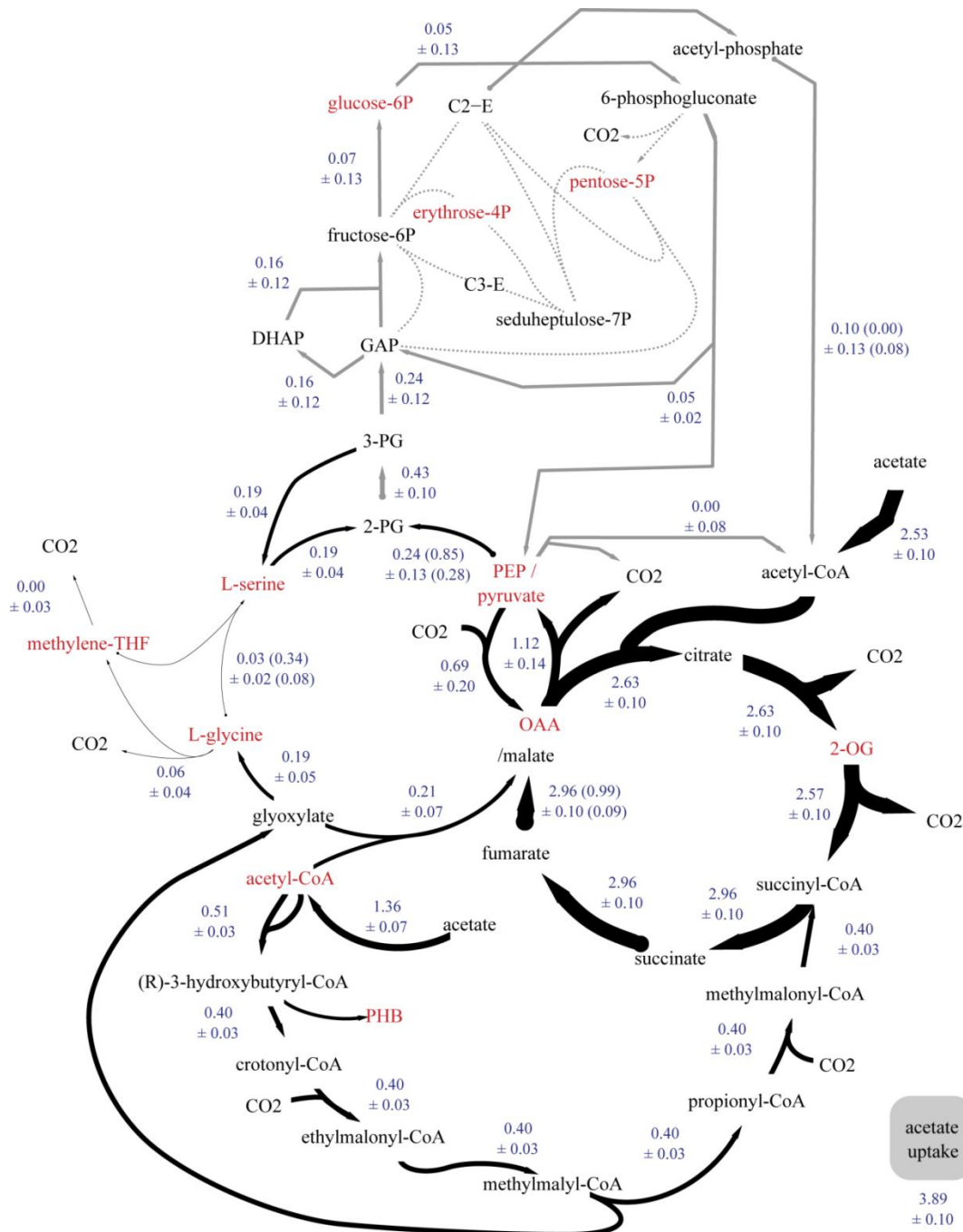
Figure III.5. Metabolic network topology showing the distribution of fluxes in the central metabolism of *M. extorquens* AM1 during growth on acetate. Net fluxes obtained from ^{13}C-labeling experiments are given in mmol·g^{-1} (CDW)·hrs^{-1}, including standard deviation; exchange fluxes are given in brackets. Arrows represent direction of fluxes; biomass exit fluxes are labeled in red. Dotted lines indicate an unidentifiable flux.
OAA: oxaloacetate; 2-OG: 2-oxoglutarate; 2/3-PG: 2/3-phosphoglycerate; DHAP: dihydroxyacetone-phosphate; GAP: glycerinaldehyd-3-phosphate; C2-E/C3-E: C2/C3 fragments bound to holoenzyme.

As mentioned above, acetyl-CoA was condensed with glyoxylate to generate malate; approximately half of the glyoxylate was converted via this route, and the remaining glyoxylate was converted to glycine by serine glycine aminotransferase. Glycine was used for

biomass synthesis (52%), cleaved by the glycine cleavage system to form methylene-H_4F (32%), or condensed with methylene-H_4F (16%) by serine hydroxymethyltransferase to generate serine. No methylene-H_4F was produced by serine hydroxymethyltransferase. Glycine production from glyoxylate by serine glyoxylate aminotransferase requires recycling of hydroxypyruvate, the product of serine deamination; all of the hydroxypyruvate produced was converted to 2-phosphoglycerate by serine cycle enzymes and subsequently to serine via the phosphoserine pathway. The labeling patterns of PEP and pyruvate were identical; both derived from C4 compounds (oxaloacetate/malate). The substrate cycle of PEP carboxylase/PEP carboxykinase described during C1 assimilation (Peyraud *et al.*, 2011) also exists during C2 growth and contributes to a significant loss of energy during growth on acetate (0.69 mmol·g^{-1}·h^{-1} of ATP). No evidence for substrate cycling via malate thiokinase/malyl-CoA thioesterase was observed during growth on acetate, which is in contrast to growth in the presence of methanol.

III. 1.6 Intracellular metabolite pools during high and low acetate concentration

Organisms like *C. glutamicum* and *E. coli* tolerate significantly higher acetate concentrations in the medium and grow faster than *M. extorquens* AM1 with acetate. *C. glutamicum* for example displayed a growth rate of 0.32 h^{-1} on 60 mM and 0.24 h^{-1} on 180 mM acetate but the growth rate of *M. extorquens* AM1 was 0.025 h^{-1} on 30 mM acetate. PHB concentration of *M. extorquens* AM1 cells grown on 30 mM acetate was 16.5 ± 0.1% of CDW and higher than with 5 mM acetate (13.2 ± 0.4) which points to inhibition of carbon assimilation with increasing acetate concentration. The addition of 2 mM methionine to the medium did not relieve growth inhibition of *M. extorquens* AM1 as shown with *E. coli* (see Chapter I. 3). To investigate if growth of *M. extorquens* AM1 is repressed by inhibition of one of the EMC pathway enzymes by the intracellular accumulation of acetate, CoA thioester concentrations were determined during growth on 5 and 30 mM acetate. In case of an enzyme inhibition intracellular pool sizes are expected to increase. However, pool size of the EMC pathway intermediates displayed a lower concentration during growth with 30 mM than with 5 mM acetate (fold change 0.2 - 0.7, 30 mM versus 5 mM acetate, Table III.4). This indicates the EMC pathway enzymes are not inhibited by accumulating acetate and inhibition of biosynthesis occurs in pathways other than the EMC pathway.

Table III.4. Changes of intracellular CoA thioester concentrations during growth on 30 mM acetate versus 5 mM acetate. Cultures of *M. extorquens* AM1 were grown on minimal medium containing 30 and 5 mM acetate as sole carbon source. Samples for CoA thioester quantification were taken during exponential growth; for quantification an internal standard was added.

Intermediate	Ratio (30 mM / 5 mM acetate)
CoA	0.85
acetyl-CoA	0.63
hydroxybutyryl-CoA	0.50
ethylmalonyl-CoA	0.23
methylsuccinyl-CoA	0.33
mesaconyl-CoA	0.34
propionyl-CoA	0.47
methylmalonyl-CoA	0.69
succinyl-CoA	1.04

III. 2 Oxalate metabolism

III. 2.1 Macrokinetic growth characterization during oxalate assimilation

M. extorquens AM1 exhibited a doubling time of six hours when grown on 5 mM potassium oxalate in a bioreactor (see also Table III.5), which is slower than that observed on methanol (4 hours (Peyraud *et al.*, 2011)) but significantly increased compared to the doubling time on acetate (10 hours, see Chapter III 1.2.). The biomass yield was 0.07 ± 0.01 (g of [C] per CDW / g of [C] from oxalate), which is six times less than that from acetate. The oxalate uptake rate was determined as 34 ± 4 mmol $\cdot$ g^{1} (CDW) $\cdot$ h^{-1} from three independent cultivations in the bioreactor. There was not the same inhibitory effect of high oxalate concentrations like observed than with high acetate concentrations.

III. 2.2 Identification of proteins present during oxalotrophic growth

To identify the enzymatic make-up of oxalate-grown cells and to find proteins that are enriched during oxalotrophic growth, a label-free semi-quantitative proteome analysis was performed. As a reference, the previously characterized proteomes during growth on methanol and acetate (Chapter III. 1.3) were used. The majority of the proteins (a total of approximately 2800, Table SI_2.2) were detected in cells grown on oxalate, methanol and acetate. The six most abundant proteins detected only in oxalate samples were the following (Figure III.6): (1) oxalyl-CoA decarboxylase (*oxc;* META1_0990), (2 and 3) formyl-CoA transferase (*frc1* and *frc2;* META1_0988 and 0999, respectively), and (4, 5, and 6) oxalate formate antiporter (*oxlT;* META1_1925, 0993, and 0992, respectively). The protein annotated as oxalyl-CoA decarboxylase has an amino acid sequence identity of 62% to

Results

oxalyl-CoA decarboxylase of *O. formigenes* (Baetz & Allison, 1989; Lung *et al.*, 1994) and catalyzes oxalyl-CoA decarboxylation to formyl-CoA. Two paralogous formyl-CoA transferases were detected with sequence identities of 62% (Frc1) and 56% (Frc2) to the homologue of *O. formigenes* (Sidhu *et al.*, 1997). In *O. formigenes,* substrate uptake is accomplished by an oxalate/formate antiporter (OxlT) (Fu *et al.*, 2001); three proteins with approximately 35% sequence identity were found in oxalate-grown *M. extorquens* AM1 cells.
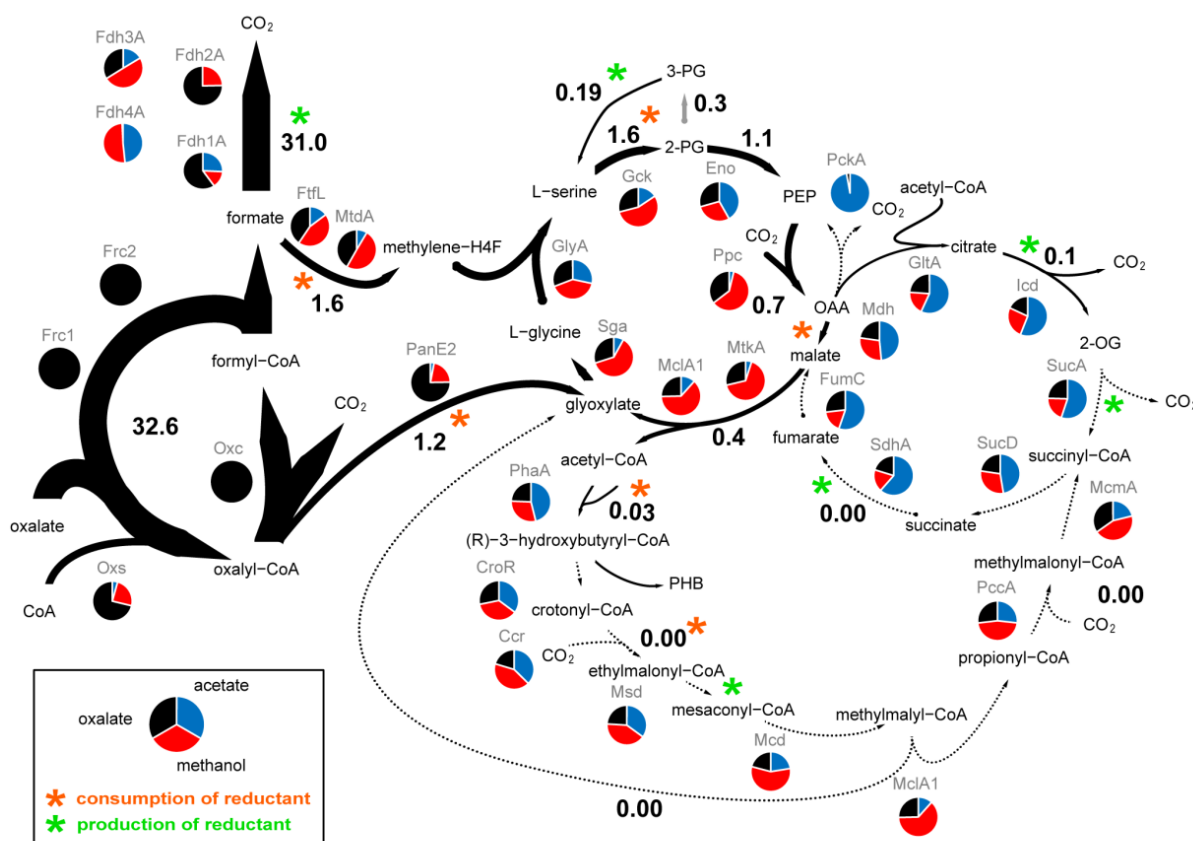
Figure III.6: Proposed network topology of the central metabolism operating during growth of *M. extorquens* AM1 on oxalate based on proteome data including flux values calculated using flux balance analysis. Theoretical flux distribution was calculated for a constrained oxalate uptake rate of 33.8 mmol · g^{-1} (CDW) · h^{-1} and a growth rate of 0.11 h^{-1}; fluxes are given in mmol · g^{-1} (CDW) · h^{-1}. Results of comparative proteome analysis are graphically included; red: methanol, blue: acetate, black: oxalate samples. Average spectral counts are represented relative of total number of spectra from the three different sample sets. Consumption (orange) and production (red) of reductant is indicated by asterisk. For a better overview not all intermediates and enzymes are shown, all enzymes of the central metabolism are listed in the supplement Table 2.

Abbreviations used for metabolites: PG: phosphoglycerate, PEP: phosphoenolpyruvate, 2-OG: 2-oxoglutarate, OAA: oxaloacetate, H$_4$F: tetrahydrofolate
Abbreviations used for proteins: (Fdh1a) (Fdh2a), (Fdh3a), (Fdh4a): formate dehydrogenase, (Frc1), (Frc2): fromyl-CoA transferase, (Oxc): oxalyl-CoA decarboxylase, (PanE2): oxalyl-CoA reductase, (Oxs): oxalyl-CoA synthetase, (FtfL): formate-H4F ligase, (MtdA): methylene-H$_4$F dehydrogenase, (Gck): glycerate kinase, (Eno): enolase, (Ppc): PEP carboxylase, (MtkA) malate thiokinase, (MclA1): malyl-CoA/β-methylmalyl-CoA lyase, (Sga): serine glyoxylate aminotransferase, (GlyA): serine hydroxymethyltransferase, (PhaA): β-ketothiolase, (CroR): crotonase, (Ccr): crotonyl-CoA carboxylase/reductase, (Msd): methylsuccinyl-CoA dehydrogenase, (Mcd): mesaconyl-CoA hydratase, (PccA): propionyl-CoA carboxylase, (McmA): methylmalonyl-CoA mutase, (GltA): citrate synthase, (Icd): isocitrate dehydrogenase, (SucA): 2-oxoglutarate dehydrogenase, (SucD): succinyl-CoA synthetase, (SdhA): succinate dehydrogenase, (FumC): fumarase, (Mdh): malate dehydrogenase.

Based on the protein identifications, it was predicted that oxalate uptake in *M. extorquens* AM1 is enabled by an oxalate/formate antiporter. The import of the two-fold negatively charged oxalate by simultaneous export of the monoanion formate contributes to an electrochemical and proton gradient across the membrane that then may be coupled to ATP synthesis (Svedruzic *et al.*, 2005). Oxalate is converted by formyl-CoA transferase and oxalyl-CoA decarboxylase to formate, which than can be oxidized to carbon dioxide by formate dehydrogenase. *M. extorquens* AM1 was previously reported to contain four different formate dehydrogenases (Fdh) (Chistoserdova *et al.*, 2007). Fdh1 is tungsten containing, NAD^+-dependent and located in the cytoplasm (Laukel *et al.*, 2003). Fdh2 activity is also dependent on NAD^+, but molybdenum containing; the two enzymes are known to be functionally equivalent (Chistoserdova *et al.*, 2004). Fdh3 is predicted to contain a TAT pathway signal, is probably located in the periplasm and uses a cytochrome as an electron acceptor. Little is known about Fdh4; *in vivo* activity of the enzyme has only been demonstrated after the inactivation of Fdh1/2/3. However, the electron acceptor remains unknown (Chistoserdova *et al.*, 2007). Cells grown on oxalate displayed an approximately four-fold higher abundance (based on normalized spectral counts) of Fdh1 and Fdh2 than methanol-grown cells (Figure III.6). Based on these data, it was proposed that the oxidation of formate to carbon dioxide proceeds with the formation of NADH in the cytoplasm. Therefore, formate must be transferred back into the cell, similarly to the process during growth on formate, by either passive diffusion or an unknown formate transporter. $NAD(P)^+$ transhydrogenase (Pnt) was approximately 10-fold more abundant in cells grown on oxalate than those grown on methanol and may thus contribute to the conversion of NADH into NADPH. Similarly to cells grown on methanol, all enzymes of the TCA cycle were detected in oxalate-grown cells but only at low abundances (Figure III.6). Thus, it was predicted that the TCA cycle is not involved in oxidative processes and operates in an incomplete and purely anabolic manner.

III. 2.3 Detection of specific metabolites present during oxalotrophic growth

The above described identification of oxalyl-CoA decarboxylase and formyl-CoA transferase in oxalate-grown cells rather than during growth on methanol or acetate suggests that their substrates and/or products are present in oxalate-grown cells. To verify the presence of these metabolites during oxalotrophic growth, CoA thioesters from *M. extorquens* AM1 grown in the bioreactor were analyzed. After metabolite extraction and analysis using HPLC-

Results

MS, oxalyl-CoA and formyl-CoA was identified in cells grown with oxalate as the carbon source (Figure III.7) but not in the previously characterized methanol- and acetate-grown cells. To validate the conversion of oxalate through oxalyl-CoA and formyl-CoA, the incorporation of [U-^{13}C]-oxalate was monitored. Only three seconds after the addition of labeled oxalate, a mass shift of plus two in oxalyl-CoA and of plus one in formyl-CoA was detected. The labeled fraction of oxalyl-CoA was 0.8 after three seconds and 1.0 after one minute. However, the labeled fraction of formyl-CoA was 0.6 after 3 seconds and 0.8 after one minute; no further increase of labeling in formyl-CoA was observed over 10 more minutes. This apparent equilibrium may be related to the reversibility of formyl-CoA transferase and the pool of unlabeled intra- and extracellular formate.
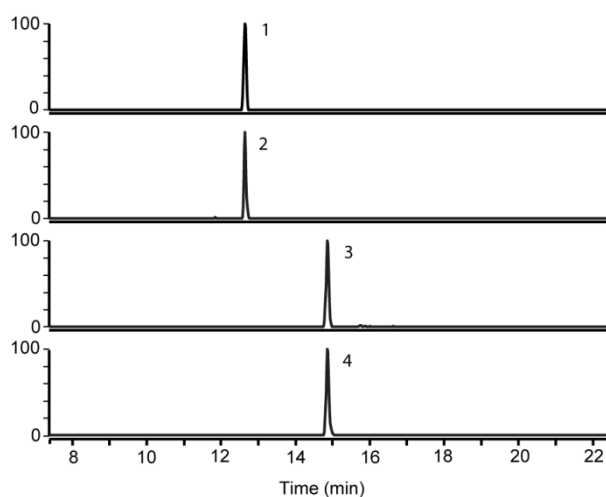
Figure III.7. LC-MS analysis of CoA thioesters in cell extracts of *M. extorquens* AM1 during growth on natural labeled oxalate and after incubation with [U-^{13}C]-oxalate.
1, oxalyl-CoA (M0); 2, oxalyl-CoA (M+2); 3, formyl-CoA (M0); 4, formyl-CoA (M+1).

III. 2.4 Growth characterization of mutants involved in oxalate oxidation

To study the role and function of the formyl-CoA transferase, knockout mutants were generated for the paralogues (*frc1* and *frc2*) and for oxalyl-CoA decarboxylase (*oxc*). Growth characterization of these mutants in the presence of oxalate as the sole source of carbon and energy was performed in shake flasks (Table III.5), and succinate was used as a control. All the strains grew normally with succinate, but the Δ*oxc* and Δ*frc1* mutants were unable to grow with oxalate as the sole carbon source; only the Δ*frc2* mutant grew similarly to the wild-type strain on oxalate. To investigate the oxidation of formate and to identify which formate dehydrogenase catalyzes the reaction, various mutant strains were tested (Δ*fdh1/2*,

Δ*fhd3*, Δ*fdh1/2/3*, Δ*fdh4* and Δ*fdh1/2/3/4*). With the exception of the triple and quadruple mutants, all of these strains were able to grow on formate (Chistoserdova *et al.*, 2004; Chistoserdova *et al.*, 2007). Whereas the single mutants (Δ*fhd3* and Δ*fdh4*) grew in the presence of oxalate, the double mutant (Δ*fhd1/2*) displayed a severe growth defect and grew only slowly on oxalate. Oxalate concentration in the supernatant of Δ*fhd1/2* mutant decreased over time, and formate secretion was detected in parallel (at a level of approximately 1 mM after 24 hours). The triple mutant Δ*fhd1/2/3*, like the quadruple mutant Δ*fdh1/2/3/4*, was unable to grow on oxalate; however, a minor decrease in oxalate concentration (approximately 1-2 mM within 24 hours) was observed with a concomitant formate buildup (1-2 mM) in the triple mutant, which was not observed in Δ*fhd1/2/3/4*. These results demonstrate that oxalate decarboxylation to formate by oxalyl-CoA decarboxylase and formyl-CoA transferase and its subsequent oxidation by formate dehydrogenase are crucial steps in generation of reductant.

Table III.5: Growth rate, oxalate uptake rate, and yield of *M. extorquens* AM1 wild-type and mutants grown on oxalate. Cultivations were carried out in either shake flasks, or in a bioreactor (wild-type, Δ*oxs*/Δ*panE2*, Δ*ccr*, Δ*pccA*) for determination of growth rate and oxalate uptake rate. All cultivations were carried out in three independent replicates.

Name	Gene Inactivated	Growth[a]	Uptake[b]	Yield[c]	Reference
wild-type		**0.106 ± 0.005**	**33.8 ± 4.4**	**0.070 ± 0.6**	
formyl-CoA transferase 1	Δ*frc1*	-	(+)	n.d.	this study
formyl-CoA transferase 2	Δ*frc2*	++	++	n.d.	this study
oxalyl-CoA decarboxylase	Δ*oxc*	-	-	n.d.	this study
formate dehydrogenase 3	Δ*fdh3*	++	++	n.d.	1
formate dehydrogenase 4	Δ*fdh4*	++	++	n.d.	1
formate dehydrogenase 1 and 2	Δ*fdh1/2*	(+)	+[ex]	n.d.	1
formate dehydrogenase 1, 2 and 3	Δ*fdh1/2/3*	-	(+)[ex]	n.d.	1
formate dehydrogenase 1, 2, 3 and 4	Δ*fdh1/2/3/4*	-	-	n.d.	2
oxalyl-CoA reductase	Δ*panE2*	-	-	n.d.	3
oxalyl-CoA synthase	Δ*oxs*	++	++	n.d.	3
oxalyl-CoA synthase and oxalyl-CoA reductase	**Δ*oxs*/Δ*panE2***	**0.089 ± 0.001**	**28.4 ± 1.5**	**0.069 ± 0.4**	**3**
glycerate kinase	Δ*gck*	-	-	n.d.	4
PEP carboxylase	Δ*ppc*	+	++	n.d.	5
malate thiokinase	Δ*mtkA*	++	++	n.d.	6
crotonyl-CoA carboxylase/reductase	**Δ*ccr***	**0.117 ± 0.007**	**37.6 ± 0.6**	**0.071 ± 0.1**	**7**
ethylmalonyl-CoA/methylmalonyl-CoA epimerase	Δ*epm*	++	++	n.d.	8
ethylmalonyl-CoA mutase	Δ*ecm*	++	++	n.d.	9
methylsuccinyl-CoA dehydrogenase	Δ*msd*	+	+	n.d.	8
mesaconyl-CoA hydratase	Δ*mcd*	-	-	n.d.	10
malyl-CoA/β-methylmalyl-CoA lyase 1 and 2	Δ*mclA1/2*	-	-	n.d.	11
propionyl-CoA carboxylase	Δ*pccA*	(+)*	(+)*	n.d.	8
methylmalonyl-CoA mutase	Δ*mcmA*	-	(+)	n.d.	8

[a] growth rate in h^{-1}; ++ growth like wildtype, +/(+) slower than wild-type /almost no growth, - no growth; * growth-rate increased during cultivation
[b] oxalate uptake rate in mmol · g^{-1} (CDW) · h^{-1}; ++ uptake rate like wild-type, +/(+) slower /almost no oxalate uptake, - no oxalate utilization detected; [ex] formate secretion
[c] yield in g of [C] per CDW / g of [C] from oxalate

References:
1 (Chistoserdova *et al.*, 2004), 2 (Chistoserdova *et al.*, 2007), 3 (Skovran), 4 (Chistoserdova & Lidstrom, 1997), 5 (Arps *et al.*, 1993), 6 (Chistoserdova & Lidstrom, 1994), 7 (Chistoserdova & Lidstrom, 1996), 8 (Korotkova *et al.*, 2002a), 9 (Smith *et al.*, 1996), 10 (Korotkova *et al.*, 2005), 11 (Okubo *et al.*, 2010)

Results

III. 2.5 Oxalate conversion to glyoxylate

The next aim was the identification of proteins involved in the assimilation of oxalate. As mentioned above, glyoxylate carboligase is a common enzyme among the oxalotrophic bacteria (Cornick & Allison, 1996a; Quayle *et al.*, 1961; Sahin, 2003) characterized thus far (Chang *et al.*, 1993) that initiates the assimilation of the C2 substrate into biomass in these organisms. However, based on activity measurements of cell-free extracts (Blackmore & Quayle, 1970) and the complete genome sequence of the methylotroph (Vuilleumier *et al.*, 2009), glyoxylate carboligase is absent in *M. extorquens* AM1. In 1970, Blackmore and Quayle detected oxalyl-CoA reductase activity in cell extracts and proposed that oxalyl-CoA reductase operates in conjunction with serine cycle enzymes during oxalotrophy (Blackmore & Quayle, 1970). To confirm the activity of oxalyl-CoA reductase, the enzyme activity was quantified based on the reverse reaction, i.e., glyoxylate oxidation (Blackmore & Quayle, 1970), in cell-free extracts from oxalate-, methanol- and acetate-grown *M. extorquens* AM1 cells. The activities were 0.54 ± 0.06 Units/mg of protein in cells grown with oxalate as the carbon source and 0.07 ± 0.02 and 0.02 ± 0.01 Units/mg of protein in the methanol- and acetate-grown cells, respectively. Based on these different activities, the proteome was searched for a reductase with the highest abundance in oxalate-grown cells relative to cells grown in the presence of methanol and acetate. One protein annotated as a putative ketopantoate reductase (*panE2*) met the requirements. This protein was 3-fold more abundant on oxalate than on methanol and 25-fold more abundant on oxalate than on acetate (Figure III.6). Furthermore, the protein levels correlated with the enzyme activities measured in cell-free extracts; the activity of an oxalate-grown cell extract was eight times higher than an extract of methanol-grown cells and 27 times higher than an extract of an acetate-grown culture. A Δ*panE2* mutant indeed confirmed this finding and led to the identification of oxalyl-CoA reductase (Skovran). Furthermore, a neighboring gene annotated as a putative acyl-CoA synthetase was identified as oxalyl-CoA synthetase (*oxs*) (Skovran). Additionally, oxalyl-CoA synthetase was found to be more abundant in oxalate-grown cells compared with those grown on methanol or acetate. These enzymes allow glyoxylate generation directly from oxalate conversion to oxalyl-CoA and its reduction. Inactivation of oxalyl-CoA reductase (Δ*panE2*) resulted in the inability of *M. extorquens* AM1 to grow on oxalate, whereas a mutant of oxalyl-CoA synthetase (Δ*oxs*) grew normally on oxalate. Notably, however, a double mutant of oxalyl-CoA synthetase and oxalyl-CoA reductase (Δ*oxs*/Δ*panE2*) grew in the bioreactor, albeit at a growth rate reduced by 15% in comparison

with the wild-type strain (Table III.5). These results suggest that the lack of growth of the Δ*panE2* mutant is due to toxicity effects rather than implying that oxalyl-CoA reductase activity is essential. Thus, one can concluded that an alternative entry into central metabolism must exist, as described below.

III. 2.6 Metabolic network topology during oxalate utilization

As mentioned above, oxalyl-CoA synthetase and oxalyl-CoA reductase may operate in conjunction with the serine cycle (Blackmore & Quayle, 1970). All serine cycle enzymes, i.e., serine hydroxymethyltransferase, serine glyoxylate aminotransferase, hydroxypyruvate reductase, glycerate kinase, enolase, phosphoenolpyruvate carboxylase, malyl-CoA/β-methylmalyl-CoA lyase, and malate thiokinase, were detected in the proteome of *M. extorquens* AM1, displaying approximately half their intensity during growth on oxalate relative to the levels on methanol (Figure III.6). Uniquely, the serine cycle enolase was equally as abundant as on methanol. Additionally, all the enzymes of the H_4F-dependent pathway were detected, which are required for formate assimilation, showing fold-changes of between 0.5 and 1 relative to the methanol samples. These findings are in accordance with the assimilation route proposed by Blackmore and Quayle (Blackmore & Quayle, 1970), wherein C3-unit synthesis from C1-units plus glyoxylate and carboxylation to C4 is feasible based on the presence of C1 assimilation and serine cycle enzymes (Figure III.8A). Malate thiokinase and malyl-CoA lyase may be involved in acetyl-CoA and glyoxylate production. However, the entire set of EMC pathway enzymes was also detected in oxalate-grown cells, with fold-changes of between 0.5 and 0.9 for the oxalate versus the methanol- and acetate-grown cells. The latter pathway may thus represent a second potential route for glyoxylate generation by the conversion of acetyl-CoA via the EMC pathway and may explain the above-mentioned phenotype of the Δ*oxs*/Δ*panE2* double mutant, which grows in the presence of oxalate (Figure III.8B).

A number of mutants were used to identify the enzymes required during oxalotrophic growth. Among the mutants of serine cycle enzymes, glycerate kinase, PEP carboxylase and malate thiokinase mutant were tested (Table III.5). A mutant with a defect in glycerate kinase did not grow on oxalate, and thus, no alternative for C3-unit synthesis exists, similarly to what has been reported for methylotrophic growth (Chistoserdova & Lidstrom, 1997). A mutant deficient in PEP carboxylase, which is indispensable during growth on methanol (Arps *et al.*, 1993), exhibited a reduced growth rate on oxalate, suggesting that an alternative

Results

route for the synthesis of C4-units must exist and is sufficient to allow growth on oxalate, e.g., the condensation of glyoxylate with acetyl-CoA. A malate thiokinase mutant unable to grow on methanol (Chistoserdova & Lidstrom, 1994) grew normally on oxalate, which indicates that malate cleavage is not required for glyoxylate and acetyl-CoA generation during oxalate assimilation. However, an alternative pathway for acetyl-CoA synthesis in the mutant must exist, possibly consisting of pyruvate decarboxylation.
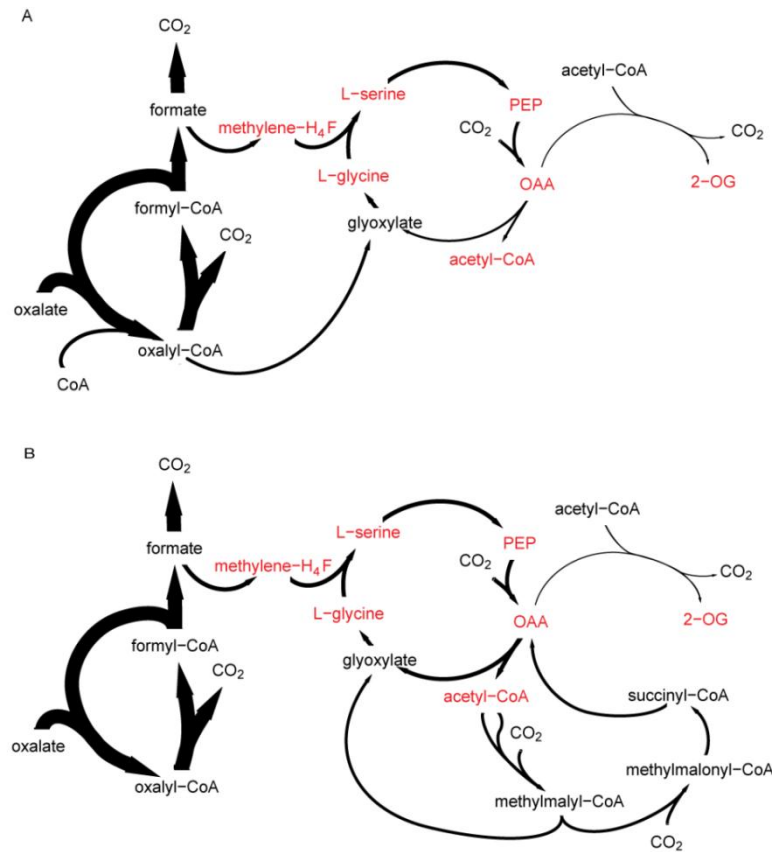
Figure III.8: Schematic view of the two different oxalate assimilation stategies. (A) Oxalate assimilation by a variant of the serine cycle including operation of oxalyl-CoA synthetase and oxalyl-CoA reductase. (B) Oxalate assimilation via C1-units by the serine cycle and EMC pathway, without oxalyl-CoA synthetase and oxalyl-CoA reductase. Precursor metabolites are labeled in red, for abbreviations see Figure 1.

In addition to the serine cycle enzymes, mutants with defects in the EMC pathway were tested. The pathway is required during C1 and C2 assimilation for the conversion of acetyl-CoA to glyoxylate (Chistoserdova & Lidstrom, 1996; Korotkova & Lidstrom, 2001; Korotkova *et al.*, 2002a). Mutant strains lacking either the key enzyme of the pathway, crotonyl-CoA carboxylase/reductase (Chistoserdova & Lidstrom, 1996), or ethylmalonyl-CoA/methylmalonyl-CoA epimerase or ethylmalonyl-CoA mutase grew with oxalate as the

carbon source in a similar manner to the wild-type (Table III.5). This observation indicates that the EMC pathway is dispensable during oxalotrophy. Remarkably, however, the inactivation of enzymes catalyzing reactions downstream of irreversible methylsuccinyl-CoA dehydrogenase, i.e., mesaconyl-CoA hydratase, malyl-CoA/β-methylmalyl-CoA, propionyl-CoA carboxylase and methylmalonyl-CoA mutase showed severe growth defects on oxalate. A methylsuccinyl-CoA dehydrogenase mutant grew on oxalate, but more slowly than the wild-type. It was hypothesized that the growth phenotype of mutants deficient in the latter group of enzymes may be caused by toxic effects as a consequence of the "trapping" of CoA thioesters, and this prediction was subsequently confirmed. The phenotypes of the mutants in the lower part of the EMC pathway indicate the operation of this pathway in the wild-type strain.

III. 2.7 Dynamic ^{13}C-oxalate incorporation

The results of the above described mutant analysis suggest the operation of a variant serine cycle without EMC pathway operation for glyoxylate regeneration during oxalate assimilation (Figure III.8A). However, oxalyl-CoA reduction is dispensable, and the phenotypes of mutants in the lower part of the EMC pathway, that were not growing on oxalate, suggest flux through the EMC pathway. A possible alternative to oxalyl-CoA reduction as a route for carbon assimilation consists of oxalate assimilation via formate and its conversion via the H_4F-dependent pathway and the serine cycle (Figure III.8B). Glyoxylate is converted by serine glyoxylate aminotransferase to glycine which is condensed with methylene-H_4F to form serine. The latter is then converted to hydroxypyruvate by serine glyoxylate aminotransferase, and reduced to glycerate, converted to phosphoglycerate and then PEP, which is carboxylated to oxaloacetate. If glyoxylate is not produced from oxalate it can alternatively be synthesized from oxaloacetate by its reduction to malate and conversion to malyl-CoA which is cleaved in acetyl-CA and glyoxylate. Acetyl-CoA is than converted by enzymes of the EMC pathway to glyoxylate. To test this hypothesis of two distinct putative assimilation strategies and to elucidate the metabolic route used for glyoxylate generation, dynamic ^{13}C-labeling experiments in the wild-type and in the Δ*oxs*/Δ*panE2* double mutant were performed. To this end, the *M. extorquens* AM1 wild-type strain and the double mutant were grown in bioreactors on naturally labeled oxalate, mixed each culture was mixed with fresh medium containing [U-^{13}C]-oxalate (at a final concentration of approximately 70% ^{13}C-oxalate) and the ^{13}C-labeling incorporation in central metabolites and

Results

CoA thioesters was followed in parallel using two designated sampling protocols, as described in the Experimental Procedures.
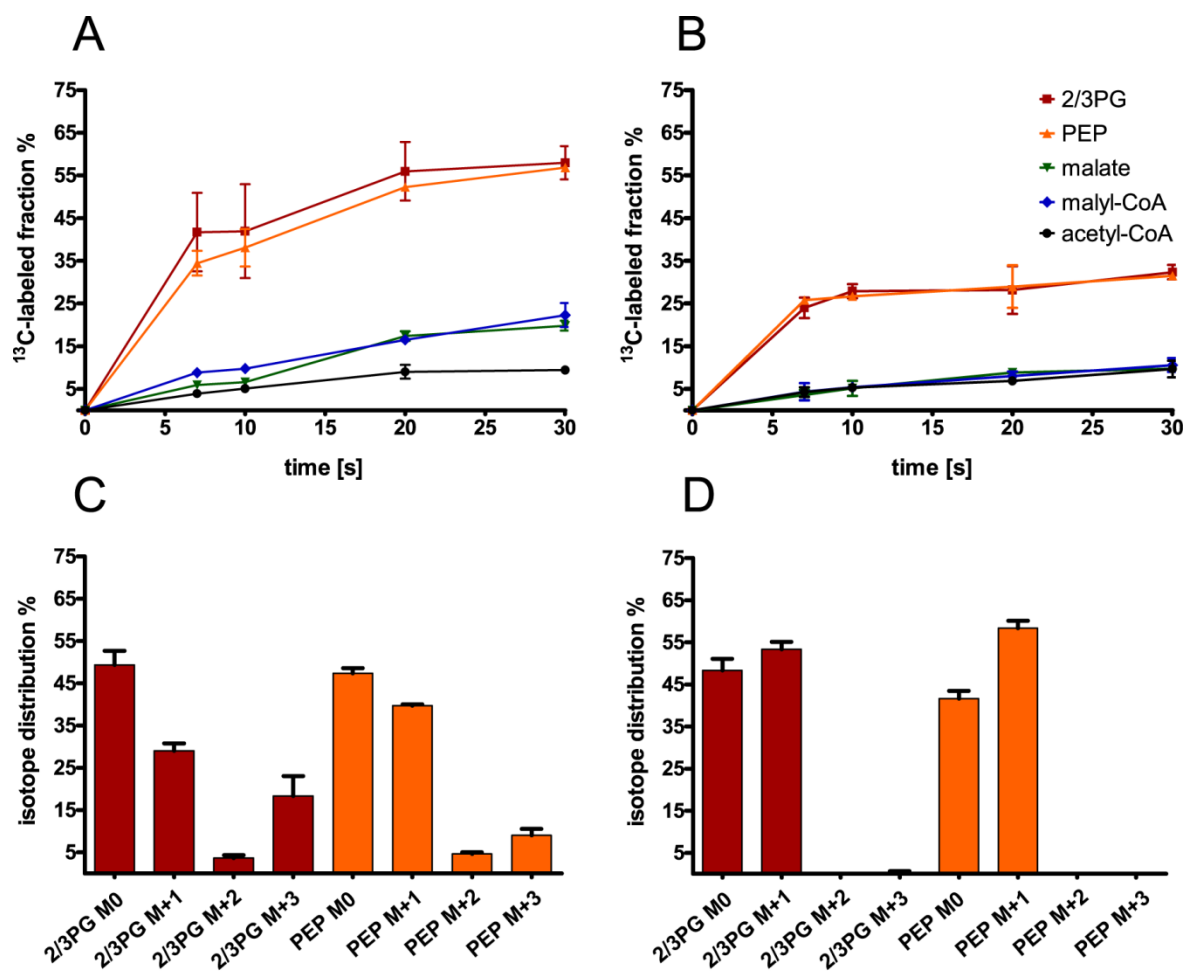
Figure III.9: Incorporation of the ^{13}C-label in central metabolites over time after incubation with [U-^{13}C]-oxalate. *M. extorquens* AM1 wild-type (A, C) and oxalyl-CoA synthetase and oxalyl-CoA reductase double mutant (Δ*oxs*/Δ*panE2*) (B, D) cells were grown on naturally labeled oxalate and mixed with fresh medium containing [U-^{13}C]-oxalate; label incorporation was measured in central metabolites at different times. The ^{13}C-labeled fractions of central metabolites (A, B) were normalized to ^{13}C-fraction of oxalate in the medium. The isotope distribution of 2/3-phosphoglycerate (2/3-PG) and PEP (C, D) was determined after 7s incubation with ^{13}C-oxalate. The medium contained 70-80% ^{13}C-oxalate. Average and standard deviation of three technical replicates are given.

Upon sampling the central metabolites, the following serine cycle intermediates were detected: 2/3-phosphoglycerate, PEP, malyl-CoA, and acetyl-CoA. During incubation of wild-type cells with ^{13}C-oxalate, 2/3-phosphoglycerate and PEP were labeled first followed by malate and malyl-CoA and then acetyl-CoA (Figure III.9A). Based on detection of malyl-CoA and the label incorporation into this metabolite before acetyl-CoA, acetyl-CoA synthesis from malyl-CoA cleavage in wild-type cells rather than pyruvate decarboxylation is suggested. The isotope distributions of 2/3-phosphoglycerate after 7 seconds of incubation with ^{13}C-labeled oxalate were in the wild-type strain 30% with one carbon-13 atom

incorporated (M+1), approximately 5% with two ^{13}C-atoms (M+2) and 20% with three ^{13}C-atoms (M+3) incorporated. The isotope distribution of PEP was similar: 40% M+1, 5% M+2, 10% M+3 (Figure III.9C). The mass shift of one can be explained by the condensation of ^{13}C-labeled methylene-H$_4$F with unlabeled [U-^{12}C]-glyoxylate. The fraction with two labeled carbon atoms originates from [U-^{13}C]-glycine (derived from [U-^{13}C]-oxalate converted via glyoxylate to glycine) and its condensation with ^{12}C-methylene-H$_4$F. In the case of the uniformly labeled C3 compound, the carbon atoms of glyoxylate and the C1-unit are predicted to be both labeled. For the $\Delta oxs/\Delta panE2$ double mutant, seven seconds after label addition a maximum of one ^{13}C-atom was incorporated (55% and 60%, respectively) in both 2/3-phosphoglycerate and PEP (Figure III.9D). These results thus demonstrate oxalyl-CoA reduction in the *M. extorquens* AM1 wild-type and its absence in the double mutant.
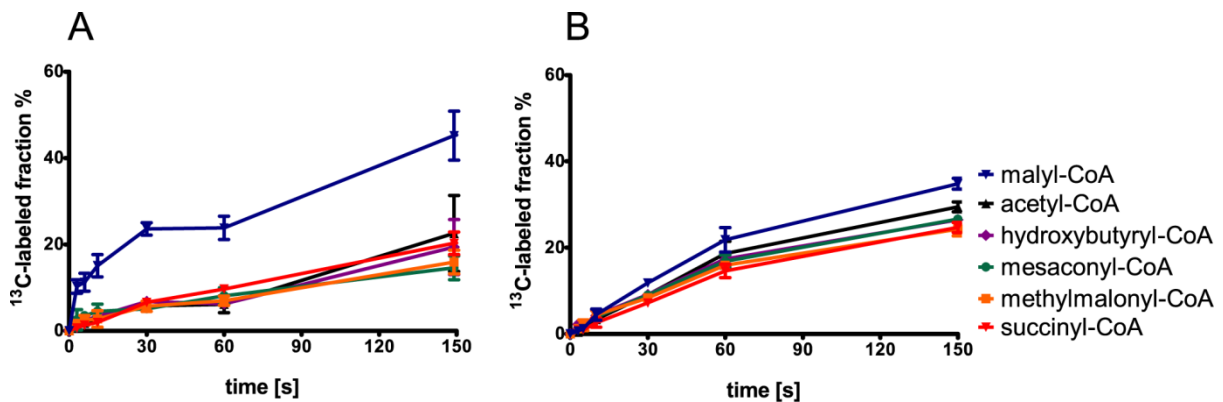
Figure III.10: Incorporation of the ^{13}C-label in CoA thioesters over time after incubation with [U-^{13}C]-oxalate. *M. extorquens* AM1 wild-type (A) and oxalyl-CoA synthetase and oxalyl-CoA reductase double mutant ($\Delta oxs/\Delta panE2$) (B) cells were grown on naturally labeled oxalate and mixed with fresh medium containing [U-^{13}C]-oxalate; label incorporation was measured at different times. The ^{13}C-labeled fractions of CoA thioesters were normalized to ^{13}C-fraction of oxalate in the medium. Average and standard deviation of three technical replicates are given.

Sampling for CoA thioesters revealed the presence of the following EMC pathway intermediates during growth on oxalate in both the wild-type strain and the $\Delta oxs/\Delta panE2$ double mutant: acetyl-CoA, hydroxybutyryl-CoA, ethylmalonyl-CoA, methylsuccinyl-CoA, mesaconyl-CoA, propionyl-CoA, methylmalonyl-CoA, succinyl-CoA, and malyl-CoA. The concentrations of the following CoA thioesters were significantly lower in the wild-type strain than in the $\Delta oxs/\Delta panE2$ double mutant (with reductions ranging from 5-90-fold; see below): ethylmalonyl-CoA, methylsuccinyl-CoA, mesaconyl-CoA, propionyl-CoA, and methylmalonyl-CoA. The reduced pool sizes may indicate a lower flux through the EMC pathway, as lower substrate concentrations are consistent with lower enzyme activity when the substrate concentrations are not greater than twice the K_M value. After incubation with

Results

[U-^{13}C]-oxalate, label incorporation in CoA thioesters in both the wild-type and Δ*oxs*/Δ*panE2* cells was deteced, first malyl-CoA followed by acetyl-CoA, and then all other CoA thioesters were labeled in parallel (Figure III.10). Malyl-CoA was labeled sooner in the wild-type than in the double mutant; however, acetyl-CoA was labeled later in the wild-type than in the double mutant. Acetyl-CoA, the product of the serine cycle, is derived from one C1-unit and one carbon dioxide. The labeled fractions of C1-units were identical in both strains (see the labeling patterns of the C3 compounds in Figure III.9), and carbon dioxide production was expected to be similar in both strains given by their similar growth rates. With respect to the similar intracellular concentrations of acetyl-CoA (see below) in the wild-type and the double mutant, the delayed labeling of acetyl-CoA is related to decreased malate cleavage in the wild-type compared with the Δ*oxs*/Δ*panE2* cells.
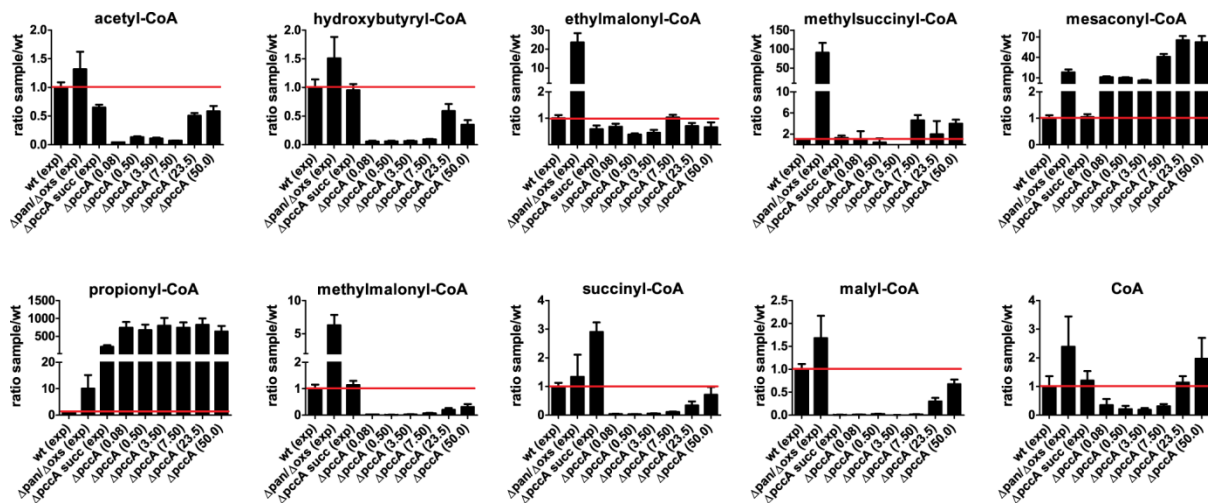
Figure III.11: Changes of intracellular CoA thioester concentrations of *M. extorquens* AM1 oxalyl-CoA synthetase and oxalyl-CoA reductase double mutant (Δ*oxs*/Δ*panE2*) versus wild-type(wt), both grown on oxalate; propionyl-CoA carboxylase (Δ*pccA*) mutant grown on succinate versus wt grown on oxalate, and Δ*pccA* mutant versus wt during different incubation times on oxalate. A pre-culture of Δ*pccA* mutant was grown on succinate, after centrifugation cells were resuspended in fresh medium containg oxalate as sole carbon source. Samples for CoA thioester quantification were taken at various times (given in brackets in hours); for quantification an internal standard was added. Samples of wt, Δ*oxs*/Δ*panE2* double mutant, and Δ*pccA* mutant were taken during exponential growth (exp). Ratios of inctracellular CoA thioester concentration were calculated using three technical replicates, average and standard deviations are given.

Additionally, EMC pathway mutants were investigated for effects on intermediates to test the hypothesis that intermediates of the pathway accumulate upon a blockage of the lower part of the pathway, which may explain the observed growth defects in these mutants. A propionyl-CoA carboxylase (Δ*pccA*) mutant was chosen to monitor the pool sizes of EMC pathway intermediates. The EMC pathway intermediate pool sizes were compared with the Δ*pccA* mutant grown on oxalate versus the wild-type cells, and versus the Δ*pccA* mutant

grown on succinate to determine whether the block is absent when growing on succinate (Figure III.11). Due to the growth defect of the Δ*pccA* mutant (Table III.5), the mutant cultures were pre-grown on succinate before being transferred to oxalate containing medium. CoA thioester samples were taken at various times after transfer to oxalate.

During the first 8 hours after the transfer of succinate grown Δ*pccA* mutant to oxalate, the intracellular concentrations of acetyl-CoA, hydroxybutyryl-CoA, methylmalonyl-CoA, succinyl-CoA, and malyl-CoA were decreased by 10-100-fold compared with the exponentially growing wild-type. However, the mesaconyl-CoA concentration was 10 times higher and propionyl-CoA concentration was 700 times higher in Δ*pccA* cells compared to wild-type. The Δ*pccA* mutant began to grow slowly after 24 hours on oxalate and continuously increased its growth rate (with a doubling time of 9 hours, 50 hours after the transfer to oxalate). After 24 hours, the pool sizes of mesaconyl-CoA (70-fold) and propionyl-CoA (700-fold) were still higher than the wild-type cells. All other CoA thioesters (upstream of methylsuccinyl-CoA dehydrogenase) displayed less than 3-fold difference in intracellular pool size compared to the wild-type. Additionally, when comparing the CoA thioester pool size of the Δ*pccA* mutant grown on oxalate to the same strain grown on succinate, the intracellular concentrations of mesaconyl-CoA and propionyl-CoA were significantly increased on oxalate (10-fold and 4-fold, respectively, during the first 8 hours and 60-fold for mesaconyl-CoA after 24 hours). These data indicate that the growth inhibition of the mutants in the lower part of the EMC pathway is caused by a toxicity effect due to a trapping of CoA thioesters between the irreversible methylsuccinyl-CoA dehydrogenase and the downstream enzyme knockouts. The conversion of acetyl-CoA in the EMC pathway results in a loss of reductant and a failure to provide sufficient C2-units for biosynthesis. Additionally, the hydrolysis of highly concentrated CoA thioesters may lead to acidification of the cytoplasm. During succinate assimilation, less carbon is "trapped" in the EMC pathway (there are lower intracellular concentrations of mesaconyl-CoA and propionyl-CoA), which is likely related to a lower flux through the EMC pathway that allows the mutant to grow on succinate.

III. 2.8 Flux balance analysis of oxalotrophy

To identify the optimal flux distribution for oxalate metabolism, a flux balance analysis using the iRP911 genome-scale metabolic model of *M. extorquens* AM1 (Peyraud *et al.*, 2011) was performed. The theoretical maximal growth rate of the cell was 0.19 h^{-1} for the

experimentally determined oxalate uptake rate. The model suggests oxalyl-CoA reduction to glyoxylate, conversion to glycine and its condensation with methylene-H_4F produced from formate reduction, which results in the formation of C3-units, and no EMC pathway operation. Acetyl-CoA is produced via cleavage of malyl-CoA which is formed by PEP carboxylase, malate dehydrogenase and malate thiokinase as part of the serine cycle. This metabolic network topology is in line with the results of ^{13}C-labeling experiments and mutant analysis described above. However, the calculated growth rate was approximately one-third higher than the experimentally determined rate. The theoretical biomass yield obtained from the flux balance analysis was 0.11 (g of [C] per CDW) / g of [C] from oxalate), which is also almost one-third higher than the experimentally determined value. With both the oxalate uptake rate and the growth rate constrained to their experimental values, the calculated yield was 0.07 (g of [C] per CDW) / g of [C] from oxalate). The simulated flux distribution of the central metabolism for the growth rate experimentally determined for *M. extorquens* AM1 during growth with oxalate is represented in Figure III.6. Notably, the enzyme activity measured *in vitro* for oxalyl-CoA reductase (which is 19.4 $mmol \cdot g^{-1}$ (CDW) $\cdot h^{-1}$, see above) is sufficient for glyoxylate generation by oxalyl-CoA reduction.

.

Chapter 4

DISCUSSION

Chapter IV Discussion

IV. 1 Acetate metabolism

M. extorquens AM1 can grow in the presence of acetate as its sole source of carbon and energy. To understand the catabolic and anabolic strategy of this isocitrate lyase-negative organism, proteome analysis and ^{13}C-labeling experiments, including metabolic flux analysis, were conducted. The glyoxylate cycle allows for complete oxidation by the TCA cycle and replenishes metabolites that leave the cycle for biosynthetic purposes. Here, it was shown that the EMC pathway functionally replaces the glyoxylate cycle during growth on acetate. This recently discovered pathway operates to refill the TCA cycle; in addition, it supplies glyoxylate for glycine and serine biosynthesis. A more detailed comparison of the operation of the metabolic network revealed a 20% and 30% higher rate of production of carbon dioxide and redox equivalents by isocitrate dehydrogenase and 2-oxoglutarate dehydrogenase in *M. extorquens* AM1 growing on acetate, compared with *C. glutamicum* (Wendisch *et al.*, 2000) and *E. coli* (Zhao & Shimizu, 2003), respectively (Table IV.1). This offers *M. extorquens* AM1 the additional gain of redox equivalents; however, these additional redox equivalents are required (by acetoacetyl-CoA reductase and crotonyl-CoA carboxylase/reductase) to operate the EMC pathway. This anaplerotic reaction sequence contains two carboxylation steps (crotonyl-CoA carboxylase/reductase and propionyl-CoA carboxylase) and recycles 20% of the carbon dioxide. The glyoxylate cycle used by *C. glutamicum* and *E. coli* neither requires redox equivalents nor contains carboxylation steps. Interestingly, despite the long and complicated reaction sequence of the EMC pathway, which operates during growth on acetate, the pathway is not disadvantageous to biomass yield.

Table IV.1: Flux values relative to acetate uptake rate of (de-)carboxylating steps of TCA cycle and EMC pathway of *C. glutamicum*, *E. coli* and *M. extorquens* AM1. Flux values were determined as indicated in the footnotes.

	C. glutamicum[a]	*E. coli*[b]	*M. extorquens* AM1[c]
Isocitrate dehydrogenase	58.1	51.0	67.6
2-Oxoglutarate dehydrogenase	56.1	49.1	66.1
Crotonyl-CoA carboxylase/reductase	-	-	10.2
Propionyl-CoA carboxylase	-	-	10.2

[a] (Wendisch *et al.*, 2000)
[b] (Zhao & Shimizu, 2003)
[c] this study

Discussion

As a consequence of the overall metabolic network topology of the EMC pathway-positive organism, the entry points into metabolism from acetyl-CoA are clearly distinct from those in organisms with a glyoxylate cycle. For isocitrate lyase-positive organisms, two entry points for acetyl-CoA exist, i.e., the TCA cycle and malate synthase, which are stoichiometrically coupled. In the case of *M. extorquens* AM1, three independent entry points were identified, in order of their contribution: (*i*) the TCA cycle, (*ii*) the EMC pathway, and (*iii*) condensation with the EMC pathway ("side-") product glyoxylate. Consequently, the network topology is more complex in the EMC pathway-positive bacterium, with the convergence of multiple pathways at different metabolites, i.e., succinyl-CoA fueled by the TCA cycle and the EMC pathway, and malate. As a result, fluxes must be tightly regulated to avoid metabolite imbalance at central metabolic nodes, and further investigation will be required to elucidate the underlying mechanism.

M. extorquens AM1 was the first EMC pathway-positive bacterium for which a genome-scale metabolic network reconstruction was performed and for which metabolic flux analysis was accomplished under methanol growth conditions (Peyraud *et al.*, 2011). The comparison of the metabolic network under methylotrophic conditions with the network present during growth on acetate revealed a high degree of overlap in the protein repertoire. Semi-quantitative proteome analysis suggests that EMC pathway enzymes are present in quantities at the same order of magnitude or lower during growth on acetate than on methanol, which is consistent with the enzymatic activities measured by Smejkalova *et al.* (Smejkalova *et al.*, 2010). The latter activities were found to be higher than the flux determined via this pathway. Only the activity of ethylmalonyl-CoA mutase (0.55 $mmol \cdot g^{-1}$ (CDW)$\cdot h^{-1}$) was in the range of the calculated flux value and could represent a growth-limiting step during acetate assimilation, which is in accordance with the earlier identification of the critical B_{12}-dependent enzyme reaction (Kiefer *et al.*, 2009). However, fluxes through the EMC pathway, normalized to their respective carbon uptake rates, were identical in cells grown on methanol and acetate. Thus, it can be concluded that the EMC pathway is required for the assimilation of both substrates to the same extent relative to their carbon amount. A striking difference was observed in the operation of the TCA cycle under both conditions. The metabolic cycle operates on acetate with a high flux through 2-oxoglutarate dehydrogenase (Figure IV.1), whereas it is incomplete under methylotrophic growth conditions (Peyraud *et al.*, 2011). The higher flux of carbon through the catabolic TCA cycle during growth on acetate relative to the assimilatory flux in the presence of methanol is consistent with TCA cycle enzymes being more abundant on acetate than on methanol. Alternative routes for substrate oxidation during

growth on acetate were determined to play only a minor role, i.e., the oxidation of one-carbon-units and pyruvate. Thus, like non-methylotrophic organisms, methylotrophs also use the TCA cycle as major pathway for the oxidation of acetyl-CoA.
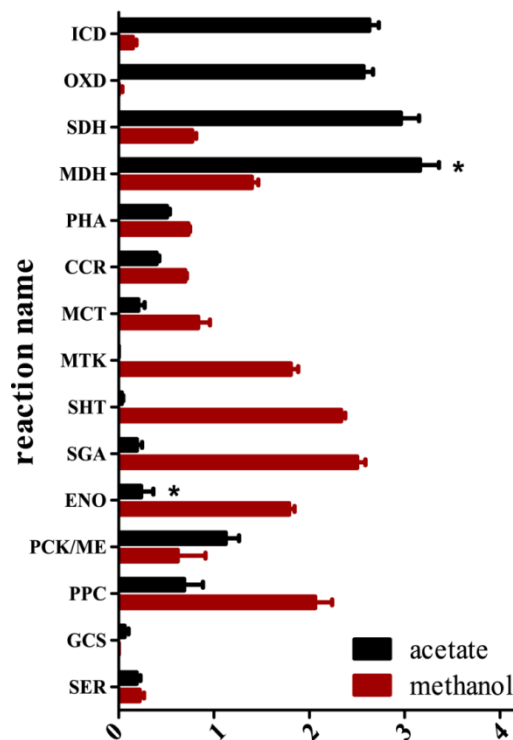
Figure IV.1. Comparison of the flux distribution in *M. extorquens* AM1 grown on acetate and methanol. Flux values are given in mmol·g^{-1} (CDW)·g^{-1}, and * indicates reversed flux on acetate relative to methanol. ICD: isocitrate dehydrogenase; OXD: 2-oxoglutarate dehydrogenase; SDH: succinate dehydrogenase; MDH: malate dehydrogenase; PHA: β-ketothiolase; CCR: crotonyl-CoA carboxylase/reductase; MCT: malyl-CoA thioesterase; MTK: malate thiokinase; SHT: serine hydroxymethyltransferase; SGA: serine glyoxylate aminotransferase; ENO: enolase; PCK/ME: PEP carboxykinase plus malic enzyme; PPC: PEP carboxylase; GCS: glycine cleavage system; and SER: phosphoserine aminotransferase.

Though a high turnover of the serine cycle is required for assimilation of one-carbon compounds to initiate the formation of multi-carbon compounds during growth on methanol, the cycle plays only a minor role during growth on acetate. This is evident from the observation that most enzymes were less abundant during growth on acetate and is consistent with the results from the flux analysis (Figure IV.1). However, in the case of serine hydroxymethyltransferase, only a minor fold-change in normalized spectral counts was observed (≈ 1.5), but flux decreased approximately 70-fold. The integration of data obtained from the flux analysis and proteomics suggests a post-translational flux control of serine hydroxymethyltransferase, for example, by substrate concentrations below the K_M value or by allosteric/competitive enzyme inhibition. Flux through the serine cycle was not only

significantly lower on acetate, but also, at some steps, the net flux direction changed, resulting in a bidirectional operation of the serine "cycle" relative to its classical operation under methylotrophic growth conditions. The flux from glyoxylate to 2-phosphoglycerate via glycine and serine operated in the same direction during growth on acetate and methanol. However, the subsequent steps of the serine cycle, the conversion of 2-phosphogycerate to malate and its subsequent cleavage to glyoxylate and acetyl-CoA, exhibited a reversed flux direction during growth on acetate, despite the irreversible enzymatic reactions catalyzed by PEP carboxylase and malate thiokinase. This is achieved by their substitution with PEP carboxykinase and malyl-CoA thioesterase, respectively. Consequently, all C3 compounds (PEP, pyruvate, and phosphoglycerate) are synthesized by decarboxylation of the C4 intermediates malate and oxaloacetate. However, glycine and serine are synthesized from glyoxylate.

Integrating proteome data and ^{13}C-metabolic flux analysis allowed correlating the abundance of proteins and their *in vivo* activities in *M. extorquens* AM1 during growth on acetate. A high degree of overlap in the proteome between acetate- and methanol-grown cells was identified, but the connectivity of the metabolic network changed, and fluxes were redirected. This feature should allow the organism to quickly adapt to changes in carbon source availability.

IV. 2 Oxalate metabolism

Growth in the presence of the highly oxidized oxalate requires an oxidative branch for the generation of reductant following cleavage of the carbon-carbon bond and an assimilation process involving oxalate reduction. The reduction of carbon is mandatory for the incorporation of oxalate into biomass, as the oxidation state of oxalate is higher than that of cellular carbon. Here, it was confirmed that *M. extorquens* AM1 assimilates oxalate in a cyclic process of CoA transfer from formyl-CoA to oxalate, whereby formyl-CoA is the product of oxalyl-CoA decarboxylation. Reductant is produced by formate oxidation via formate dehydrogenase (Blackmore & Quayle, 1970). Two different assimilation strategies for oxalate in *M. extorquens* AM1 were identified, whereby either of the two allows growth. The strategy that predominates in the wild-type is based on a minimal set of enzymes to produce all precursor metabolites (Figure III.8A). Oxalyl-CoA is reduced to glyoxylate, which upon condensation with C1-units deriving from formate by the operation of a variant of the serine cycle, results in the synthesis of C3- and C4-units (Blackmore & Quayle, 1970).

The serine cycle is modified, as it does not require malyl-CoA cleavage and EMC pathway operation for glyoxylate regeneration. However acetyl-CoA for biosynthesis may be produced either by malyl-CoA cleavage or pyruvate decarboxylation. Three of the TCA cycle enzymes are required for the synthesis of C5-precursor metabolites.

A second assimilation strategy, which was used when the oxalyl-CoA synthetase and oxalyl-CoA reductase were inactivated, consists of oxalate assimilation exclusively via C1-units (Figure III.8B). Here, oxalate is decarboxylated to formate and subsequently converted into glyoxylate via the H_4F-dependent pathway in connection with the serine cycle and the EMC pathway. The second assimilation strategy was also found to operate in wild-type cells, although to a limited extent and was dispensable.

The two separate oxalate assimilation strategies differ in their metabolic flux distributions of the assimilatory and oxidative branches. To obtain the same growth rate during oxalate assimilation exclusively via C1-units compared to oxalate assimilation by the variant of the serine cycle, the organism must operate the EMC pathway and generate higher fluxes through the serine cycle for the C1 assimilation. Moreover higher rates through oxalyl-CoA decarboxylase, formyl-CoA transferase, and formate dehydrogenase are required to account for the additional synthesis of C1-units and reductant needed for assimilation. In fact, a lower growth rate was observed for the $\Delta oxs/\Delta panE2$ double mutant than the wild-type strain, which implies that the *M. extorquens* AM1 double mutant is not able to generate the higher rates required in the oxidative and/or assimilatory branches and thus, one or more of these enzymes constitute metabolic bottlenecks during oxalate assimilation. Based on a flux analysis of methanol-grown cells, one can conclude that neither the serine cycle nor the EMC pathway can be the rate-limiting step. The organism is able to generate fluxes through both pathways required for C1 assimilation, accounting for a growth rate of at least 0.17 h^{-1} (Peyraud *et al.*, 2011). However, enzymes in the oxidative branch operate at very high rates, in the range of 30-32 mmol $\cdot$ g^{-1} (CDW) $\cdot$ h^{-1}. This range is twice as high as the rates observed during methanol assimilation (e.g., 13 mmol $\cdot$ g^{-1} (CDW) $\cdot$ h^{-1} for formate dehydrogenase (Peyraud *et al.*, 2011)). Therefore, it is suggested that oxalyl-CoA decarboxylase, formyl-CoA transferase, and/or formate dehydrogenase are the metabolic bottleneck(s) in the C1 oxalate assimilation strategy and thus restrict growth. As mentioned above, it was found that the C1 assimilation strategy also operates in the wild-type strain to a limited extent. The C1 assimilation strategy is blocked when crotonyl-CoA carboxylase/reductase is inactivated; the Δccr mutant showed a slight tendency for an increased growth rate compared with the wild-type (Table III.5). This is confirming the

hypothesis that the operation of the EMC pathway reduces growth during oxalate assimilation. Taken together, the lifestyle of *M. extorquens* AM1 during oxalate utilization seems to be limited in the oxidative branch, and oxalyl-CoA reductase is required to overcome the bottleneck and thus allows for a higher growth rate on oxalate.

Although oxalate is a low-energy carbon compound, the flux balance analysis suggests that central metabolism is not operating under optimal energetic conditions with this carbon source. A higher growth rate and yield were calculated by the flux balance analysis than were observed experimentally, which is likely related to the presence of substrate cycles, as demonstrated in *M. extorquens* AM1 during methanol (Peyraud *et al.*, 2011) and acetate assimilation (Chapter III. 1.5). During growth on oxalate, a carbon flux through the EMC pathway was detected. This is one example of a pathway operating during growth on oxalate being dispensable and decreasing the growth rate. It is likely that other substrate cycles found during C1 and C2 assimilation, e.g., PEP carboxylase/PEP carboxykinase and malate thiokinase/malyl-CoA thioesterase (Peyraud *et al.*, 2011), are also functional during oxalate utilization and thus reducing biomass yield. The presence of such substrate cycles and EMC pathway operation may allow the organism to quickly adapt its metabolism to the availability of different carbon compounds such as methanol and other C1 compounds, acetate, and various substrates entering the central metabolism at the level of acetyl-CoA. Rapid metabolic adaptations to changes in carbon source availability may contribute to the fitness of this bacterium and provide a growth advantage in low-nutrient habitats such as the phyllosphere.

IV. 3 Conclusions and Outlook

The goal of this thesis was to obtain a better understanding of the central metabolism of *M. extorquens* AM1 and the function of the EMC pathway with respect to assimilation of two carbon substrates. Acetate was used as a model compound for all substrates that enter the central metabolism on the level of acetyl-CoA. Oxalate produced by plants (Franceschi & Nakata, 2005) was of interest as it might be available for the bacterium in its plant-associated habitat (Bravo *et al.*, 2011). Thus, growth with acetate and oxalate as the carbon and energy source was investigated.

Acetate and oxalate are structurally very similar; both are two-carbon compounds. Acetate is a mono-, and oxalate a dicarboxylic acid. However, they are metabolized

differently. Both carbon compounds are initially activated to their corresponding CoA thioester. CoA thioester synthesis by an acyl-CoA synthetase costs one ATP per reaction.

Acetate oxidation occurs from conversion of acetyl-CoA into the TCA cycle and redox equivalents are generated from the following enzymes: isocitrate dehydrogenase, 2-oxoglutarate dehydrogenase, succinate dehydrogenase, and malate dehydrogenase. The oxidation of one molecule acetyl-CoA yields 3 NAD(P)H and 1 ubiquinone. Upon respiration 36 protons can be translocated and 9 ATP generated (Fuchs, 2007). Thus, the activation of acetate corresponds to roughly 10% of the ATP yield from the acetyl-CoA oxidation.

Oxalate oxidation occurs via oxalyl-CoA decarboxylation to formyl-CoA and conversion to formate; by formate dehydrogenase one NADH is generated per molecule oxalate. During respiration 10 protons can be translocated and thus, 2.5 ATP produced. If oxalate activation is conducted by oxalyl-CoA synthetase, it costs 40% of the ATP yield. As oxalate is a rather 'poor' substrate in terms of energy, the organism necessarily uses formyl-CoA transferase to synthesize the oxalyl-CoA which is subjected to decarboxylation. This enzyme allows the direct transfer of CoA from formyl-CoA to oxalate without the cost of ATP.

Not only the catabolism of both C2 compounds is different, also assimilation strategies are not the same. The EMC pathway is a prerequisite for the formation of glyoxylate from acetate; however, the pathway is not required for oxalate assimilation, though active. Oxalate is reduced to glyoxylate after it is activated by oxalyl-CoA synthase. Only around 4% of the oxalyl-CoA generated is reduced to glyoxylate and thus, produced by oxalyl-CoA synthetase.

M. extorquens is one of the major plant colonizers; the bacterium is known to utilize methanol released by plants during cell wall synthesis but apart from that other nutrients are available in the phyllosphere (Sy *et al.*, 2005; Tukey, 1966). The plant surface known as a habitat rather poor of nutrients (Lindow & Brandl, 2003) might give a growth advantage to colonizers being able to co-metabolize different carbon sources and to be ready for catabolism/anabolism of carbon sources that (might) become available (Egli, 2010). The investigation of the central metabolism of *M. extorquens* AM1 during growth on C1 and C2 carbon substrates revealed the common usage of central pathways but with flux redirection for adaptations to the present carbon source. This feature of a plastic central metabolism could allow the organism to co-metabolize different substrates that have diverging entry points for the central metabolism. Furthermore, the presence of substrate cycles, and a de-repression of the EMC pathway could enable *M. extorquens* to quickly adapt to changes in carbon source availability. Investigation of co-consumption of different carbon sources and

pulse feeding experiments with altering carbon substrates could give further insights in the metabolic properties of *M. extorquens*.

In laboratory growth conditions like shake flasks and bioreactors, mostly excess of substrate is applied, which do not necessarily reflect the growth conditions of the phyllosphere and other "low nutrient"-habitats. The state of "hunger" inferred by very low-nutrient concentrations confronts the cell with two problems; available nutrients have to be trapped as efficiently as possible and the scare availability of energy and building blocks makes the cell virtually unable to respond to changing environmental conditions and stresses (Egli, 2010). Therefore, growth under carbon/energy-limiting conditions could allow to mimic the growth conditions in phyllosphere and to understand the behavior of *M. extorquens* AM1 in its natural habitat. To study the metabolic network and the cellular proteome during growth under low-nutrient conditions could reveal new insights in the metabolic strategy which *M. extorquens* is applying during colonization of the phyllosphere and other habitats.

SUPPLEMTAL

INFORMATION

Supplementary Information 1: acetate metabolism

Table SI_1.1. FTBL file describing the central network model used for flux calculation. Biomass exit was calculated from biomass composition determined on acetate. Experimental data was used from NMR and MS analysis. Internal ^{13}C-labeled CO_2 was set to 5%. Simplifications: malate was merged with malyl-CoA and oxaloacetate, and PEP with pyruvate. H_4F-, H_4MPT-pathway and formate dehydrogenase were merged to one reaction. The half reaction model was included instead of the traditional model of the pentosephosphate pathway. Reactions of the Enter-Doudoroff pathway were merged in one reaction. Abbreviation of reaction names are given in Table SI_1.2B.

Table SI_1.2. (A) Results of flux calculation and sensitivity analysis using ^{13}C-FLUX software. (B) Abbreviations uses in A and Table SI_1.1.

<u>**Accessible on attached CD:**</u>

Table SI_1.1 and SI_1.2 see above

Table SI_1.3. Fitting results of the amino acid positional and mass isotopomers obtained by NMR and LC-MS measurements of three biological replicates.

Table SI_1.4. List of all proteins detected by 1D-SDS-PAGE and LC-MS/MS in three biological replicates of cells grown on acetate and methanol.

Table SI_1.5. List of proteins with a p-value smaller than 0.05 and a fold change of spectral counts (acetate versus methanol) above 2 or below 0.5 including proteins detected only on methanol and only on acetate.

Supplementary Information 1: acetate metabolism

Table SI_1.1

// Uptake substrates

ac_up	ac_ext		ac	//acetate uptake
	#AB		#AB	
accoas	ac		accoa	
	#AB		#AB	
co2_upt	co2_ext		co2	//co2 uptake
	#A		#A	

// serine cycle

SHMT	gly	mlh4f	Lser	
	#AB	#a	#ABa	
SGA1	glyox		gly	
	#AB		#AB	
SGA2	Lser		hpyr	
	#ABC		#ABC	
HPR	hpyr		Dglyc	
	#ABC		#ABC	
GCK	Dglyc		D2pg	
	#ABC		#ABC	
ENO	D2pg		pyr	
	#ABC		#ABC	
PEPCL	co2	pyr	oaamal	
	#A	#abc	#abcA	
MCOASL	accoa	glyox	oaamal	
	#AB	#ab	#abBA	

//C1 pathways

FDH	mlh4f		co2	//simplified THF/MPTH pathway
	#A		#A	
GCS	gly		co2_out	mlh4f
	#AB		#A	#B

//Phosphoserine pathway

PHPR	D3pg		Phypr
	#ABC		#ABC
AMT	Phypr		Pser
	#ABC		#ABC
PSP	Pser		Lser
	#ABC		#ABC

//PHB biosynthesis

ACOAAT	accoa	accoa	aaccoa
	#AB	#ab	#ABab
AACOAR_1	aaccoa		R3hbcoa
	#ABCD		#ABCD
PHBP	R3hbcoa		PHB
	#ABCD		#ABCD

//Ethylmalonyl-CoA Pathway

AACOAR_2	aaccoa		S3hbcoa
	#ABCD		#ABCD
HBCOADH	S3hbcoa		crcoa
	#ABCD		#ABCD
CCOARC	co2	crcoa	ethmcoa
	#A	#abcd	#abAcd
EMM	ethmcoa		msuccoa
	#ABCDE		#ADBCE
MSCCOADH	msuccoa		mesacoa
	#ABCDE		#ABCDE
MESACOAH	mesacoa		Smmlycoa
	#ABCDE		#ABCDE
MMCOAL	Smmlycoa		glyox	ppcoa
	#ABCDE		#DC	#ABE
PPCOAC	ppcoa	co2	Smmcoa
	#ABC	#a	#ABaC
EPM	Smmcoa		Rmmcoa
	#ABCD		#ABCD
MMCOAM	Rmmcoa		scccoa

```
                #ABCD           #ADBC

//TCA cycle
        CS      accoa   oaamal  cit
                #AB     #abcd   #dcbBAa
        ACN     cit             tDict   //R-048
                #ABCDEF         #ABCDEF
        ICDH    tDict           co2_out akg
                #ABCDEF         #F      #ABCDE
        AKGDH   akg             co2_out scccoa
                #ABCDE          #A      #BCDE
        SCH_1   scccoa          suc
                #ABCD           #ABCD
        SCH_2   scccoa          suc
                #ABCD           #DCBA
        SDH_1   suc             fum
                #ABCD           #ABCD
        SDH_2   suc             fum
                #ABCD           #DCBA
        FUM_1   fum             oaamal
                #ABCD           #ABCD
        FUM_2   fum             oaamal
                #ABCD           #DCBA

//pyruvate metabolism
        PYRDH   pyr             co2_out accoa
                #ABC            #A      #BC


//gluconeogenesis
        PEPCK   oaamal          co2_out pyr
                #ABCD           #D      #ABC
        PGM     D2pg            D3pg
                #ABC            #ABC
        PGK     D3pg            pglyp
                #ABC            #ABC
        GAPDH   pglyp           glych3p
                #ABC            #ABC
        TPI     glych3p         dhap
                #ABC            #CBA
        FBA     dhap    glych3p fru16bp
                #ABC    #abc    #ABCabc
        F16BP   fru16bp         f6p
                #ABCDEF         #ABCDEF
        PGI     f6p             g6p
                #ABCDEF         #ABCDEF

//pentose phosphate pathway
        G6PDH   g6p             glucol6p
                #ABCDEF         #ABCDEF
        PGL     glucol6p        pgluc
                #ABCDEF         #ABCDEF
        PGDH    pgluc           co2_out rib5p
                #ABCDEF         #A      #BCDEF
        PAT     e2              accoa
                #AB             #BA
        HR1     rib5p           glych3p e2
                #ABCDE          #CDE    #AB
        HR2     f6p             ery4p   e2
                #ABCDEF         #CDEF   #AB
        HR3     f6p             glych3p e3
                #ABCDEF         #DEF    #ABC
        HR4     rib5p   e2      sedh7p
                #ABCDE  #ab     #abABCDE
        HR5     ery4p   e3      sedh7p
                #ABCD   #abc    #abcABCD
        HR6     sedh7p          ery4p   e3
                #ABCDEFG                #DEFG   #ABC
        HR7     sedh7p          rib5p   e2
                #ABCDEFG                #CDEFG  #AB

//Entner-Doudoroff pathway
        EDP     pgluc           pyr     glych3p //simplified
                #ABCDEF         #ABC    #DEF
```

Supplementary Information 1: acetate metabolism

// biomass exit flux - simplified reactions with key amino acids considered

```
bf_mlh4f   mlh4f                BMmlh4f
           #A                   #A
bf_gly     gly                  BMgly
           #AB                  #AB
bf_Lser    Lser                 BMLser
           #ABC                 #ABC
bf_oaa     oaamal               BMoaa
           #ABCD                #ABCD
bf_accoa   accoa                BMaccoa
           #AB                  #AB
bf_pyr     pyr                  BMpyr
           #ABC                 #ABC
bf_akg     akg                  BMakg
           #ABCDE               #ABCDE
bf_g6p     g6p                  BMg6p
           #ABCDEF              #ABCDEF
bf_rib5p   rib5p                BMrib5p
           #ABCDE               #ABCDE
bf_ery4p   ery4p                BMery4p
           #ABCD                #ABCD
bf_PHB     PHB                  BMPHB
           #ABCD                #ABCD
bs_Ile1    oaamal   pyr         Ile        Ileres
           #ABCD    #abc        #ABbCD     #ac
bs_Ile2    Ile                  BMIle
           #ABCDE               #ABCDE
bs_Ile3    Ileres               BMIleres
           #AB                  #AB
bs_AKV     pyr      pyr         akv        co2_out
           #ABC     #abc        #ABbcC     #a
bs_Leu1    akv      accoa       leu        co2_out
           #ABCDE   #ab         #abBCDE    #A
bs_Leu2    leu                  BMleu
           #ABCDEF              #ABCDEF
bs_Phe1    pyr      ery4p       dahp
           #ABC     #abcd       #ABCabcd
bs_Phe2    pyr      dahp        Chor
           #ABC     #abcdefg    #ABCabcdefg
bs_Phe3a   Chor                 Phe        co2_out
           #ABCDEFGHIJ          #ABCEFGHIJ          #D
bs_Phe3b   Chor                 Phe        co2_out
           #ABCDEFGHIJ          #ABCEJIHGF          #D
bs_Phe3    Phe                  BMPhe
           #ABCDEFGHI           #ABCDEFGHI
bs_Tyr4a   Chor                 Tyr        co2_out
           #ABCDEFGHIJ          #ABCEFGHIJ          #D
bs_Tyr4b   Chor                 Tyr        co2_out
           #ABCDEFGHIJ          #ABCEJIHGF          #D
bs_Tyr4    Tyr                  BMTyr
           #ABCDEFGHI           #ABCDEFGHI
```

// Exit Flux

```
exit_co2   co2_out              co2_exit
           #A                   #A
```

FLUXES
NET

NAME	FCD	VALUE(F/C)	ED_WEIGHT	LOW(F)	INC(F)

// entry flux

ac_up	F	3.6			
accoas	D				
co2_upt	D				

// serine cycle

SHMT	D				
SGA1	D				
SGA2	D				
HPR	D				
GCK	D				
ENO	D				
PEPCL	F	0			
MCOASL	D				

//Phosphoserine pathway

PHPR	F	0.01
AMT	D	
PSP	D	

//C1,glycine and serine biosynthesis hypothesis

FDH	F	0.01
GCS	D	

//PHB biosynthesis

ACOAAT	D	
AACOAR_1	D	
PHBP	D	

//Ethylmalonyl-CoA pathway

AACOAR_2	D	
HBCOADH	D	
CCOARC	F	0.5
EMM	D	
MESACOAH	D	
MSCCOADH	D	
MMCOAL	D	
PPCOAC	D	
EPM	D	
MMCOAM	D	

//TCA cycle

CS	D
ACN	D
ICDH	D
AKGDH	D
SCH_1	D
SCH_2	D
SDH_1	D
SDH_2	D
FUM_1	D
FUM_2	D

//pyruvate metabolism

PYRDH	F	0.001

//gluconeogenesis

PEPCK	D
PGM	D
PGK	D
GAPDH	D
TPI	D
FBA	D
F16BP	D
PGI	D

//pentose phosphate pathway

G6PDH	D	
PGL	D	
PGDH	D	
PAT	F	0.02
HR1	D	
HR2	D	
HR3	D	
HR4	D	
HR5	D	
HR6	F	0.02
HR7	F	0.02

//Entner-Doudoroff pathway

EDP	F	0.02

//biomass exit flux

bf_mlh4f	C	0.0286	
bf_gly	C	0.09399	
bf_Lser	C	0.02835	
bf_oaa	C	0.0963	// 0.2060 -0.0160 for ile
bf_accoa	C	0.13832	// 0.2532 -0.0002 for leu

bf_pyr	C	0.22417	"// 0.2337 -0.0160 for ile; -0.0004 for val; -0.0004 for leu"
bf_akg	C	0.05779	
bf_TP	C	0	
bf_g6p	C	0.02353	
bf_rib5p	C	0.02301	
bf_ery4p	C	0.02185	"// 0.0363 -0.0003 for phe; -0.0003 for tyr"
bf_PHB	C	0.10771	
bs_Ile1	D		
bs_Ile2	D		
bs_Ile3	C	0.008	
bs_AKV	D		
bs_Leu1	D		
bs_Leu2	C	0.0002	
bs_Phe1	C	0.006	
bs_Phe2	D		
bs_Phe3a	D		
bs_Phe3b	D		
bs_Phe3	C	0.003	
bs_Tyr4a	D		
bs_Tyr4b	D		
bs_Tyr4	D	0.003	

// exit flux

exit_co2	D

XCH

NAME	FCD	VALUE(F/C)	ED_WEIGHT	LOW(F)	INC(F)

// entry flux

ac_up	D	
accoas	C	0
co2_upt	D	

// serine cycle

SHMT	F	0.001
SGA1	C	0
SGA2	C	0
HPR	C	0
GCK	C	0
ENO	F	0.01
PEPCL	C	0
MCOASL	C	0

//C1,glycine and serine biosynthesis hypothesis

GCS	C	0
FDH	C	0

//Phosphoserine pathway

PHPR	C	0
AMT	C	0
PSP	C	0

//PHB biosynthesis

ACOAAT	C	0
AACOAR_1	C	0
PHBP	C	0

//Ethylmalonyl-CoA Pathway

AACOAR_2	C	0
HBCOADH	C	0
CCOARC	C	0
EMM	C	0
MESACOAH	C	0
MSCCOADH	C	0
MMCOAL	C	0
PPCOAC	C	0
EPM	C	0
MMCOAM	C	0

//TCA cycle

CS	C	0

ACN	C	0	
ICDH	C	0	
AKGDH	C	0	
SCH_1	C	0	
SCH_2	D		
SDH_1	C	0	
SDH_2	D		
FUM_1	F	0.99	
FUM_2	D		

//pyruvate metabolism

PYRDH	C	0

//gluconeogenesis

PEPCK	C	0
PGM	C	0
PGK	C	0
GAPDH	C	0
TPI	C	0
FBA	C	0
F16BP	C	0
PGI	C	0

//pentose phosphate pathway

G6PDH	C	0
PGL	C	0
PGDH	C	0
PAT	F	0.001
HR1	F	0.01
HR2	F	0.01
HR3	F	0.01
HR4	C	0
HR5	C	0
HR6	C	0
HR7	C	0

//Entner-Doudoroff pathway

EDP	C	0	//0.01

//biomass exit flux

bf_mlh4f	D	
bf_gly	D	
bf_Lser	D	
bf_oaa	D	
bf_accoa	D	
bf_pyr	D	
bf_akg	D	
bf_TP	D	
bf_g6p	D	
bf_rib5p	D	
bf_ery4p	D	
bf_PHB	D	
bs_Ile1	C	0
bs_Ile2	D	
bs_Ile3	D	
bs_AKV	C	0
bs_Leu1	C	0
bs_Leu2	D	
bs_Phe1	C	0
bs_Phe2	C	0
bs_Phe3a	C	0
bs_Phe3b	C	0
bs_Phe3	D	
bs_Tyr4a	C	0
bs_Tyr4b	C	0
bs_Tyr4	D	

// exit flux

exit_co2	D

EQUALITIES
    NET

VALUE	FORMULA
0	SCH_1-SCH_2

Supplementary Information 1: acetate metabolism

0	SDH_1-SDH_2
0	FUM_1-FUM_2
0	bs_Phe3a-bs_Phe3b
0	bs_Tyr4a-bs_Tyr4b
0	SGA1-SGA2

XCH

VALUE	FORMULA
0	SCH_1-SCH_2
0	SDH_1-SDH_2
0	FUM_1-FUM_2

INEQUALITIES

NET

VALUE	COMP	FORMULA

// Inequalities for Input and Output Fluxes are generated automatically

// C2 assimilation

0.001	<=	accoas

// serine cycle

0.0001	<=	PEPCL

//C1,glycine and serine biosynthesis hypothesis

0.0001	<=	GCS
0.0001	<=	FDH

//PHB biosynthesis

0.0001	<=	ACOAAT
0.0001	<=	AACOAR_1
0.0001	<=	PHBP

//Ethylmalonyl-CoA Pathway

0.0001	<=	AACOAR_2
0.0001	<=	HBCOADH
0.0001	<=	CCOARC
0.0001	<=	EMM
0.0001	<=	MESACOAH
0.0001	<=	MSCCOADH
0.0001	<=	PPCOAC
0.0001	<=	EPM
0.0001	<=	MMCOAM

//TCA cycle

0.0001	<=	CS
0.0001	<=	ACN
0.0001	<=	ICDH
0.0001	<=	AKGDH
0.0001	<=	SCH_1
0.0001	<=	SCH_2
0.0001	<=	SDH_1
0.0001	<=	SDH_2

//pyruvate metabolism

0.0001	<=	PYRDH

//gluconeogenesis

//pentose phosphate pathway

0.0001	<=	PGDH
0.0001	<=	HR4
0.0001	<=	HR5
0.0001	<=	HR6
0.0001	<=	HR7

//Entner-Doudoroff pathway

0.0001	<=	EDP

//biomass exit flux

0.0001	<=	bs_Ile1
0.0001	<=	bs_Ile2
0.0001	<=	bs_AKV
0.0001	<=	bs_Leu1

```
          0.0001    <=        bs_Phe3
          0.0001    <=        bs_Tyr4

     XCH
               VALUE   COMP    FORMULA
// Inequalities for Input and Output Fluxes are generated automatically
```

```
FLUX_MEASUREMENTS
          FLUX_NAME        VALUE   DEVIATION        //                Val      Dev

          ac_up    3.63     0.1

LABEL_INPUT
          META_NAME        ISOTOPOMER      VALUE

// 13CLabeled methanol + unlabeled co2

          ac_ext   #01      0.778557114
                   #10      0.001002004
                   #11      0.213426854
                   #00      0.007014028

          co2_ext  #0       0.95
                   #1       0.05
```

Supplementary Information 1: acetate metabolism

Table SI_1.2

Table SI_1.2A

Abbreviation	Replicate 1				Replicate 2				Replicate 3			
	net flux	dev	exchange flux	dev	net flux	dev.	exchange flux	dev.	net flux	dev	exchange flux	dev
ac_up	3.43	0.10	0.00	0.00	3.89	0.10	0.00	0.00	4.43	0.10	0.00	0.00
accoas	3.43	0.10	0.00	0.00	3.89	0.10	0.00	0.00	4.43	0.10	0.00	0.00
co2_upt	1.23	0.10	0.00	0.00	1.48	0.15	0.00	0.00	1.88	0.14	0.00	0.00
SHMT	0.01	0.01	0.24	0.05	0.03	0.02	0.34	0.08	0.03	0.02	0.36	0.08
SGA1	0.15	0.04	0.00	0.00	0.19	0.05	0.00	0.00	0.22	0.06	0.00	0.00
SGA2	0.15	0.04	0.00	0.00	0.19	0.05	0.00	0.00	0.22	0.06	0.00	0.00
HPR	0.15	0.04	0.00	0.00	0.19	0.05	0.00	0.00	0.22	0.06	0.00	0.00
GCK	0.15	0.04	0.00	0.00	0.19	0.05	0.00	0.00	0.22	0.06	0.00	0.00
ENO	-0.19	0.03	0.39	0.18	-0.24	0.13	0.85	0.28	-0.27	0.08	0.57	0.22
PEPCL	0.49	0.11	0.00	0.00	0.69	0.20	0.00	0.00	0.98	0.17	0.00	0.00
MCOASL	0.22	0.04	0.00	0.00	0.21	0.07	0.00	0.00	0.23	0.06	0.00	0.00
FDH	0.00	0.02	0.00	0.00	0.00	0.03	0.00	0.00	0.01	0.03	0.00	0.00
GCS	0.05	0.03	0.00	0.00	0.06	0.04	0.00	0.00	0.08	0.04	0.00	0.00
PHPR	0.17	0.03	0.00	0.00	0.19	0.04	0.00	0.00	0.22	0.04	0.00	0.00
AMT	0.17	0.03	0.00	0.00	0.19	0.04	0.00	0.00	0.22	0.04	0.00	0.00
PSP	0.17	0.03	0.00	0.00	0.19	0.04	0.00	0.00	0.22	0.04	0.00	0.00
ACOAAT	0.48	0.02	0.00	0.00	0.51	0.03	0.00	0.00	0.58	0.03	0.00	0.00
AACOAR_1	0.11	0.00	0.00	0.00	0.11	0.00	0.00	0.00	0.13	0.00	0.00	0.00
PHBP	0.11	0.00	0.00	0.00	0.11	0.00	0.00	0.00	0.13	0.00	0.00	0.00
AACOAR_2	0.37	0.02	0.00	0.00	0.40	0.03	0.00	0.00	0.46	0.03	0.00	0.00
HBCOADH	0.37	0.02	0.00	0.00	0.40	0.03	0.00	0.00	0.46	0.03	0.00	0.00
CCOARC	0.37	0.02	0.00	0.00	0.40	0.03	0.00	0.00	0.46	0.03	0.00	0.00
EMM	0.37	0.02	0.00	0.00	0.40	0.03	0.00	0.00	0.46	0.03	0.00	0.00
MSCCOADH	0.37	0.02	0.00	0.00	0.40	0.03	0.00	0.00	0.46	0.03	0.00	0.00
MESACOAH	0.37	0.02	0.00	0.00	0.40	0.03	0.00	0.00	0.46	0.03	0.00	0.00
MMCOAL	0.37	0.02	0.00	0.00	0.40	0.03	0.00	0.00	0.46	0.03	0.00	0.00
PPCOAC	0.37	0.02	0.00	0.00	0.40	0.03	0.00	0.00	0.46	0.03	0.00	0.00
EPM	0.37	0.02	0.00	0.00	0.40	0.03	0.00	0.00	0.46	0.03	0.00	0.00
MMCOAM	0.37	0.02	0.00	0.00	0.40	0.03	0.00	0.00	0.46	0.03	0.00	0.00
CS	2.16	0.09	0.00	0.00	2.63	0.10	0.00	0.00	2.98	0.10	0.00	0.00
ACN	2.16	0.09	0.00	0.00	2.63	0.10	0.00	0.00	2.98	0.10	0.00	0.00
ICDH	2.16	0.09	0.00	0.00	2.63	0.10	0.00	0.00	2.98	0.10	0.00	0.00
AKGDH	2.10	0.09	0.00	0.00	2.57	0.10	0.00	0.00	2.91	0.10	0.00	0.00
SCH_1	1.24	0.05	0.00	0.00	1.48	0.05	0.00	0.00	1.68	0.05	0.00	0.00
SCH_2	1.24	0.05	0.00	0.00	1.48	0.05	0.00	0.00	1.68	0.05	0.00	0.00
SDH_1	1.24	0.05	0.00	0.00	1.48	0.05	0.00	0.00	1.68	0.05	0.00	0.00
SDH_2	1.24	0.05	0.00	0.00	1.48	0.05	0.00	0.00	1.68	0.05	0.00	0.00
FUM_1	1.24	0.05	0.98	0.13	1.48	0.05	0.99	0.09	1.68	0.05	0.99	0.06
FUM_2	1.24	0.05	0.98	0.13	1.48	0.05	0.99	0.09	1.68	0.05	0.99	0.06
PYRDH	0.01	0.04	0.00	0.00	0.00	0.08	0.00	0.00	0.01	0.07	0.00	0.00
PEPCK	0.92	0.10	0.00	0.00	1.12	0.14	0.00	0.00	1.48	0.13	0.00	0.00
PGM	0.35	0.04	0.00	0.00	0.43	0.10	0.00	0.00	0.49	0.07	0.00	0.00
PGK	0.18	0.03	0.00	0.00	0.24	0.12	0.00	0.00	0.27	0.08	0.00	0.00
GAPDH	0.18	0.03	0.00	0.00	0.24	0.12	0.00	0.00	0.27	0.08	0.00	0.00
TPI	0.10	0.03	0.00	0.00	0.16	0.12	0.00	0.00	0.19	0.08	0.00	0.00
FBA	0.10	0.03	0.00	0.00	0.16	0.12	0.00	0.00	0.19	0.08	0.00	0.00
F16BP	0.10	0.03	0.00	0.00	0.16	0.12	0.00	0.00	0.19	0.08	0.00	0.00
PGI	0.05	0.03	0.00	0.00	0.07	0.13	0.00	0.00	0.09	0.08	0.00	0.00
G6PDH	0.02	0.03	0.00	0.00	0.05	0.13	0.00	0.00	0.07	0.08	0.00	0.00
PGL	0.02	0.03	0.00	0.00	0.05	0.13	0.00	0.00	0.07	0.08	0.00	0.00
PGDH	0.00	0.03	0.00	0.00	0.00	0.14	0.00	0.00	0.00	0.08	0.00	0.00
PAT	0.04	0.03	0.00	0.02	0.10	0.13	0.00	0.08	0.10	0.08	0.00	0.06
HR1	-0.01	0.03	0.21	0.00	0.01	0.13	0.99	0.00	0.00	0.08	0.54	0.00
HR2	0.04	0.00	0.11	0.00	0.06	0.01	0.88	0.00	0.06	0.01	0.33	0.00
HR3	0.01	0.00	0.09	0.00	0.03	0.01	0.00	0.00	0.03	0.01	0.23	0.00
HR4	0.00	0.00	0.00	0.00	0.00	0.01	0.00	0.00	0.00	0.01	0.00	0.00
HR5	0.08	0.00	0.00	0.00	0.18	0.01	0.00	0.00	0.11	0.01	0.00	0.00
HR6	0.07	0.00	0.00	0.00	0.15	0.00	0.00	0.00	0.08	0.00	0.00	0.00
HR7	0.01	0.00	0.00	0.00	0.03	0.00	0.00	0.00	0.03	0.00	0.00	0.00
EDP	0.02	0.01	0.00	0.00	0.05	0.02	0.00	0.00	0.07	0.02	0.00	0.00

bf_mlh4f	0.03	0.00	0.00	0.00	0.03	0.00	0.00	0.00	0.03	0.00	0.00	0.00
bf_gly	0.10	0.00	0.00	0.00	0.10	0.00	0.00	0.00	0.11	0.00	0.00	0.00
bf_Lser	0.03	0.00	0.00	0.00	0.03	0.00	0.00	0.00	0.03	0.00	0.00	0.00
bf_oaa	0.10	0.00	0.00	0.00	0.10	0.00	0.00	0.00	0.11	0.00	0.00	0.00
bf_accoa	0.14	0.00	0.00	0.00	0.14	0.00	0.00	0.00	0.16	0.00	0.00	0.00
bf_pyr	0.23	0.00	0.00	0.00	0.23	0.00	0.00	0.00	0.26	0.00	0.00	0.00
bf_akg	0.06	0.00	0.00	0.00	0.06	0.00	0.00	0.00	0.07	0.00	0.00	0.00
bf_g6p	0.02	0.00	0.00	0.00	0.02	0.00	0.00	0.00	0.03	0.00	0.00	0.00
bf_rib5p	0.02	0.00	0.00	0.00	0.02	0.00	0.00	0.00	0.03	0.00	0.00	0.00
bf_ery4p	0.02	0.00	0.00	0.00	0.02	0.00	0.00	0.00	0.03	0.00	0.00	0.00
bf_PHB	0.11	0.00	0.00	0.00	0.11	0.00	0.00	0.00	0.13	0.00	0.00	0.00
bs_Ile1	0.01	0.00	0.00	0.00	0.01	0.00	0.00	0.00	0.01	0.00	0.00	0.00
bs_Ile2	0.01	0.00	0.00	0.00	0.01	0.00	0.00	0.00	0.01	0.00	0.00	0.00
bs_Ile3	0.01	0.00	0.00	0.00	0.01	0.00	0.00	0.00	0.01	0.00	0.00	0.00
bs_AKV	0.00	0.00	0.00	0.00	0.00	0.00	0.00	0.00	0.00	0.00	0.00	0.00
bs_Leu1	0.00	0.00	0.00	0.00	0.00	0.00	0.00	0.00	0.00	0.00	0.00	0.00
bs_Leu2	0.00	0.00	0.00	0.00	0.00	0.00	0.00	0.00	0.00	0.00	0.00	0.00
bs_Phe1	0.01	0.00	0.00	0.00	0.01	0.00	0.00	0.00	0.01	0.00	0.00	0.00
bs_Phe2	0.01	0.00	0.00	0.00	0.01	0.00	0.00	0.00	0.01	0.00	0.00	0.00
bs_Phe3a	0.00	0.00	0.00	0.00	0.00	0.00	0.00	0.00	0.00	0.00	0.00	0.00
bs_Phe3b	0.00	0.00	0.00	0.00	0.00	0.00	0.00	0.00	0.00	0.00	0.00	0.00
bs_Phe3	0.00	0.00	0.00	0.00	0.00	0.00	0.00	0.00	0.00	0.00	0.00	0.00
bs_Tyr4a	0.00	0.00	0.00	0.00	0.00	0.00	0.00	0.00	0.00	0.00	0.00	0.00
bs_Tyr4b	0.00	0.00	0.00	0.00	0.00	0.00	0.00	0.00	0.00	0.00	0.00	0.00
bs_Tyr4	0.00	0.00	0.00	0.00	0.00	0.00	0.00	0.00	0.00	0.00	0.00	0.00
exit_co2	5.24	0.28	0.00	0.00	6.39	0.29	0.00	0.00	7.47	0.30	0.00	0.00

Table SI_1.2B

Abbreviation	Name	Abbreviation	Name
ac_up	acetate uptake	PYRDH	pyuvate dehydrogenase
accoas	acetyl-CoA synthetase	PEPCK	PEP carboxykinase
co2_upt	carbon dioxide uptake	PGM	phophoglycerate mutase
SHMT	serine hydroxymethyl transferase	PGK	glyceraldehyde-3-phosphate dehydrogenase
SGA1	serine glycine aminotransferase	GAPDH	glyceraldehyde-3-phosphate dehydrogenase
SGA2	serine glycine aminotransferase	TPI	triosephosphate isomerase
HPR	gydroxxypyruvate reductase	FBA	fructose-bisphosphate aldolase
GCK	glycerate kinase	F16BP	fructose-1,6-bisphosphatase
ENO	enolase	PGI	transaldolase phosphoglucose isomerase
PEPCL	PEP carboxylase	G6PDH	glucose-6-phosphate 1-dehydrogenase
MCOASL	malyl-CoA lyase	PGL	6-phosphogluconolactonas
FDH	formate dehydrogenase	PGDH	6-phosphogluconate dehydrogenase
GCS	glycine cleavage system	PAT	phosphoacetyl-CoA transferase
PHPR	phosphohydroxypyruvate reductase	HR1	pentosephosphate pathway half reaction model
AMT	phosphoserine aminotransferase	HR2	pentosephosphate pathway half reaction model
PSP	phoshoserine phosphatase	HR3	pentosephosphate pathway half reaction model
ACOAAT	beta-ketothiolase	HR4	pentosephosphate pathway half reaction model
AACOAR_1	acetoacetyl-CoA reductase	HR5	pentosephosphate pathway half reaction model
PHBP	PHB polymerase	HR6	pentosephosphate pathway half reaction model
AACOAR_2	acetoacetyl-CoA reductase	HR7	pentosephosphate pathway half reaction model
HBCOADH	crotonase	EDP	Entner Doudoroff pathway
CCOARC	crotonyl-CoA carboxylase/reductase		
EMM	ethylmalonyl-CoA epimerase/mutase	bf_mlh4f	biomass exit flux m-THF
MSCCOADH	methylsuccinyl-CoA dehydrogenase	bf_gly	biomass exit flux glycine
MESACOAH	mesaconyl-CoA hydratase	bf_Lser	biomass exit flux serine
MMCOAL	beta-methylmalyl-CoA lyase	bf_oaa	biomass exit flux oxalacetate
PPCOAC	propionyl-CoA carboxylase	bf_accoa	biomass exit flux acetyl-CoA
EPM	methylmalonyl-CoA epimerase	bf_pyr	biomass exit flux pyruvate
MMCOAM	methylmalonyl-CoA mutase	bf_akg	biomass exit flux 2-oxoglutarate
CS	citrate synthase	bf_g6p	biomass exit flux glucose-6-phophate
ACN	aconitate hydratase	bf_rib5p	biomass exit flux ribose-5-phosphate
ICDH	isocitrate dehydrogenase	bf_ery4p	biomass exit flux erytrose-4-phosphate
AKGDH	2-oxoglutarate dehydrogenase	bf_PHB	biomass exit flux PHB
SCH_1	succinyl-CoA hydratase	bs_Ile1-3	biomass exit flux isoleucine
SCH_2	succinyl-CoA hydratase	bs_AKV	biomass synthesis leucine
SDH_1	succinate dehydrogenase	bs_Leu1-2	biomass exit flux leucine
SDH_2	succinate dehydrogenase	bs_Phe1-3	biomass exit flux phenylalanine
FUM_1	fumarase	bs_Tyr4a,b	biomass exit flux tyrosine
FUM_2	fumarase	exit_co2	exit flux carbon dioxide

Supplementary Information 2: oxalate metabolism

Table SI_2.1. List of proteins of the central metabolism detected in oxalate-grown cells and compared with methanol and acetate cells, including average spectral counts, p-value and fold change.

Accessible on attached CD:

Table SI_2.1 see above

Table SI_2.2. List of all proteins detected by 1D-SDS-PAGE and LC-MS/MS in three biological replicates of cells grown on oxalate including previously published acetate and methanol samples.

Table SI_2.3. Results of flux balance analysis, including constrains used for flux optimization

Table SI_2.1

Gene Number	Gene	Description (gene name)	oxalate vs acetate		oxalate vs methanol		Normalized sprectra (‰)		
			fold-change	p-value	fold-change	p-value	Acetate	Methanol	Oxalate
Oxalate metabolism									
META1_0988	*frc1*	formyl-CoA transferase, NAD(P)-binding	n.d.	0.00	n.d.	0.00	0.00	0.00	11.53
META1_0990	*oxc*	oxalyl-CoA decarboxylase (oxc, yfdU)	n.d.	0.00	n.d.	0.00	0.00	0.00	11.61
META1_0992	*oxlT*	oxalate/formate antiporter	n.d.	0.00	n.d.	0.00	0.00	0.00	0.67
META1_0993	*oxlT*	oxalate/formate antiporter	n.d.	0.00	n.d.	0.00	0.00	0.00	1.08
META1_0999	*frc2*	formyl-CoA transferase, NAD(P)-binding	n.d.	0.00	n.d.	0.00	0.00	0.00	1.47
META1_1925	*oxlT*	putative oxalate/formate antiporter	n.d.	0.00	n.d.	0.00	0.00	0.00	1.30
META1_2127	*oxlT*	putative oxalate/formate antiporter	n.d.	0.00	17.00	0.25	0.00	0.04	0.69
META1_2129	*panE2*	oxalyl-CoA reductase	24.85	0.00	3.46	0.00	0.10	0.72	2.48
META1_2130	*oxs*	oxalyl-CoA synthetase	16.50	0.89	2.92	0.00	0.10	0.56	1.65
C1 oxidation									
META1_5031	*fdh1B*	tungsten-containing formate Dh β SU	1.52	0.07	4.78	0.00	0.76	0.24	1.16
META1_5032	*fdh1A*	tungsten-containing formate Dh α SU	2.31	0.02	4.10	0.00	1.42	0.80	3.27
META1_4846	*fdh2C*	NAD-dep. formate Dh, Mo containing, γSU	n.d.	0.00	7.07	0.18	0.00	0.05	0.36
META1_4847	*fdh2B*	NAD-dep. formate Dh, Mo containing, β SU	n.d.	0.00	n.d.	0.02	0.00	0.00	0.00
META1_4848	*fdh2A*	NAD-dep. formate Dh, Mo containing, α SU	n.d.	0.00	3.05	0.00	0.00	1.47	4.50
META1_4849	*fdh2D*	NAD-linked formate Dh, Mo containing, Δ SU	n.d.	0.00	1.68	0.44	0.00	0.25	0.42
META1_0303	*fdh3A*	formate Dh α SU precursor (tat signal)	2.06	0.46	0.68	0.83	33.57	101.82	69.22
META1_0304	*fdh3B*	formate Dh iron-sulfur (β) SU	n.d.	0.00	0.95	0.35	0.00	14.11	13.44
META1_0305	*fdh3C*	formate Dh γ(cytochrome) SU	0.56	0.95	0.67	0.98	7.26	6.05	4.03
META1_2093	*fdh4B*	formate Dh SU B	0.00	0.37	n.d.	0.12	0.04	0.00	0.00
META1_2094	*fdh4A*	formate Dh SU A	0.02	0.32	0.01	0.35	0.87	0.92	0.01
Energy metabolism									
META1_2956	*pntAA*	NAD(P)+ transhydrogenase, SU α part 1.	0.78	0.34	9.58	0.00	10.28	0.84	8.02
META1_2957	*pntAB*	NAD(P) transhydrogenase, SU α part 2	0.86	0.37	8.19	0.37	3.06	0.32	2.64
META1_3299	*hppa*	H+ translocating pyrophosphate synthase	0.70	0.01	n.d.	0.00	0.62	0.00	0.43
TCA cycle									
META1_2531	*acs*	acetyl-CoA synthetase	0.72	0.00	2.14	0.00	4.65	1.57	3.36
META1_5129	*gltA*	citrate synthase	0.42	0.01	1.24	0.08	4.93	1.66	2.07
META1_2828	*acnA*	aconitate hydratase	0.36	0.01	0.71	0.06	6.32	3.25	2.29
META1_3354	*icd*	NADP-dep. isocitrate Dh	0.32	0.00	0.70	0.15	4.46	2.07	1.44
META1_1540	*sucA*	2-oxoglutarate Dh complex, E1 component	0.45	0.00	1.21	0.06	5.44	2.01	2.43
META1_1541	*sucB*	2-oxoglutarate Dh complex, dihydrolipoamide succinyltransferase	0.34	0.00	1.07	0.43	3.43	1.11	1.18
META1_1542	*lpd*	2-oxoglutarate Dh, dihydrolipoamide Dh	0.29	0.00	0.97	0.63	2.70	0.81	0.78
META1_1538	*sucC*	succinyl-CoA synthetase, β SU	0.36	0.00	0.67	0.07	3.77	2.00	1.34
META1_1539	*sucD*	succinyl-CoA synthetase, α SU	0.48	0.02	0.76	0.09	2.33	1.47	1.12
META1_3860	*sdhD*	succinate Dh Δ SU	0.74	0.95	1.11	0.50	0.05	0.03	0.03
META1_3861	*sdhA/B*	succinate Dh, flavoprotein SU	0.33	0.00	1.11	0.46	2.08	0.61	0.69
META1_3863	*sdhB*	succinate Dh, iron-sulfur SU	0.28	0.01	0.97	0.08	0.38	0.11	0.11
META1_2857	*fumC*	fumarase C	0.48	0.01	1.50	0.03	3.15	1.02	1.53
META1_1537	*mdh*	malate Dh	0.47	0.01	0.79	0.13	3.69	2.19	1.73
EMC pathway									
META1_3700	*phaA*	β-ketothiolase	0.53	0.02	0.82	0.04	6.31	4.04	3.32
META1_3701	*phaB*	acetoacetyl-CoA reductase	0.59	0.03	0.71	0.32	1.97	1.63	1.16
META1_3675	*croR*	crotonase	0.80	0.69	0.77	0.29	0.44	0.46	0.36
META1_0178	*ccr*	crotonyl-CoA carboxylase/reductase	0.54	0.01	0.48	0.00	2.78	3.14	1.51
META1_0839	*epm*	ethylmalonyl-CoA/methylmalonyl-CoA epimerase	0.74	0.27	0.85	0.27	0.34	0.29	0.25
META1_0180	*ecm*	ethylmalonyl-CoA mutase	1.01	0.73	0.70	0.02	2.00	2.85	2.01
META1_2223	*msd*	methylsuccinyl-CoA Dh	0.69	0.01	0.59	0.02	2.95	3.45	2.02
META1_4153	*mcd*	mesaconyl-CoA hydratase	0.93	0.88	0.37	0.00	0.60	1.51	0.56
META1_0172	*pccB*	propionyl-CoA carboxylase β-chain	0.66	0.04	0.67	0.03	3.08	3.04	2.04

META1_3203	*pccA*	propionyl-CoA carboxylase α SU	1.00	0.96	0.58	0.03	2.67	4.64	2.67
META1_2390	*mcmB*	methylmalonyl-CoA mutase, α SU	1.14	0.15	0.89	0.82	1.22	1.56	1.40
META1_5251	*mcmA*	methylmalonyl-CoA mutase, α SU	1.64	0.01	0.79	0.15	0.96	2.01	1.58
META1_2137	*mcl2*	malyl-CoA thioesterase	1.06	0.49	1.45	0.06	0.72	0.52	0.76
PHB metabolism									
META1_3304	*phaC*	poly(3-hydroxyalkanoate) polymerase	0.56	0.25	3.89	0.62	1.69	0.24	0.94
META1_0419	*depA*	intracellular PHB depolymerase	1.35	0.56	1.40	0.41	0.20	0.19	0.27
Serine cycle									
META1_3384	*glyA*	serine hydroxymethyltransferase	1.09	0.55	0.76	0.00	4.19	6.04	4.56
META1_1726	*sga*	serine glyoxylate aminotransferase	3.74	0.00	0.48	0.00	1.42	11.02	5.32
META1_1727	*hprA*	hydroxypyruvate reductase, NAD(P)H-dep.	3.20	0.01	0.63	0.02	0.48	2.44	1.54
META1_2944	*gck*	glycerate kinase	1.86	0.00	0.52	0.00	0.63	2.22	1.16
META1_2984	*eno*	enolase	0.70	0.01	1.02	1.00	2.85	1.97	2.00
META1_1732	*ppc*	phosphoenolpyruvate carboxylase	9.48	0.00	0.58	0.00	0.23	3.70	2.15
META1_1731	*mtkB*	malate thiokinase, small SU	3.78	0.00	0.46	0.00	0.64	5.21	2.40
META1_1730	*mtkA*	malate thiokinase, large SU	5.81	0.00	0.43	0.00	0.23	3.04	1.32
META1_1733	*mclA1*	malyl-CoA lyase/β-methylmalyl-CoA lyase	2.18	0.00	0.40	0.00	1.76	9.51	3.84
C1 pathways									
META1_1729	*fch*	methenyl H$_4$F cyclohydrolase	3.27	0.03	0.59	0.05	0.37	2.07	1.22
META1_1728	*mtdA*	NADP-dep. methylene- H$_4$MPT/ methylene-H$_4$F Dh	4.86	0.00	0.84	0.64	0.81	4.67	3.92
META1_0329	*ftfL*	formate-H$_4$F ligase (formyl-H$_4$F synthetase)	2.74	0.00	0.91	0.21	1.36	4.10	3.73
META1_1766	*fae*	formaldehyde-activating enzyme	0.73	0.16	0.45	0.01	3.77	6.09	2.76
META1_1761	*mtdB*	NAD(P)-dep. methylene H$_4$MPT Dh	1.18	0.21	0.99	0.06	1.40	1.84	1.22
META1_1763	*mch*	N(5),N(10)-methenyl- H$_4$MPT (methenyl-H$_4$MPT) cyclohydrolase	0.87	0.21	0.66	0.07	1.40	1.84	1.22
META1_1755	*fhcC*	formyltransferase/hydrolase complex Fhc SU C	0.57	0.23	1.01	0.93	0.57	0.72	0.73
META1_1756	*fhcD*	formyltransferase/hydrolase complex Fhc SU D	0.47	0.95	0.62	0.03	0.47	0.79	0.49
META1_1757	*fhcA*	formyltransferase/hydrolase complex Fhc SU A	0.87	0.73	0.89	0.43	0.87	0.98	0.87
META1_1758	*fhcB*	formyltransferase/hydrolase complex Fhc SU B	0.82	1.00	0.66	0.01	0.82	1.16	0.77
Serine / glycine metabolism									
META1_0620	*gcvP*	glycine decarboxylase, PLP-dep., SU (protein P) of glycine cleavage complex	1.10	0.55	29.09	0.92	3.75	0.14	4.11
META1_0622	*gcvT*	glycine cleavage complex protein T, aminomethyltransferase, H4F-dep.	2.08	0.08	72.22	0.31	1.05	0.03	2.18
META1_0485	*serC*	phosphoserine aminotransferase	1.22	0.39	0.52	0.02	0.21	0.49	0.26
META1_2848	-	putative phosphoserine phosphatase (serB-like)	1.42	0.31	1.40	0.40	0.21	0.21	0.30
META1_0105	*serA*	D-3-phosphoglycerate Dh	0.45	0.00	1.13	0.37	2.88	1.14	1.29
META1_0486	*serA*	phosphoglycerate Dh	1.35	0.38	0.90	0.95	0.21	0.31	0.28
C3 metabolism									
META1_1533	*pck*	phosphoenolpyruvate carboxykinase	0.03	0.99	n.d.	0.12	1.37	0.00	0.04
META1_3097	*ppdK*	pyruvate phosphate dikinase (pyruvate, orthophosphate dikinase)	0.61	0.01	1.08	0.56	5.90	3.34	3.60
META1_2941	*pyk*	pyruvate kinase	1.19	0.35	0.34	0.00	0.62	2.14	0.73
META1_0594	*dme*	NAD-dependent malic enzyme	0.44	0.00	1.55	0.01	5.38	1.51	2.35
META1_2987	*pdhB*	pyruvate Dh E1 β SU	0.40	0.01	1.71	0.02	4.00	0.95	1.62
META1_2986	*pdhA*	pyruvate Dh E1 α SU	0.33	0.01	1.55	0.04	2.01	0.43	0.67
META1_2989	*pdhC*	dihydrolipoamide acetyltransferase	0.27	0.00	2.20	0.03	5.44	0.67	1.47
META1_2990	*lpd*	dihydrolipoamide Dh, E3 Component of pyruvate Dh multienzyme complex	0.31	0.00	3.33	0.00	3.98	0.37	1.24

Abbreviations: SU: subunit, dep.: dependent Dh: dehydrogenase

REFERENCES

References

Abe, K., Ruan, Z. S. & Maloney, P. C. (1996). Cloning, sequencing, and expression in *Escherichia coli* of OxlT, the oxalate:formate exchange protein of *Oxalobacter formigenes*. *J Biol Chem* **271**, 6789-6793.

Alber, B. E., Spanheimer, R., Ebenau-Jehle, C. & Fuchs, G. (2006). Study of an alternate glyoxylate cycle for acetate assimilation by *Rhodobacter sphaeroides*. *Mol Microbiol* **61**, 297-309.

Albers, H. & Gottschalk, G. (1976). Acetate metabolism in *Rhodopseudomonas gelatinosa* and several other Rhodospirillaceae. *Arch Microbiol* **111**, 45-49.

Allison, M. J., Dawson, K. A., Mayberry, W. R. & Foss, J. G. (1985). *Oxalobacter formigenes* gen. nov., sp. nov.: oxalate-degrading anaerobes that inhabit the gastrointestinal tract. *Arch Microbiol* **141**, 1-7.

Allison, M. J., Cook, H. M., Milne, D. B., Gallagher, S. & Clayman, R. V. (1986). Oxalate degradation by gastrointestinal bacteria from humans. *J Nutr* **116**, 455-460.

Ames, G. F. (1968). Lipids of *Salmonella typhimurium* and *Escherichia coli* - structure and metabolism. *Journal of Bacteriology* **95**, 833-843.

Anesti, V., Vohra, J., Goonetilleka, S., McDonald, I. R., Straubler, B., Stackebrandt, E., Kelly, D. P. & Wood, A. P. (2004). Molecular detection and isolation of facultatively methylotrophic bacteria, including *Methylobacterium podarium* sp. nov., from the human foot microflora. *Environ Microbiol* **6**, 820-830.

Anesti, V., McDonald, I. R., Ramaswamy, M., Wade, W. G., Kelly, D. P. & Wood, A. P. (2005). Isolation and molecular detection of methylotrophic bacteria occurring in the human mouth. *Environ Microbiol* **7**, 1227-1238.

Anthony, C. (1982). The biochemistry of methylotrophs. *London: Academic Press*.

Anthony, C. (2011). How half a century of research was required to understand bacterial growth on C1 and C2 compounds; the story of the serine cycle and the ethylmalonyl-CoA pathway. *Sci Prog* **94**, 109-137.

Arps, P. J., Fulton, G. F., Minnich, E. C. & Lidstrom, M. E. (1993). Genetics of serine pathway enzymes in *Methylobacterium extorquens* AM1: phosphoenolpyruvate carboxylase and malyl coenzyme A lyase. *J Bacteriol* **175**, 3776-3783.

Baetz, A. L. & Allison, M. J. (1989). Purification and characterization of oxalyl-coenzyme A decarboxylase from *Oxalobacter formigenes*. *J Bacteriol* **171**, 2605-2608.

Baetz, A. L. & Allison, M. J. (1990). Purification and characterization of formyl-coenzyme A transferase from *Oxalobacter formigenes*. *J Bacteriol* **172**, 3537-3540.

References

Bantscheff, M., Schirle, M., Sweetman, G., Rick, J. & Kuster, B. (2007). Quantitative mass spectrometry in proteomics: a critical review. *Anal Bioanal Chem* **389**, 1017-1031.

Blackmore, M. A. & Quayle, J. R. (1970). Microbial growth on oxalate by a route not involving glyoxylate carboligase. *Biochem J* **118**, 53-59.

Bolten, C. J., Kiefer, P., Letisse, F., Portais, J. C. & Wittmann, C. (2007). Sampling for metabolome analysis of microorganisms. *Anal Chem* **79**, 3843-3849.

Bosch, G., Skovran, E., Xia, Q., Wang, T., Taub, F., Miller, J. A., Lidstrom, M. E. & Hackett, M. (2008). Comprehensive proteomics of *Methylobacterium extorquens* AM1 metabolism under single carbon and nonmethylotrophic conditions. *Proteomics* **8**, 3494-3505.

Bousfield, I. J. & Green, P. N. (1985). Reclassification of bacteria of the genus *Protomonas* Urakami and Komagata 1984 in the genus *Methylobacterium* (Patt, Cole, and Hanson) Emend Green and Bousfield 1983. *Int J Syst Bacteriol* **35**, 209-209.

Braissant, O., Cailleau, G., Aragno, M. & Verrecchia, E. P. (2004). Biologically induced mineralization in the tree *Milicia excelsa* (Moraceae): its causes and consequences to the environment. *Geobiology* **2**, 59-66.

Braunegg, G., Sonnleitner, B. & Lafferty, R. M. (1978). Rapid gas-chromatographic method for determination of poly-beta-hydroxybutyric acid in microbial biomass. *Eur J Appl Microbiol Biotechnol* **6**, 29-37.

Bravo, D., Braissant, O., Solokhina, A., Clerc, M., Daniels, A. U., Verrecchia, E. & Junier, P. (2011). Use of an isothermal microcalorimetry assay to characterize microbial oxalotrophic activity. *FEMS Microbiol Ecol* **78**, 266-274.

Casal, M., Cardoso, H. & Leao, C. (1996). Mechanisms regulating the transport of acetic acid in *Saccharomyces cerevisiae*. *Microbiology* **142 (Pt 6)**, 1385-1390.

Chang, Y. Y., Wang, A. Y. & Cronan, J. E., Jr. (1993). Molecular cloning, DNA sequencing, and biochemical analyses of *Escherichia coli* glyoxylate carboligase. An enzyme of the acetohydroxy acid synthase-pyruvate oxidase family. *J Biol Chem* **268**, 3911-3919.

Chistoserdova, L. & Lidstrom, M. E. (1997). Identification and mutation of a gene required for glycerate kinase activity from a facultative methylotroph, *Methylobacterium extorquens* AM1. *J Bacteriol* **179**, 4946-4948.

Chistoserdova, L., Chen, S. W., Lapidus, A. & Lidstrom, M. E. (2003). Methylotrophy in *Methylobacterium extorquens* AM1 from a genomic point of view. *J Bacteriol* **185**, 2980-2987.

Chistoserdova, L., Laukel, M., Portais, J. C., Vorholt, J. A. & Lidstrom, M. E. (2004). Multiple formate dehydrogenase enzymes in the facultative methylotroph *Methylobacterium extorquens* AM1 are dispensable for growth on methanol. *J Bacteriol* **186**, 22-28.

Chistoserdova, L., Crowther, G. J., Vorholt, J. A., Skovran, E., Portais, J. C. & Lidstrom, M. E. (2007). Identification of a fourth formate dehydrogenase in *Methylobacterium extorquens* AM1 and confirmation of the essential role of formate oxidation in methylotrophy. *J Bacteriol* **189**, 9076-9081.

Chistoserdova, L. V. & Lidstrom, M. E. (1994). Genetics of the serine cycle in *Methylobacterium extorquens* AM1: identification, sequence, and mutation of three new genes involved in C1 assimilation, *orf4*, *mtkA*, and *mtkB*. *J Bacteriol* **176**, 7398-7404.

Chistoserdova, L. V. & Lidstrom, M. E. (1996). Molecular characterization of a chromosomal region involved in the oxidation of acetyl-CoA to glyoxylate in the isocitrate-lyase-negative methylotroph *Methylobacterium extorquens* AM1. *Microbiology* **142**, 1459-1468.

Cornick, N. A. & Allison, M. J. (1996a). Assimilation of oxalate, acetate, and CO_2 by *Oxalobacter formigenes*. *Can J Microbiol* **42**, 1081-1086.

Cornick, N. A. & Allison, M. J. (1996b). Anabolic Incorporation of oxalate by *Oxalobacter formigenes*. *Appl Environ Microbiol* **62**, 3011-3013.

Dawes, E. A. (1988). Polyhydroxybutyrate: an intriguing biopolymer. *Biosci Rep* **8**, 537-547.

Delmotte, N., Knief, C., Chaffron, S., Innerebner, G., Roschitzki, B., Schlapbach, R., von Mering, C. & Vorholt, J. A. (2009). Community proteogenomics reveals insights into the physiology of phyllosphere bacteria. *Proc Natl Acad Sci USA* **106**, 16428-16433.

Diez-Gonzalez, F. & Russell, J. B. (1997a). The ability of *Escherichia coli* O157:H7 to decrease its intracellular pH and resist the toxicity of acetic acid. *Microbiology* **143**, 1175-1180.

Diez-Gonzalez, F. & Russell, J. B. (1997b). Effects of carbonylcyanide-m-chlorophenylhydrazone (CCCP) and acetate on *Escherichia coli* O157:H7 and K-12: uncoupling versus anion accumulation. *FEMS Microbiol Lett* **151**, 71-76.

Dutton, M. V. & Evans, C. S. (1996). Oxalate production by fungi: Its role in pathogenicity and ecology in the soil environment. *Can J Microbiol* **42**, 881-895.

Egli, T. (2010). How to live at very low substrate concentration. *Water Res* **44**, 4826-4837.

Eisenreich, W., Strauss, G., Werz, U., Fuchs, G. & Bacher, A. (1993). Retrobiosynthetic analysis of carbon fixation in the phototrophic eubacterium *Chloroflexus aurantiacus*. *Eur J Biochem* **215**, 619-632.

Ensign, S. A. (2006). Revisiting the glyoxylate cycle: alternate pathways for microbial acetate assimilation. *Mol Microbiol* **61**, 274-276.

Erb, T. J., Berg, I. A., Brecht, V., Müller, M., Fuchs, G. & Alber, B. E. (2007). Synthesis of C5-dicarboxylic acids from C2-units involving crotonyl-CoA carboxylase/reductase: the ethylmalonyl-CoA pathway. *Proc Natl Acad Sci USA* **104**, 10631-10636.

References

Erb, T. J., Retey, J., Fuchs, G. & Alber, B. E. (2008). Ethylmalonyl-CoA mutase from *Rhodobacter sphaeroides* defines a new subclade of coenzyme B_{12}-dependent acyl-CoA mutases. *J Biol Chem* **283**, 32283-32293.

Erb, T. J. (2009). The ethylmalonyl-CoA pathway: a novel acetyl-CoA assimilation strategy. In *Insitute of Microbiology*. Freiburg: University of Freiburg.

Erb, T. J., Brecht, V., Fuchs, G., Müller, M. & Alber, B. E. (2009a). Carboxylation mechanism and stereochemistry of crotonyl-CoA carboxylase/reductase, a carboxylating enoyl-thioester reductase. *Proc Natl Acad Sci USA* **106**, 8871-8876.

Erb, T. J., Fuchs, G. & Alber, B. E. (2009b). (2S)-Methylsuccinyl-CoA dehydrogenase closes the ethylmalonyl-CoA pathway for acetyl-CoA assimilation. *Mol Microbiol* **73**, 992-1008.

Erb, T. J., Frerichs-Revermann, L., Fuchs, G. & Alber, B. E. (2010). The apparent malate synthase activity of *Rhodobacter sphaeroides* is due to two paralogous enzymes, (3S)-malyl-coenzyme A (CoA)/{beta}-methylmalyl-CoA lyase and (3S)-malyl-CoA thioesterase. *J Bacteriol* **192**, 1249-1258.

Fall, R. & Benson, A. A. (1996). Leaf methanol - The simplest natural product from plants. *Trends in Plant Sci* **1**, 296-301.

Franceschi, V. R. & Nakata, P. A. (2005). Calcium oxalate in plants: Formation and function. *Annu Rev Plant Biol* **56**, 41-71.

Fu, D., Sarker, R. I., Abe, K., Bolton, E. & Maloney, P. C. (2001). Structure/function relationships in OxlT, the oxalate-formate transporter of *Oxalobacter formigenes*. Assignment of transmembrane helix 11 to the translocation pathway. *J Biol Chem* **276**, 8753-8760.

Fuchs, G. (2007). Allgemeine Mikrobiologie: Thieme.

Galbally, I. E. & Kirstine, W. (2002). The production of methanol by flowering plants and the global cycle of methanol. *J Atmos Chem* **43**, 195-229.

Gerstmeir, R., Wendisch, V. F., Schnicke, S., Ruan, H., Farwick, M., Reinscheid, D. & Eikmanns, B. J. (2003). Acetate metabolism and its regulation in *Corynebacterium glutamicum*. *J Biotechnol* **104**, 99-122.

Gottschal, J. C. & Kuenen, J. G. (1980). Mixotrophic growth of *Thiobacillus*-A2 on acetate and thiosulfate as growth limiting substrates in the chemostat. *Arch Microbiol* **126**, 33-42.

Green, P. N. (2006). *Methylobacterium*, 3rd edn. New York: Springer.

Hagemeier, C. H., Chistoserdova, L., Lidstrom, M. E., Thauer, R. K. & Vorholt, J. A. (2000). Characterization of a second methylene tetrahydromethanopterin dehydrogenase from *Methylobacterium extorquens* AM1. *Eur J Biochem* **267**, 3762-3769.

Han, L. & Reynolds, K. A. (1997). A novel alternate anaplerotic pathway to the glyoxylate cycle in streptomycetes. *J Bacteriol* **179**, 5157-5164.

Hansen, R. W. & Hayashi, J. A. (1962). Glycolate metabolism in *Escherichia coli*. *J Bacteriol* **83**, 679-687.

Harder, W. & Quayle, J. R. (1971). The biosynthesis of serine and glycine in *Pseudomonas* AM1 with special reference to growth on carbon sources other than C1 compounds. *Biochem J* **121**, 753-762.

Heider, J. (2001). A new family of CoA-transferases. *FEBS Lett* **509**, 345-349.

Herbert, D. P., P.J., Strange, R.E. (1971). Chemical analysis of microbial cells. In *Meth Microbiol*, pp. 209-344. Edited by J. R. Norris, D.W. London and New York: Academic Press.

Holms, H. (1996). Flux analysis and control of the central metabolic pathways in *Escherichia coli*. *FEMS Microbiol Rev* **19**, 85-116.

Jan, S., Roblot, C., Goethals, G., Courtois, J., Courtois, B., Saucedo, J. E. N., Seguin, J. P. & Barbotin, J. N. (1995). Study of parameters affecting poly(3-hydroxybutyrate) quantification by gas-chromatography. *Anal Biochem* **225**, 258-263.

Khambata, S. R. & Bhat, J. V. (1953). Studies on a new oxalate-decomposing bacterium, *Pseudomonas oxalaticus*. *J Bacteriol* **66**, 505-507.

Khammar, N., Martin, G., Ferro, K., Job, D., Aragno, M. & Verrecchia, E. (2009). Use of the *frc* gene as a molecular marker to characterize oxalate-oxidizing bacterial abundance and diversity structure in soil. *J Microbiol Methods* **76**, 120-127.

Kiefer, P., Heinzle, E. & Wittmann, C. (2002). Influence of glucose, fructose and sucrose as carbon sources on kinetics and stoichiometry of lysine production by *Corynebacterium glutamicum*. *J Ind Microbiol Biotechnol* **28**, 338-343.

Kiefer, P., Portais, J. C. & Vorholt, J. A. (2008). Quantitative metabolome analysis using liquid chromatography-high-resolution mass spectrometry. *Anal Biochem* **382**, 94-100.

Kiefer, P., Buchhaupt, M., Christen, P., Kaup, B., Schrader, J. & Vorholt, J. A. (2009). Metabolite profiling uncovers plasmid-induced cobalt limitation under methylotrophic growth conditions. *PLoS One* **4**, e7831.

Kiefer, P., Delmotte, N. & Vorholt, J. A. (2011). Nanoscale ion-pair reversed-phase HPLC-MS for sensitive metabolome analysis. *Anal Chem* **83**, 850-855.

Klamt, S., Saez-Rodriguez, J. & Gilles, E. D. (2007). Structural and functional analysis of cellular networks with CellNetAnalyzer. *BMC Syst Biol* **1**, 2.

Kleijn, R. J., van Winden, W. A., van Gulik, W. M. & Heijnen, J. J. (2005). Revisiting the C-13-label distribution of the non-oxidative branch of the pentose phosphate pathway based upon kinetic and genetic evidence. *FEBS J* **272**, 4970-4982.

References

Knief, C., Delmotte, N., Chaffron, S., Stark, M., Innerebner, G., Wassmann, R., von Mering, C. & Vorholt, J. A. (2011). Metaproteogenomic analysis of microbial communities in the phyllosphere and rhizosphere of rice. *ISME J.*

Kolb, S. (2009). Aerobic methanol-oxidizing Bacteria in soil. *FEMS Microbiol Lett* **300**, 1-10.

Konovalova, H. M., Shylin, S. O. & Rokytko, P. V. (2007). Characteristics of carotinoids of methylotrophic bacteria of *Methylobacterium genus*. *Mikrobiol Z* **69**, 35-41.

Kornberg, H. L. & Beevers, H. (1957a). The glyoxylate cycle as a stage in the conversion of fat to carbohydrate in castor beans. *Biochim Biophys Acta* **26**, 531-537.

Kornberg, H. L. & Beevers, H. (1957b). A mechanism of conversion of fat to carbohydrate in castor beans. *Nature* **180**, 35-36.

Kornberg, H. L. & Krebs, H. A. (1957). Synthesis of cell constituents from C2-units by a modified tricarboxylic acid cycle. *Nature* **179**, 988-991.

Kornberg, H. L. & Gotto, A. M. (1959). Formation of malate from glycollate by *Pseudomonas ovalis* Chester. *Nature* **183**, 1791-1793.

Kornberg, H. L. & Gotto, A. M. (1961). Metabolism of C2 compounds in micro-organisms .6. Synthesis of cell constituents from glycollate by *Pseudomonas* sp. *Biochem J* **78**, 69-&.

Kornberg, H. L. & Sadler, J. R. (1961). Metabolism of C2-compounds in micro-organisms .8. A dicarboxylic acid cycle as a route for oxidation of glycollate by *Escherichia coli*. *Biochem J* **81**, 503-513.

Korotkova, N. & Lidstrom, M. E. (2001). Connection between poly-beta-hydroxybutyrate biosynthesis and growth on C(1) and C(2) compounds in the methylotroph *Methylobacterium extorquens* AM1. *J Bacteriol* **183**, 1038-1046.

Korotkova, N., Chistoserdova, L., Kuksa, V. & Lidstrom, M. E. (2002a). Glyoxylate regeneration pathway in the methylotroph *Methylobacterium extorquens* AM1. *J Bacteriol* **184**, 1750-1758.

Korotkova, N., Chistoserdova, L. & Lidstrom, M. E. (2002b). Poly-beta-hydroxybutyrate biosynthesis in the facultative methylotroph *Methylobacterium extorquens* AM1: identification and mutation of *gap11*, *gap20*, and *phaR*. *J Bacteriol* **184**, 6174-6181.

Korotkova, N., Lidstrom, M. E. & Chistoserdova, L. (2005). Identification of genes involved in the glyoxylate regeneration cycle in *Methylobacterium extorquens* AM1, including two new genes, *meaC* and *meaD*. *J Bacteriol* **187**, 1523-1526.

Large, P. J., Quayle, J. R. & Peel, D. (1961). Microbial growth on C1 compounds. II. Synthesis of cell constituents by methanol- and formate-grown *Pseudomonas AM 1*, and methanol-grown *Hyphomicrobium vulgare*. *Biochem J* **81**, 470-480.

Laukel, M., Chistoserdova, L., Lidstrom, M. E. & Vorholt, J. A. (2003). The tungsten-containing formate dehydrogenase from *Methylobacterium extorquens* AM1: purification and properties. *Eur J Biochem* **270**, 325-333.

Laukel, M., Rossignol, M., Borderies, G., Volker, U. & Vorholt, J. A. (2004). Comparison of the proteome of *Methylobacterium extorquens* AM1 grown under methylotrophic and nonmethylotrophic conditions. *Proteomics* **4**, 1247-1264.

Lehninger, A. L. (1975). *Biochemistry*, 2nd edn. New York: Worth Publi. Inc.

Lindow, S. E. & Brandl, M. T. (2003). Microbiology of the phyllosphere. *Appl Environ Microbiol* **69**, 1875-1883.

Loew, O. (1892). Ueber ein Bacillus, welcher Ameinsensäure und Formaldehyd assimiliren kann. *Centralblatt Bakteriologie Parasitenkunde, Infektionskrankheiten Hygiene, Abteilung II* **I2**, 462-465.

Lung, H. Y., Baetz, A. L. & Peck, A. B. (1994). Molecular cloning, DNA sequence, and gene expression of the oxalyl-coenzyme A decarboxylase gene, *oxc*, from the bacterium *Oxalobacter formigenes*. *J Bacteriol* **176**, 2468-2472.

Marx, C. J. & Lidstrom, M. E. (2001). Development of improved versatile broad-host-range vectors for use in methylotrophs and other gram-negative bacteria. *Microbiology* **147**, 2065-2075.

Marx, C. J. & Lidstrom, M. E. (2002). Broad-host-range cre-lox system for antibiotic marker recycling in gram-negative bacteria. *Biotechniques* **33**, 1062-1067.

Marx, C. J. (2008). Development of a broad-host-range sacB-based vector for unmarked allelic exchange. *BMC Res Notes* **1**, 1.

Massou, S., Nicolas, C., Letisse, F. & Portais, J. C. (2007a). Application of 2D-TOCSY NMR to the measurement of specific C-13-enrichments in complex mixtures of C-13-labeled metabolites. *Metab Eng* **9**, 252-257.

Massou, S., Nicolas, C., Letisse, F. & Portais, J. C. (2007b). NMR-based fluxomics: Quantitative 2D NMR methods for isotopomers analysis. *Phytochemistry* **68**, 2330-2340.

Neidhardt, F. C. (1996). Chemical composition of *Escherichia coli*. In *Escherichia coli and Salmonella: Cellular and Molecular Biology*, pp. 3-6. Edited by F. C. Neidhardt, Curtiss, R., Ingraham, J. L., Lin, E. C. C., Low, K. B., Magasanik, B., et al. Washington, D.C.: ASM Press.

Oh, M. K., Rohlin, L., Kao, K. C. & Liao, J. C. (2002). Global expression profiling of acetate-grown *Escherichia coli*. *J Biol Chem* **277**, 13175-13183.

Okubo, Y., Skovran, E., Guo, X., Sivam, D. & Lidstrom, M. E. (2007). Implementation of microarrays for *Methylobacterium extorquens* AM1. *OMICS* **11**, 325-340.

References

Okubo, Y., Yang, S., Chistoserdova, L. & Lidstrom, M. E. (2010). Alternative route for glyoxylate consumption during growth on two-carbon compounds by *Methylobacterium extorquens* AM1. *J Bacteriol* **192**, 1813-1823.

Orth, J. D., Thiele, I. & Palsson, B. O. (2010). What is flux balance analysis? *Nat Biotechnol* **28**, 245-248.

Patel, T. R. & McFadden, B. A. (1978). *Caenorhabditis elegans* and *Ascaris suum*: fragmentation of isocitrate lyase in crude extracts. *Exp Parasitol* **44**, 72-81.

Peel, D. & Quayle, J. R. (1961). Microbial growth on C1 Compounds .I. Isolation and characterization of *Pseudomonas AM1*. *Biochem J* **81**, 465-469.

Peng, L. & Shimizu, K. (2003). Global metabolic regulation analysis for *Escherichia coli* K12 based on protein expression by 2-dimensional electrophoresis and enzyme activity measurement. *Appl Microbiol Biotechnol* **61**, 163-178.

Peyraud, R., Kiefer, P., Christen, P., Massou, S., Portais, J. C. & Vorholt, J. A. (2009). Demonstration of the ethylmalonyl-CoA pathway by using ^{13}C metabolomics. *Proc Natl Acad Sci USA* **106**, 4846-4851.

Peyraud, R., Schneider, K., Kiefer, P., Massou, S., Vorholt, J. A. & Portais, J. C. (2011). Genome-scale reconstruction and system level investigation of the metabolic network of *Methylobacterium extorquens* AM1. *BMC Syst Biol* **5**, 189.

Pham, T. V., Piersma, S. R., Warmoes, M. & Jimenez, C. R. (2010). On the beta-binomial model for analysis of spectral count data in label-free tandem mass spectrometry-based proteomics. *Bioinformatics* **26**, 363-369.

Quayle, J. R. & Keech, D. B. (1959a). Carbon assimilation by *Pseudomonas oxalaticus* (OX 1). 2. Formate and carbon dioxide utilization by cell-free extracts of the organism grown on formate. *Biochem J* **72**, 631-637.

Quayle, J. R. & Keech, D. B. (1959b). Carbon assimilation by *Pseudomonas oxalaticus* (OX 1). 1. Formate and carbon dioxide utilization during growth on formate. *Biochem J* **72**, 623-630.

Quayle, J. R. & Keech, D. B. (1960). Carbon assimilation by *Pseudomonas oxalaticus* (OX1). 343. Oxalate utilization during growth on oxalate. *Biochem J* **75**, 515-523.

Quayle, J. R., Keech, D. B. & Taylor, G. A. (1961). Carbon assimilation by *Pseudomonas oxalaticus* (OXI). 4. Metabolism of oxalate in cell-free extracts of the organism grown on oxalate. *Biochem J* **78**, 225-236.

Quayle, J. R. & Taylor, G. A. (1961). Carbon assimilation by *Pseudomonas oxalaticus* (OXI). 5. Purification and properties of glyoxylic dehydrogenase. *Biochem J* **78**, 611-615.

Quayle, J. R. (1963a). Carbon assimilation by *Pseudomonas oxalaticus* (OX1). 6. Reactions of oxalyl-coenzyme A. *Biochem J* **87**, 368-373.

Quayle, J. R. (1963b). Carbon assimilation by *Pseudomonas Oxalaticus* (Ox1). 7. Decarboxylation of oxalyl-coenzyme a to formyl-coenzyme A. *Biochem J* **89**, 492-503.

Reddy, C. S., Ghai, R., Rashmi & Kalia, V. C. (2003). Polyhydroxyalkanoates: an overview. *Bioresour Technol* **87**, 137-146.

Roe, A. J., McLaggan, D., Davidson, I., O'Byrne, C. & Booth, I. R. (1998). Perturbation of anion balance during inhibition of growth of *Escherichia coli* by weak acids. *J Bacteriol* **180**, 767-772.

Roe, A. J., O'Byrne, C., McLaggan, D. & Booth, I. R. (2002). Inhibition of *Escherichia coli* growth by acetic acid: a problem with methionine biosynthesis and homocysteine toxicity. *Microbiology* **148**, 2215-2222.

Russell, J. B. (1992). Another explanation for the toxicity of fermentation acids at low pH - Anion accumulation versus uncoupling. *J Appl Bacteriol* **73**, 363-370.

Sahin, N. (2003). Oxalotrophic bacteria. *Res Microbiol* **154**, 399-407.

Sahin, N. & Aydin, S. (2006). Identification of oxalotrophic bacteria by neural network analysis of numerical phenetic data. *Folia Microbiol (Praha)* **51**, 87-91.

Sahin, N., Kato, Y. & Yilmaz, F. (2008). Taxonomy of oxalotrophic *Methylobacterium* strains. *Naturwissenschaften* **95**, 931-938.

Salmond, C. V., Kroll, R. G. & Booth, I. R. (1984). The effect of food preservatives on pH homeostasis in *Escherichia coli*. *J Gen Microbiol* **130**, 2845-2850.

Sapan, C. V., Lundblad, R. L. & Price, N. C. (1999). Colorimetric protein assay techniques. *Biotechnol Appl Biochem* **29**, 99-108.

Sasser, M. (1990). Identification of bacteria through fatty acid analysis. In *Methods in Phytobacteriology*, pp. 199-204. Edited by Z. Klement, Rudolph, K., Sands, D. C. Budapest: Akademiai Kiado.

Sauer, U. (2006). Metabolic networks in motion: ^{13}C-based flux analysis. *Mol Syst Biol* **2**, 62.

Schneider, K., Asao, M., Carter, M. S. & Alber, B. E. (2012). *Rhodobacter sphaeroides* uses a reductive route via propionyl coenzyme A to assimilate 3-hydroxypropionate. *J Bacteriol* **194**, 225-232.

Schrader, J., Schilling, M., Holtmann, D., Sell, D., Filho, M. V., Marx, A. & Vorholt, J. A. (2009). Methanol-based industrial biotechnology: current status and future perspectives of methylotrophic bacteria. *Trends Biotechnol* **27**, 107-115.

Sidhu, H., Ogden, S. D., Lung, H. Y., Luttge, B. G., Baetz, A. L. & Peck, A. B. (1997). DNA sequencing and expression of the formyl coenzyme A transferase gene, *frc*, from *Oxalobacter formigenes*. *J Bacteriol* **179**, 3378-3381.

References

Sidhu, H., Hoppe, B., Hesse, A., Tenbrock, K., Bromme, S., Rietschel, E. & Peck, A. B. (1998). Absence of *Oxalobacter formigenes* in cystic fibrosis patients: a risk factor for hyperoxaluria. *Lancet* **352**, 1026-1029.

Skovran, E., Yang, S., Palmer, A.D., Lidstrom, M.E. Oxalyl-CoA reductase (PanE2) is part of a novel glyoxylate production and detoxification pathway in *Methylobacterium extorquens* AM1. *In preparation*.

Smejkalova, H., Erb, T. J. & Fuchs, G. (2010). Methanol assimilation in *Methylobacterium extorquens* AM1: demonstration of all enzymes and their regulation. *PLoS One* **5**, e13001.

Smith, L. M., Meijer, W. G., Dijkhuizen, L. & Goodwin, P. M. (1996). A protein having similarity with methylmalonyl-CoA mutase is required for the assimilation of methanol and ethanol by *Methylobacterium extorquens* AM1. *Microbiology* **142**, 675-684.

Smith, P. K., Krohn, R. I., Hermanson, G. T. & other authors (1985a). Measurement of protein using bicinchoninic acid. *Anal Biochem* **150**, 76-85.

Smith, R. L., Strohmaier, F. E. & Oremland, R. S. (1985b). Isolation of anaerobic oxalate-degrading bacteria from fresh-water lake-sediments. *Arch Microbiol* **141**, 8-13.

Sokol, S., Millard, P. & Portais, J. C. (2012). influx_s: increasing numerical stability and precision for metabolic flux analysis in isotope labelling experiments. *Bioinformatics* **28**, 687-693.

Steiner, P. & Sauer, U. (2003). Overexpression of the ATP-dependent helicase RecG improves resistance to weak organic acids in *Escherichia coli*. *Appl Microbiol Biotechnol* **63**, 293-299.

Svedruzic, D., Jonsson, S., Toyota, C. G., Reinhardt, L. A., Ricagno, S., Lindqvist, Y. & Richards, N. G. (2005). The enzymes of oxalate metabolism: unexpected structures and mechanisms. *Arch Biochem Biophys* **433**, 176-192.

Sy, A., Timmers, A. C., Knief, C. & Vorholt, J. A. (2005). Methylotrophic metabolism is advantageous for *Methylobacterium extorquen*s during colonization of *Medicago truncatula* under competitive conditions. *Appl Environ Microbiol* **71**, 7245-7252.

Tukey, H. B. (1966). Leaching of Metabolites from above-Ground Plant Parts and Its Implications. *B Torrey Bot Club* **93**, 385-401.

Vandamme, P. & Coenye, T. (2004). Taxonomy of the genus *Cupriavidus*: a tale of lost and found. *Int J Syst Evol Microbiol* **54**, 2285-2289.

Vorholt, J. A., Chistoserdova, L., Lidstrom, M. E. & Thauer, R. K. (1998). The NADP-dependent methylene tetrahydromethanopterin dehydrogenase in *Methylobacterium extorquens* AM1. *J Bacteriol* **180**, 5351-5356.

Vorholt, J. A. (2002). Cofactor-dependent pathways of formaldehyde oxidation in methylotrophic bacteria. *Arch Microbiol* **178**, 239-249.

Vuilleumier, S., Chistoserdova, L., Lee, M. C. & other authors (2009). *Methylobacterium* genome sequences: a reference blueprint to investigate microbial metabolism of C1 compounds from natural and industrial sources. *PLoS One* **4**, e5584.

Walsh, K. & Koshland, D. E., Jr. (1984). Determination of flux through the branch point of two metabolic cycles. The tricarboxylic acid cycle and the glyoxylate shunt. *J Biol Chem* **259**, 9646-9654.

Wendisch, V. F., de Graaf, A. A., Sahm, H. & Eikmanns, B. J. (2000). Quantitative determination of metabolic fluxes during coutilization of two carbon sources: comparative analyses with *Corynebacterium glutamicum* during growth on acetate and/or glucose. *J Bacteriol* **182**, 3088-3096.

Wiechert, W. (2001). ^{13}C metabolic flux analysis. *Metab Eng* **3**, 195-206.

Wiechert, W., Mollney, M., Petersen, S. & de Graaf, A. A. (2001). A universal framework for ^{13}C metabolic flux analysis. *Metab Eng* **3**, 265-283.

Zhao, J. & Shimizu, K. (2003). Metabolic flux analysis of *Escherichia coli* K12 grown on ^{13}C-labeled acetate and glucose using GC-MS and powerful flux calculation method. *J Biotechnol* **101**, 101-117.

108

Acknowledgements

Curriculum Vitae

Kathrin Schneider

Born July 21st, 1978, in Konstanz, Germany

Academic Education

12/2008-present	**Doctoral Thesis** **Eidgenössische Technische Hochschule Zurich, Switzerland** Institute of Microbiology, Supervisor: Prof. Dr. J.A. Vorholt

10/2003- **Diploma Student (Biology)**, Graduation as Biologist (Diploma)
11/2008 **University of Freiburg, Germany**

Diploma Thesis (12 month)
The Ohio State University, USA
Department of Microbiology, Supervisor Prof. Dr. B.E. Alber, Prof. Dr. G. Fuchs
"Investigation of 3-hydroxypropionate metabolism in *Rhodobacter sphaeroides*"

Erasmus EU Exchange Program (4 months)
University of Wolverhampton, England

Work Experience

11/2005- **Undergraduate Research Assistant**
09/2007 **University of Freiburg, Germany**
Institute of Microbiology, Supervisor Prof. Dr. B.E. Alber, Prof. Dr. G. Fuchs

07/2002- **Midwife**
09/2005 **Frauenklink Rheinfelden, Germany**

Internship and Training

04/1999- **Training as Midwife**
03/2002 **University Hospital of Freiburg, Germany**

10/1998- **Volunteer Work in the Social Sector (Freiwilliges Soziales Jahr)**
03/1999 **Malteser Hilfsdienst Konstanz, Germany**

09/1997- **Medical Internships**,
08/1998 **University Hospital Jena and Civic Hospital Konstanz, Germany**

1997 Abitur, Konstanz, Germany